Title
The cytosol must flow: physiological signals coordinate transport through plasmodesmata

Author
Brunkard, Jacob O.

Publication Date
2015

Peer reviewed|Thesis/dissertation

The cytosol must flow: physiological signals coordinate transport through plasmodesmata

by

Jacob Oliver Brunkard

A dissertation submitted in partial satisfaction
of the requirements for the degree of

Doctor of Philosophy

in

Plant Biology

in the

Graduate Division

of the

University of California, Berkeley

Committee in charge:

Patricia C. Zambryski, Chair
Gian Garriga
Sarah C. Hake
Peter H. Quail

Summer 2015

Abstract

The cytosol must flow: physiological signals coordinate transport through plasmodesmata

by

Jacob Oliver Brunkard

Doctor of Philosophy in Plant Biology

University of California, Berkeley

Professor Patricia C. Zambryski, Chair

Plant cells are connected by nanoscopic channels in the cell wall called plasmodesmata (PD). PD allow neighboring cells to exchange cytosol, permitting small and large molecules (including water, ions, sugars, hormones, proteins, RNA, and viruses) to move from cell to cell. PD are absolutely essential for plant life: all land plants have PD, and no mutant lacking PD has ever been identified. Despite their importance to a range of biology, including hormonal signaling, transcription factor trafficking, and the movement of resources and nutrients, very little is currently known about how PD transport is regulated.

The Zambryski lab conducted a forward genetic screen for mutants severely defective in regulating PD transport during embryogenesis, and identified five mutants with increased PD transport (*ise1–ise5*) and one mutant with decreased PD transport (*dse1*) at the mid-torpedo stages of embryogenesis. After mapping and characterizing these mutants, I discovered that two major metabolic pathways regulate PD transport during development of plant embryos and shoots: chloroplast biogenesis and sugar signaling. Here, I use a combination of approaches from cell biology, transcriptomics, and physiology to unravel the complex pathways linking chloroplasts, sugars, and PD.

Upon discovering that two mutants defective in chloroplast biogenesis, *ise1* and *ise2*, affect the expression of thousands of nuclear genes—including many that are not clearly related to chloroplast function—and prevent the restriction of PD transport during embryogenesis, I decided to pursue an open hypothesis that chloroplasts (and other plastid types) could transmit signals within the cell through thin, tubular projections called “stromules” (stroma-filled tubules). Previous work has shown that stromules physically associate with the nucleus, ER, mitochondria, and other subcellular locations, but there was no evidence that signals initiated within the plastid affected stromule activity. I demonstrate that stromules are induced during the day and that they respond to light-sensitive redox signaling pathways within the chloroplast. Furthermore, I show that stromules can form independently outside of their cellular context. In combination,

these results support the hypothesis that stromules are potential routes for intracellular signal transduction (Chapter Two).

Previous work had suggested that PD transport is tightly regulated over developmental time scales and in response to abiotic and biotic stress. Our discovery that chloroplasts coordinate PD transport led us to explore whether intercellular trafficking changes over physiological time scales, particularly in response to light. I show that cytosol moves through PD much faster during the day than the night in leaves, and that this increase in PD transport during the day is light-dependent. Light is insufficient to induce high levels of PD transport at night, however, suggesting that PD transport is regulated by the circadian clock (Chapter Three).

PD transport decreases as leaves age, which promotes allocation of nutritional resources to younger, growing leaves in the shoot. Although well-studied, the mechanism of this transition from high to low PD transport remained unclear. I use the *ise4* mutant as a starting point: ISE4 is a chaperone subunit required to activate a kinase, TOR, that is a central metabolic sensor in all eukaryotes. I show that TOR senses sugar availability to coordinate the restriction of PD transport during embryogenesis and during shoot development, and that TOR regulates plant growth and aging (Chapter Four).

For Molly

Table of contents

List of figures, tables, symbols

Figures

Tables

Abbreviations

$35S_{PRO}$	35S promoter derived from *Cauliflower mosaic virus*
3D-SIM	Three-dimensional structured illumination microscopy
ABA	Abscisic acid
ABI3	ABA-INSENITIVE 3
AZD-8055	5-{2,4-Bis[(3S)-3-methylmorpholin-4-yl]pyrido[2,3-d]pyrimidin-7-yl}-2-methoxyphenyl)methanol
Col-0	*Arabidopsis thaliana* ecotype Columbia-0
DNA	Deoxyribonucleic acid
DSE1	DECREASED SIZE EXCLUSION LIMIT 1
E	Einstein, one mole of photosynthetically active photons
FITC	Fluorescein isothiocyanate
GFP	GREEN FLUORESCENT PROTEIN
GUN2	GENOMES UNCOUPLED 2 (also HO1, HY1)
h	hour
HO1	HEME OXYGENASE 1 (also GUN2, HY1)
HY1	ELONGATED HYPOCOTYL 1 (also GUN2, HO1)
HPTS	8-hydroxpyrene-1,3,6-trisulfonic acid
ISE1–5	INCREASED SIZE EXCLUSION LIMIT 1–5
MS	Murashige and Skoog growth medium
Nb-1	*Nicotiana benthamiana* ecotype Nb-1
NTRC	NADPH-DEPENDENT THIOREDOXIN REDUCTASE C
PD	Plasmodesma
PIE1	PHOTOPERIOD-INDEPENDENT EARLY FLOWERING 1
ROS	Reactive oxygen species
RNA	Ribonucleic acid
SHAM	Salicyl hydroxamic acid
TF	Transcription factor
TOR	TARGET OF RAPAMYCIN
TRV	*Tobacco rattle virus*
VIGS	Virus-induced gene silencing
WT	Wild-type
Y2H	Yeast two-hybrid

Acknowledgments

First and foremost, I must acknowledge my advisor, Pat Zambryski, who encouraged me to pursue projects according to my curiousity, and always had time to meet and discuss the latest experiment or kernel of an idea.

Many friends and colleagues have contributed to this work, for which I am very grateful. Special thanks to my early mentors, Tessa Burch-Smith and Min Xu, post-doctoral researchers in the Zambryski lab who guided me as I began these projects. Thanks also to my Zambryski labmates over the years for their advice, friendship, and labor: graduate students Julieta Aguilar, Solomon Stonebloom, Todd Cameron, James Anderson-Furgeson, and Anne Runkel; undergraduate mentees Lauren Kivlen, Mary Ahern, Jacob Leroux, Vemmy Matsutnan, and Christine Regan; postdoctoral researchers Elena Shemyakina and Romain Grangeon; and senior scientists Howard Goodman and John Zupan. Steve Ruzin and Denise Schichnes have offered invaluable assistance with microscopy, and their enthusiasm has brightened days spent sequestered in dark rooms with lasers and slides. Claire Bendix and Megan Cohn provided constant emotional support, intellectual criticism, and friendship.

The faculty of the Plant and Microbial Biology department have been excellent mentors. Thanks to my pedagogical advisors, Sheng Luan, Renee Sung, and especially Kathleen Ryan, who took a risk in letting a plant biologist assist in her microbiology course (to my great benefit). Mary Wildermuth has encouraged my development as a scientist and as a member of the Berkeley community, offering opportunities to participate in curriculum development and educational outreach programs. Henrik Scheller provided constructive input during my second year when he served on my qualifying exam committee. My thesis committee members, Sarah Hake, Peter Quail, and Gian Garriga, have each been attentive, friendly, and inquisitive, making my committee meetings fun and productive. Barbara Baker is a dear friend, mentor, and colleague, offering her incredible insight to many of the experiments in this dissertation, and providing consistent support, in many forms, since I rotated in her lab at the beginning of my graduate studies.

I cannot possibly thank all of the friends and family who have supported me during this process enough, nor even list all of their names. My mother, Kathy, fostered my particular brand of critical thinking and work ethic, has been my most careful editor (of this dissertation, grant proposals, and publications), and is a constant inspiration. She also provided technical assistance for various projects, including providing some biological samples (e.g., of *Polytrichum commune*) and sharing her extensive knowledge of plant morphology and physiology. My father, Jimmy, tuned my thinking to mathematics and probabilities, to histories and politics and literature, and spent decades learning in our gardens with me. A team of scientist friends of the family who have encouraged me for the past twenty years must be mentioned: Tracy Whitford, John Smith, and especially Jeri Jewett-Smith, who has always been my most reliable cheerleader and advocate. Sergio Sanchez has kept me grounded and focused, and can always make me laugh. Most especially, thanks to my sister, Molly, my best friend, who is my constant companion and source of inspiration.

Chapter One: The cytosol must flow: intercellular transport through plasmodesmata, an introduction

The following chapter is a modified version of an article published in *Current Opinion in Cell Biology* (Brunkard et al., 2015a), along with excerpts from an article published in *Current Opinion in Plant Biology* (Brunkard et al., 2013).

Abstract

Plant cells are connected across cell walls by nanoscopic channels called plasmodesmata (PD), which allow plant cells to share resources and exchange signaling molecules. Several protein components of PD membranes have been identified, and recent advances in superresolution live-cell microscopy are illuminating PD ultrastructure. Restricting transport through PD is crucial for morphogenesis, since hormones and hundreds of transcription factors regularly move through PD, and this transport must stop to allow cells to begin differentiating. Chloroplasts and mitochondria regulate PD function through signal transduction networks that coordinate plant physiology and development. Recent discoveries on the relationships of land plants and their algal relatives suggest that PD have evolved independently in several lineages, emphasizing the importance of cytosolic bridges in multicellular biology.

Plasmodesmata: a primer

Multicellularity arose independently in a handful of lineages, which have evolved incredible morphological, physiological, and ecological diversity. The major multicellular lineages today include animals, some fungi, some algae, and plants. Multicellularity requires two fundamental features: cell–cell adhesion and cell–cell signaling (Niklas and Newman, 2013). Whereas animals rely on an extracellular matrix for adhesion that permits close contact for communication between cells that can be motile during development, plant cells generate sturdy cellulosic cell walls that provide structural support and defense, but prevent movement or physical connection between cells. Animals use gap junctions and cytonemes to directly exchange signals and resources between cells (Niklas, 2014; Roy et al., 2014). In plants, intercellular transport and communication rely primarily on plasmodesmata (PD).

Cell–cell signaling and transport in plants is facilitated by nanoscopic channels called PD, often as small as 30 nm in diameter and 100 nm in length, that cross the cell wall and connect neighboring cells (Brunkard et al., 2013; Burch-Smith and Zambryski, 2012; Ehlers and Große Westerloh, 2014; Sager and Lee, 2014) (Figure 1.1). PD have three distinct structural components: a central strand of tightly compressed endoplasmic reticulum (ER), called the ‘desmotubule’; a surrounding membrane that is continuous with the plasma membrane of the cells it connects; and in between these membranes, a cytosolic sleeve that allows molecules to move between cells. Water, ions, hormones, sugars, and other small molecules easily traffic through most PD, as do many larger molecules, including proteins and RNAs (Benkovics and Timmermans, 2014; Furuta et al., 2012; Gallagher et al., 2014; Niehl and Heinlein, 2011) (Figure 1.2).

PD connect almost all cells to their neighbors, with a few exceptions in highly specialized cell types that degrade or occlude PD for cellular isolation (Palevitz and Hepler, 1985; Willmer and Sexton, 1979). Despite several forward genetic screens (Benitez-Alfonso et al., 2009; Fernandez-Calvino et al., 2011; Kim et al., 2002; Xu et al., 2012a, 2011; Zambryski and Crawford, 2000), no mutant lacking PD has ever been recovered, and many mutants with strongly altered PD function are lethal. Since plant viruses are obliged to spread through PD, and many viral movement proteins localize at PD (Figure 1.2b) and alter PD function, early efforts to study PD by molecular biologists focused on the mechanisms of viral movement. Later studies of mobile transcription factors emphasized the possibility that some endogenous proteins might also alter PD function to promote their own movement, but there is no clear model for how this might occur, and early experiments supporting this model using microinjection techniques should be reconsidered in light of the accumulating evidence that microinjection perturbs PD function and is often misleading (Storms et al., 1998). We leave detailed discussion of viral movement through PD and putative selective/facilitated transport of a handful of endogenous proteins through PD to other reviews (Gallagher et al., 2014; Heinlein, 2015; Niehl and Heinlein, 2011; Sevilem et al., 2015), and focus here on the more general, experimentally supported principle that 'the cytosol must flow' through PD by default. We review recent advances in understanding PD structure and function, the role of PD in morphogenesis, emerging perspectives on how PD are regulated by intracellular signaling pathways, and new insights on the evolution of PD.

The structure of PD

For decades, most of our knowledge of PD relied on ultrastructural studies using transmission electron microscopy (TEM). These studies revealed that PD form either during cell division (primary PD) when strands of ER are trapped as the cell plate forms, or after cell division (secondary PD) through unknown mechanisms that rely on localized modification of the cell wall (Burch-Smith et al., 2011a). Many PD are straight channels, but some are branched and complex, especially in the nonvascular tissue of older leaves, where this complexity is correlated with decreased transport through PD. Electron dense material is often found within the cytosolic sleeve of PD, and includes cytoskeletal proteins, such as actin and myosin (White and Barton, 2011). The desmotubule, which is continuous with the ER, is so tightly constricted that it contains little lumenal space, and, in fact, the desmotubule membrane is among the most appressed membranes in biology (Tilsner et al., 2011). Therefore, although some molecules may move between cells through the desmotubule, most intercellular transport occurs instead via the cytosolic sleeve. PD are often surrounded by callose (β-1,3-glucan) in the cell wall (Dettmer et al., 2011; Zavaliev et al., 2011). Large callose deposits form around PD, especially during stress, pathogen attack, and organogenesis, which probably inhibit transport through PD by restricting the size of the cytosolic sleeve (Dettmer et al., 2011; Lee et al., 2011; Wang et al., 2013; Zavaliev et al., 2011).

Proteomic approaches have attempted to identify the molecular components of PD, but efforts to isolate pure PD have not succeeded, because PD are very small and are intimately connected to the cell wall, ER, and plasma membrane (Fernandez-Calvino et al., 2011; Levy et al., 2007). Nonetheless, a handful of proteins that often

localize specifically to PD and impact PD function have been characterized. In Arabidopsis, eight PD-localized proteins (PDLPs) were identified by amino acid similarity to PDLP1, which was discovered during a survey of cell wall-associated membrane-bound proteins fused to GFP (Amari et al., 2010; Thomas et al., 2008). PDLP1 and PDLP6 (Fernandez-Calvino et al., 2011), and PDLP5 (Lee et al., 2011), were later found in independent proteomic screens of PD-enriched membrane isolations. PDLPs are transmembrane proteins with a short cytosolic tail and two extracellular DUF26 domains (cysteine-rich receptor-like kinase domains of unknown function) that often localize to PD. In the same survey, another PD-localized protein, PD callose binding protein 1 (PDCB1), was also identified (Simpson et al., 2009). Phenotypes resulting from mutating or overexpressing these genes support the conclusion that PDCBs and PDLPs contribute to callose deposition at PD, but their biochemical functions remain unclear. A separate proteomic study of PD-rich membrane fractions identified a β-glucanase that instead participates in degrading callose deposits at PD (Levy et al., 2007). Finally, two PD germin-like proteins (PDGLP1 and PDGLP2) that promote PD transport in roots were detected in coimmunoprecipitates with a PD-localized viral protein (Ham et al., 2012). Recent studies have shown that plasma membrane proteins, such as receptor-like kinases, can also accumulate within the plasma membrane of PD, but these proteins have no known direct function in regulating PD transport (Faulkner et al., 2013; Stahl et al., 2013). Against some models first proposed more than fifteen years ago (Lee et al., 2000), none of the identified PD proteins appear to facilitate putative targeted, selective transport of endogenous plant proteins between cells.

Advanced microscopy techniques are also being applied to uncover details of PD structure. PD are remarkably sensitive to most fixation techniques used for TEM; fluorescence microscopy, on the other hand, allows rapid live-cell visualization of PD. Besides callose stains, the most reliable markers of PD are the movement proteins (MPs) of certain plant viruses that modify PD structure to promote trafficking of viral proteins and RNA (Heinlein, 2015; Mushegian and Elena, 2015; Niehl and Heinlein, 2011) (Figure 1.2b). Fitzgibbon et al. used three dimensional structured illumination microscopy to visualize GFP-tagged MPs at subdiffraction resolution (‘superresolution’, in this case ~100 nm), and confirmed TEM reports that callose accumulates at the ‘necks’ of PD (closest to the ends of PD where the cytosolic sleeve opens to the cytoplasm) while some MPs accumulate mostly in the ‘central cavity’ of complex PD where multiple PD branches intersect (Fitzgibbon et al., 2010, 2013). Ongoing superresolution microscopy studies will hopefully resolve whether PD proteins, such as the PDLPs, localize throughout PD and/or the plasma membrane, or are restricted to subdomains within PD, as suggested by TEM approaches (Lee et al., 2011).

Transport through PD

Molecules move rapidly through the cytoplast, mostly through convection generated by cytoplasmic streaming (with diffusion contributing to a lesser extent), where they will eventually encounter PD (Pickard, 2003). Since nearly all plant cells are connected by PD, this means that most molecules — including proteins — have ample opportunity to move from one cell to another. This is confirmed by the simple observations that heterologous fluorescent proteins, such as GFP, and large fluorescent

dyes, such as fluorescein derivatives bound to dextrans, readily move from cell to cell (Brunkard et al., 2015c; Crawford and Zambryski, 2001a; Kim and Zambryski, 2005; Kim et al., 2005a, 2005b; Oparka et al., 1999a; Roberts et al., 1997a; Wu et al., 2003). In fact, unlike in animals, the question in plants is not what features promote protein movement between cells, but how are proteins retained by a cell (Wu et al., 2003)? To date, we only have a few answers: first, protein size; second, subcellular targeting; and third, sequestration by interacting proteins (the 'nuclear trapping' hypothesis). The first feature regulating movement is the most simple: larger proteins move more slowly from cell to cell, and very large proteins are unable to move via PD. While GFP (27 kDa) quickly moves into neighboring cells (to levels detectable by fluorescence microscopy within minutes or hours), 2xGFP (54 kDa) moves much more slowly, and 3xGFP (81 kDa) is often unable to exit the cell where it is expressed (Brunkard et al., 2015c; Kim and Zambryski, 2005; Kim et al., 2005b). Indeed, broad surveys determining the mobility of a total of nearly 100 transcription factors (TFs) fused to fluorescent proteins in roots have found that, at minimum, about one-third of TFs can move through PD, and that protein size strongly correlates with the distance TFs move from their original cells (Lee et al., 2006; Rim et al., 2011). The second feature known to affect protein movement is subcellular targeting. Proteins encoding strong subcellular localization signals are often sequestered before they encounter PD, for example in the ER lumen or in organelles (Crawford and Zambryski, 2000).

Sequestration is a third mechanism that regulates the intercellular movement of proteins. In this model, often called the 'nuclear trapping' hypothesis, a protein's movement is affected by the presence of interacting partners that limit its availability for movement by sequestering the protein in the nucleus, a principle first described for the SHORT ROOT transcription factor (Cui et al., 2007; Schiefelbein et al., 2014) (Figure 1.3). A recently elaborated example is a complex of proteins including TRANSPARENT TESTA GLABRA 1 (TTG1, a WD40 repeat protein), GLABRA 3 (GL3, a bHLH TF), and GLABRA 1 (GL1, a Myb TF) that promote differentiation of scattered cells on the leaf surface to generate trichomes ('leaf hairs') (Balkunde et al., 2011; Bouyer et al., 2008). TTG1 freely moves between cells in the epidermis in the absence of GL3, but in cells where GL3 is expressed, TTG1 becomes 'trapped' in the nucleus with GL3 (Balkunde et al., 2011) (Figure 1.3a). TTG1 is then retained by that cell, which becomes a sink for TTG1 protein from nearby cells that are not expressing GL3, effectively depleting TTG1 levels from the region (Figure 1.3b), which probably contributes to the formation of a pattern of evenly dispersed trichomes across the leaf surface (Figure 1.3c) (Bouyer et al., 2008). In another example of sequestration, intercellular movement of the WUSCHEL TF is restricted by its homodimerization domain, which likely limits its ability to exit the nucleus and/or move through PD due to increased size as a dimer (Daum et al., 2014; Yadav et al., 2011).

Two further, speculative mechanisms that could prevent protein mobility remain under-examined. First, some proteins might restrict PD transport to limit their own movement. For example, a TF might promote expression of callose synthase genes that deposit callose around PD to limit intercellular transport, effectively preventing that TF from moving. Second, a cell may inhibit the activity of mobile proteins through protein degradation or deformation. This proposal is supported by the discovery that a TF fusion, GL1–KN1, requires refolding by chaperonins to function in the epidermis after

ectopic expression in adjacent tissue (Kragler et al., 1998; Xu et al., 2011). While we do not know whether only an unfolded conformation of GL1–KN1 is available for trafficking through PD in the first place, or whether movement through PD somehow disrupts GL1–KN1 structure, this study opens the possibility that cells could preferentially degrade or alter the structure of incoming proteins from neighboring cells to restrict their activity.

PD control differentiation and development

Since plant cells are in constant communication via PD, cells often need to isolate themselves by reducing PD transport to differentiate and acquire a new genetic program. Indeed, PD transport is often drastically restricted around regions of cells during morphogenesis, including during embryogenesis, inflorescence development, and lateral root formation (Benitez-Alfonso et al., 2013; Gisel et al., 1999, 2002; Kim and Zambryski, 2005; Kim et al., 2005a, 2005b; Maule et al., 2013; Rinne and van der Schoot, 1998; Sager and Lee, 2014) (Figure 1.4). Exploring the lateral root example, Benitez-Alfonso et al. showed that PD transport around differentiating lateral roots is inhibited by callose deposition. Furthermore, this reduction in PD transport is required for regular lateral root formation, and excess lateral roots form in mutants with increased callose deposition at PD in roots (Benitez-Alfonso et al., 2013). This takes the hypothesis one step further: not only does restricted intercellular communication permit differentiation and developmental reprogramming, but reducing PD transport is sufficient to induce ectopic organogenesis. How does PD transport have such a powerful effect on plant development?

In the case of initiating lateral roots, cellular isolation allows the phytohormone auxin to accumulate to a high concentration. Auxin is directed to these progenitor cells through the activity of plasma membrane transporters, where auxin is perceived by intracellular receptors that promote the expression of callose synthase (Han et al., 2014). Without callose deposition, PD allow auxin to passively flow backwards along the concentration gradient (against the direction of active transport by transmembrane efflux carriers) (Rutschow et al., 2011); with callose deposition, the auxin can accumulate to higher and higher levels. Thus, a positive feedback loop trapping auxin in a small region of cells allows sufficient auxin buildup to trigger organogenesis. These findings illustrate the central role of dynamically regulated PD transport in plant development, and highlight the need to integrate growing knowledge of PD biology with research on morphogenesis and phytohormone signaling.

Differentiation of guard cells in the shoot epidermis is also regulated by PD transport. Stomatal guard cell differentiation is initiated by a transcription factor, SPEECHLESS (SPCH) (Vatén and Bergmann, 2012). Forward genetic screens for defective guard cell patterning identified two mutants, *chorus* and *kobito1*, both with increased PD transport that allows SPCH to traffic out of a differentiating guard cell and initiate spurious guard cell formation (Guseman et al., 2010; Kong et al., 2012). This results in clusters of guard cells instead of evenly spaced, separate stomata across the leaf surface.

chorus is a weak recessive allele of *GLUCAN SYNTHASE-LIKE 8* (*GSL8*), a gene that encodes a putative callose synthase (Chen et al., 2009; Guseman et al., 2010; Zavaliev et al., 2011). Callose is a cell wall polysaccharide, β-1,3-glucan, that restricts intercellular transport when deposited just outside PD (Figure 1.1), and is also

deposited at the cell plate during cytokinesis (Zavaliev et al., 2011). Plants with a strong loss-of-function allele of *gsl8* are defective in cell division and have an extremely disorganized epidermis, including aggregation of guard cells, possibly due to incomplete cytokinesis or due to changes in PD transport of developmental signals (Chen et al., 2009). In *chorus* mutants, which do not show strong defects in cell division, callose does not accumulate to wild-type levels at PD, and PD transport increases accordingly (Guseman et al., 2010). Moreover, whereas SPCH-YFP does not move from cell to cell in wild-type plants, SPCH-YFP readily travels through PD in *chorus* mutants (Guseman et al., 2010). These findings support the conclusion that callose-mediated restriction of PD transport to isolate differentiating cells is required for epidermal patterning.

Similar to *chorus*, plants with a recessive allele of *KOBITO1* form clusters of guard cells and have increased PD transport permitting intercellular transport of SPCH (Kong et al., 2012). Unlike *chorus*, however, *kobito1* mutants do not show defects in callose deposition at PD, and may even overproduce callose. KOBITO1 is a putative glycosyltransferase-like protein of unknown function previously implicated in cellulose biosynthesis (Brocard-Gifford et al., 2004; Pagant et al., 2002). Mutants defective in cellulose biosynthesis do not show kob1-like phenotypes, however, suggesting that KOBITO1 functions in another, as yet uncharacterized pathway restricting PD movement.

Intracellular regulators of intercellular transport: organelle-nucleus-PD signaling

In the last decade, three mutant screens were conducted to identify genes regulating PD transport. The first looked for altered movement of fluorescent tracers in embryo-defective mutants, reasoning that any mutant with strong effects on PD transport would exhibit severely disrupted development [3]. From this screen, four mutants have been characterized so far: *increased size exclusion limit 1* and *2* (*ise1* and *ise2*), which have increased PD transport, and *decreased size exclusion limit 1* (*dse1*), which has decreased PD transport (Burch-Smith et al., 2011b; Kim et al., 2002; Kobayashi et al., 2007; Stonebloom et al., 2009; Xu et al., 2012a). A follow-up study of ISE2 function led to the identification another embryo-defective mutant with increased PD transport, *clp protease proteolytic subunit 2* (*clpr2*) (Carlotto et al., 2015). Two other screens searched for mutants with decreased protein movement either from the phloem to surrounding tissues or from the mesophyll to the epidermis. These efforts led to the characterization of two PD mutants: *gfp arrested trafficking 1* (*gat1*) and *chaperonin containing TCP1* 8 (*cct8*) (Benitez-Alfonso et al., 2009; Fichtenbauer et al., 2012; Xu et al., 2011). Unexpectedly, none of the genes recovered from these screens encode proteins that localize to PD. ISE1 and ISE2 are RNA helicases that localize to mitochondria and plastids, respectively; DSE1 is a WD40-repeat containing protein found in the cytoplasm and nucleus; GAT1 is a plastid-localized thioredoxin; and CCT8 is a cytoplasmic chaperonin subunit.

Intriguingly, four of these six mutants contribute to a single narrative: PD function and formation are strongly regulated by intracellular signals originating from mitochondria and plastids. Beyond dramatically increasing PD transport and formation [14], loss of either ISE1 or ISE2 affects the expression of ~3000 genes; genes that encode chloroplast proteins are remarkably overrepresented in both transcriptomes

(Burch-Smith et al., 2011b). Loss of ClpR2, an essential component of the chloroplast Clp protease machinery that is required for chloroplast biogenesis, has similar impacts on chloroplast genome expression as *ise2*, and probably affects PD transport through the same pathways as the *ise1* and *ise2* mutants (Carlotto et al., 2015). PD transport is severely reduced in mutants lacking the plastid thioredoxin m3, which overproduce hydrogen peroxide (H2O2), a known upstream signal impacting intracellular processes and nuclear gene expression (Benitez-Alfonso et al., 2009). Together, these results demonstrate that there must be extensive signaling among organelles, the nucleus, and PD to coordinate intercellular transport (Brunkard et al., 2013; Burch-Smith et al., 2011b). Physiological studies reinforced this model by showing that changes in the redox states of mitochondria or chloroplasts serve as upstream signals to rapidly alter PD transport (Stonebloom et al., 2012). All of these findings have been extensively discussed (Brunkard et al., 2013; Burch-Smith and Zambryski, 2012), and are summarized in Figure 1.5a; here, I will focus on studies that lend further support to this model.

Research on viral pathogenesis often provides insights into PD function, since viruses pirate PD for their spread through plant tissues (Harries and Ding, 2011; Niehl and Heinlein, 2011). In a stunning convergence of discoveries across different fields, several studies revealed that chloroplast proteins can inhibit or enhance the spread of tobamoviruses, potentially by modifying PD function (Figure 1.5c). *Tobacco mosaic virus* (TMV) spreads more rapidly in tobacco plants that have silenced expression of the plastid-localized *ATP synthase gamma subunit* (*AtpC*) or *RuBisCO activase* (*RCA*) [18]. On the other hand, silencing expression of the *RuBisCO small subunit* (*RbcS*) delays the spread of *Tomato mosaic tobamovirus* (ToMV) [19]. These observed changes in pathogenesis could be related to several aspects of viral spread, such as altered viral replication. In light of the mounting evidence that chloroplasts coordinate PD transport, and that loss of ISE1 or ISE2 causes increased PD transport of tobamovirus movement proteins in particular [14], future studies should also consider that disrupting chloroplast function can have downstream effects on PD transport, and that these changes in PD transport could be partially responsible for the observed abnormal viral spread.

Studies focused on PD proteins have further emphasized the relationship between chloroplasts and PD. Not only do chloroplasts regulate PD — changes in PD transport in turn disrupt chloroplast function (Figure 1.5b). First, overexpression of PDLP5 (a protein specifically localized at PD; see below), which decreases PD transport [20 and 21], leads to chlorosis and overaccumulation of salicylic acid (SA), a phytohormone synthesized in plastids [22]. Second, transgenic expression of the TMV movement protein (P30), which predominantly localizes to PD and promotes viral transport, leads to increased H_2O_2 accumulation, overaccumulation of SA, and transcriptional induction of SA-response and chloroplast ROS-scavenging genes [23]. Older studies showed that transgenic P30 expression also decreases the rate of photosynthetic carbon assimilation [24]. In concert, these discoveries imply that chloroplasts are sensitive to alterations in PD function.

The parallel evolution of PD

PD-like structures have evolved independently in multiple lineages of brown and green algae [71] (Figure 1.6), leading to the prevailing hypothesis that PD support the evolution of complex, parenchymatous multicellular forms [1] in organisms whose cells are surrounded by cellulosic cell walls. PD form in all land plants (embryophytes) studied to date, including liverworts, mosses, hornworts, and polysporangiophytes (‘vascular’ plants). Our understanding of embryophyte PD evolution needs revision in light of recent evidence on the relationships among land plants and three closely related groups of green algae, Zygnematales, Coleochaetales, and Charales [72]. Current phylogenies, based on strong molecular evidence, suggest that the closest relatives of embryophytes are the Zygnematales or a clade composed of both Zygnematales and Coleochaetales, which diverged from land plants over 450 million years ago. Previous phylogenies had instead placed Charales as the sister clade to embryophytes, and since many Charales species have PD-like channels between their cells, it was long held that algal and embryophyte PD are homologous [71]. The Zygnematales, however, do not have PD, and while Coleochaetales have channels between cells that are similar to PD, their ‘PD’ generally lack the desmotubule found in all embryophyte PD. Therefore, the ‘PD’ of green algae may not be homologous to the PD of embryophytes, but possibly arose independently through parallel evolution. While comparative studies of these various ‘PD’ are informative, we can no longer presume that the PD of green algae are necessarily homologous to embryophyte PD, and at least provisionally consider land plant PD to be a unique shared trait (synapomorphy).

Conclusion

Since the divergence of animals, plants, fungi, and algae from a single-celled eukaryote over 1.5 billion years ago, each of these lineages independently evolved multicellularity. Cell–cell signaling in complex multicellular organisms requires extensive adaptations, including some parallel adaptations (e.g., remarkably similar PD in brown algae, various green algae, and plants) and many divergent adaptations (gap junctions, for example, have very little similarity to PD). Unlike animal cells, plant cells are not autonomous by default, due to the constant exchange of signals between cells by PD. Instead, plant morphogenesis relies on locally inhibiting PD transport, which establishes autonomous domains that permit differentiation and development.

Going forward, PD biologists are getting closer to answering long-standing questions and face many exciting new questions. There is growing evidence that callose deposition at PD is only one mechanism to restrict PD transport, but these other mechanisms remain unknown. Genetic approaches, such as further characterization of dse1, a mutant with decreased PD transport but no large callose deposits at PD, hold promise for discovering these callose-independent mechanisms of regulating PD function [18]. We still do not know how PD form after cell division, a major missing piece in our knowledge of PD; again, genetics will lead the way, since our first clue is mutants in the ONPS pathway that increase PD formation [4, 5 and 69]. Several critical protein components of PD have been characterized; while proteomic studies suggest that many more proteins can localize near PD, we do not yet know if these proteins have biologically important roles in regulating PD function. All recent evidence demonstrates that there is dynamic and coordinated regulation of PD transport.

Chloroplasts and mitochondria regulate PD at the intracellular level, while PD and phytohormones interact on larger scales during growth and development. As the pieces of the puzzle are assembled, the next major task for PD biologists will be to integrate cellular and physiological perspectives on PD biology to develop a complete picture of how these remarkable structures facilitate multicellular plant life.

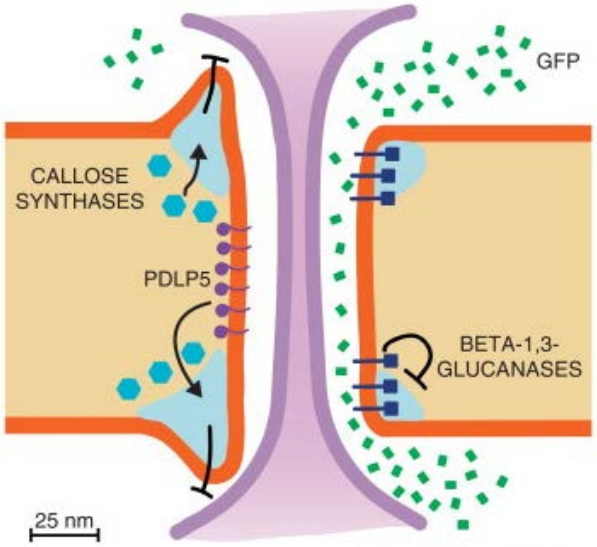

Figure 1.1. Scaled cartoon model of a plasmodesma, following Tilsner et al. [55]. Plasmodesmata are plasma membrane-lined channels that cross the cell wall, containing cytosol and a central, tightly compressed strand of endoplasmic reticulum called the desmotubule (purple). The cytosol is continuous between adjacent cells, allowing small and large molecules to move from one cell to the next. Here, GFP (green) is moving via diffusion through PD. Callose deposition bordering PD (light blue areas) negatively regulates PD transport, and is mediated by callose synthases (blue squares, left). Degradation of callose bordering PD positively regulates PD transport, and is mediated by β-1,3-glucanases (dark blue hexagons with membrane-spanning tails, right). Some PD proteins affect PD transport through unclear mechanisms, such as PDLP5 (purple circles with membrane-spanning tails, left), which here is shown inhibiting GFP transport, possibly by promoting local callose synthesis.

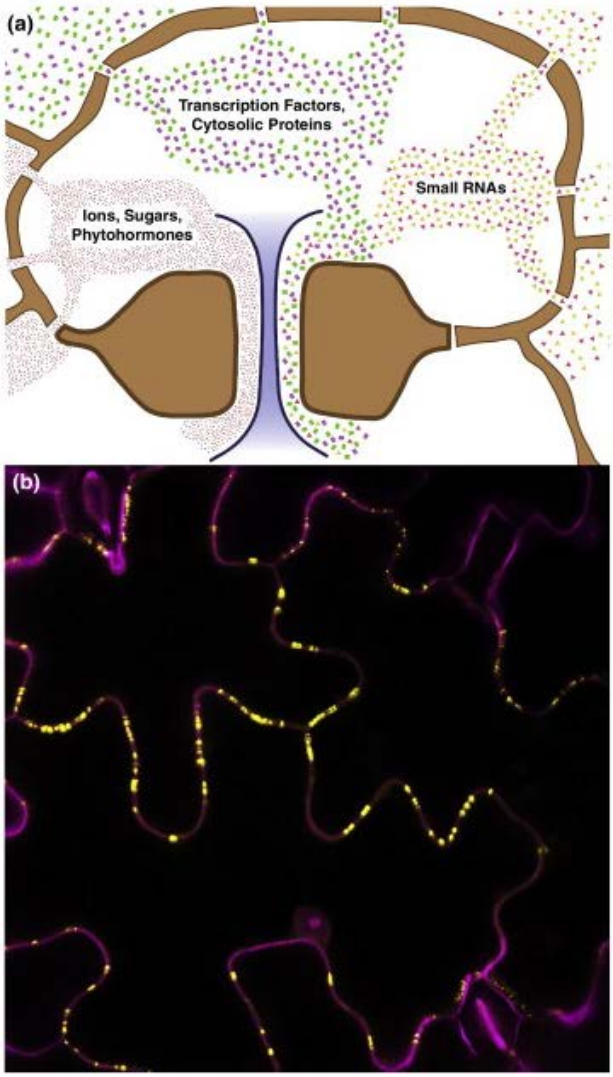

Figure 1.2. Plasmodesmata are conduits through the cell wall that allow cytosolic flow between neighboring cells. (a) Molecules in the cytosol, whether small molecules, like ions, sugars, and phytohormones, or large molecules, such as transcription factors and RNAs, can move across the cell wall boundary (brown) through PD (white interruptions in the cell wall). A single PD is enlarged to illustrate ultrastructure (center): the external PD membrane (dark brown) is continuous with the plasma membrane, the internal desmotubule (dark blue membranes, light blue lumen) is tightly compressed ER that can have almost no lumenal space, and the cytosolic sleeve between these membranes (white) allows molecules to flow between cells. (b) PD (yellow) are dispersed around the cell walls (magenta) of plant cells in the leaf epidermis. PD are marked by the movement protein of Tobacco mosaic virus fused to YFP (transiently expressed in a tobacco relative, *Nicotiana benthamiana*), and the cell walls and nuclei are stained with propidium iodide.

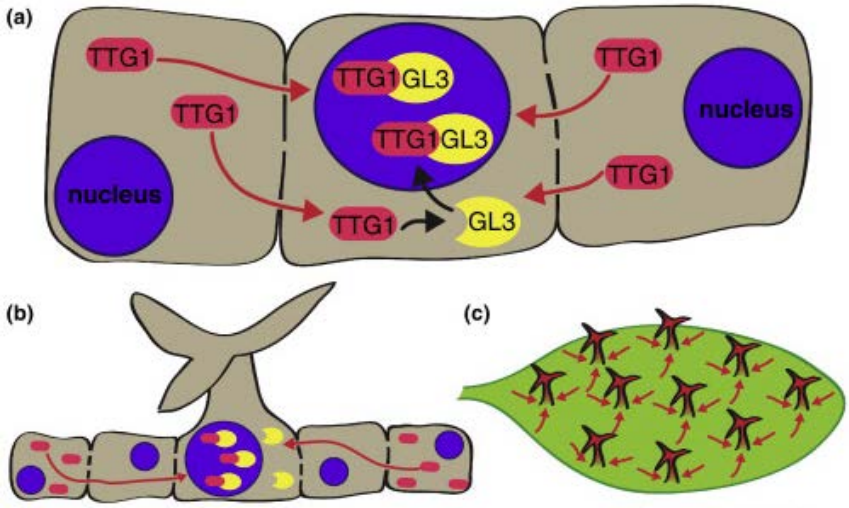

Figure 1.3. Subcellular sequestration of proteins creates intercellular concentration gradients that drive developmental patterning. (a) TTG1 (a WD40-repeat protein, red) is expressed throughout the epidermis, but when it encounters cells expressing GL3 (yellow), TTG1 and GL3 interact and are sequestered in the nucleus (blue), where they initiate trichome development. (b) TTG1 proteins move freely between cells via PD, but are rapidly sequestered in the developing trichome by GL3. This effectively depletes TTG1 levels in cells near the trichome. (c) TTG1 is depleted from regions surrounding developing trichomes (TTG1 concentration gradient indicated by red arrows). Without TTG1, cells near the developing trichome are unable to initiate trichome differentiation. Thus, regional reduction of TTG1 establishes a disperse pattern of trichomes.

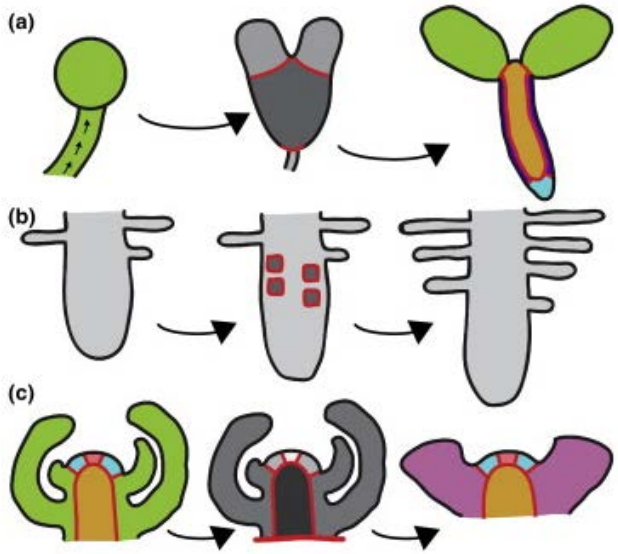

Figure 1.4. PD transport decreases to facilitate plant morphogenesis by isolating differentiating cells. (a) PD transport is unrestricted in young, globular stage embryos (left, green), which receive resources from the rest of the developing seed by a suspensor (green stalk). As the embryo develops, PD transport becomes restricted (red lines), especially at the boundaries of developing organs (middle). Eventually, several domains are established (right: cotyledons (embryonic leaves), green; shoot-root axis, gold; epidermis, purple; root cap, light blue). Molecules freely transport within each domain, but PD transport is limited between the domains (red lines). (b) As the root grows, the progenitor cells of new lateral roots become temporarily isolated (middle, dark gray regions surrounded by red lines) while they initiate organogenesis. PD transport to the developing lateral roots is later restored (right). (c) The vegetative shoot apex, shown here in longitudinal section, is also divided into several domains (indicated by red lines where PD transport is restricted). Stem cells (pink) are isolated from differentiating cells (blue), leaf primordia (green), and the underlying central zone (gold). During the transition from vegetative to reproductive growth, the apex is temporarily isolated from the rest of the plant (middle, gray; red line at base of apex indicates restricted PD transport), but transport into the apex is restored once the inflorescence meristem is established (right; floral primordia, mauve).

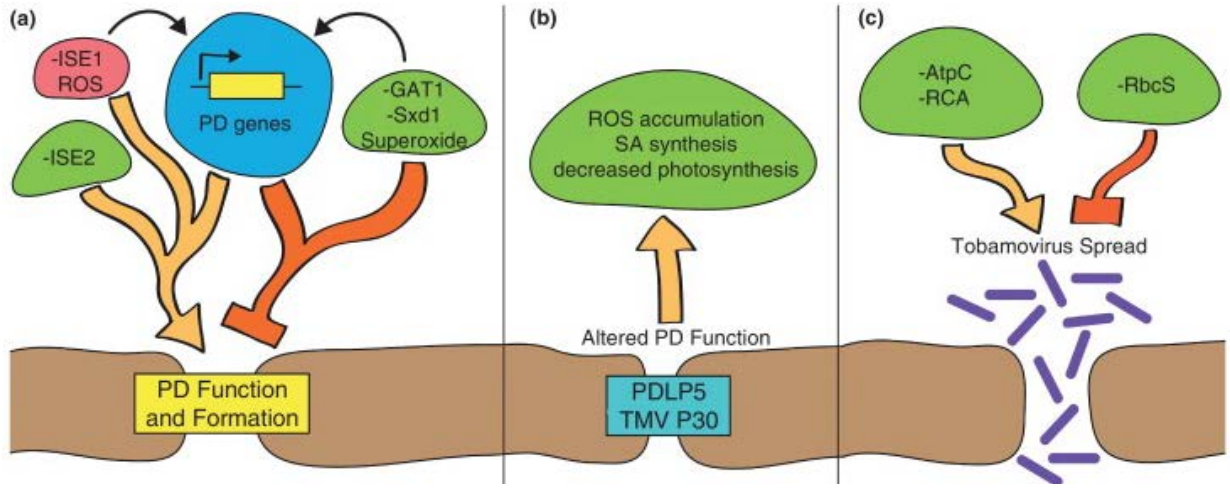

Figure 1.5. (a) Plasmodesmata function and formation are coordinated by changes in chloroplast (green) and mitochondrial (red) function. These changes alter expression of nuclear genes (blue) through organelle retrograde signaling pathways (black arrows). Loss of organelle RNA helicases (ISE1 or ISE2) causes dramatic changes in nuclear gene expression and increases PD transport and biogenesis. ROS produced specifically in the mitochondria also positively regulates PD function. On the other hand, superoxide formation in the chloroplast or loss of either GAT1 or Sxd1 [56 and 57] (which also leads to oxidation of the chloroplast redox state) negatively regulate PD function. (b) PD function regulates chloroplast physiology: PDLP5 or P30 expression cause increased ROS formation, SA biosynthesis, and decreased photosynthesis. (c) Various chloroplast proteins also impact tobamoviral spread, possibly through effects on PD function.

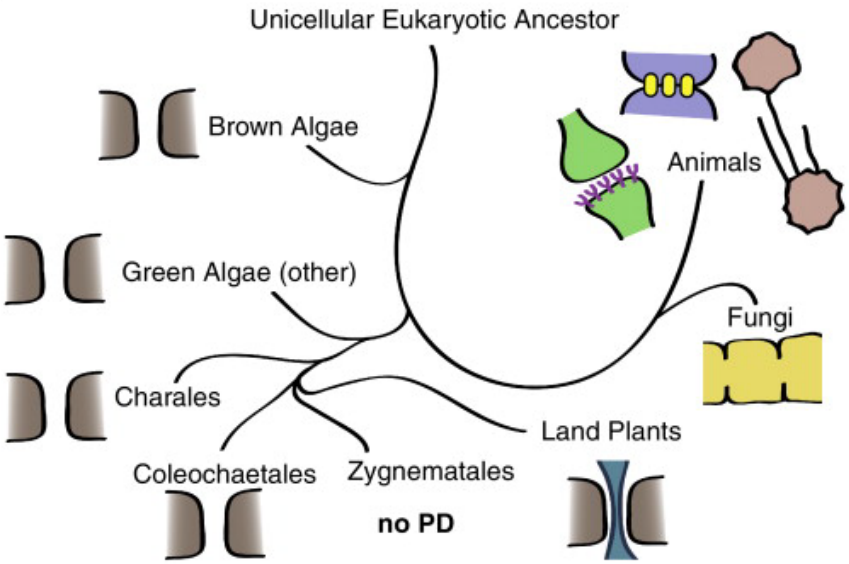

Figure 1.6. Evolution of multicellularity and adaptations that facilitate intercellular transport and signaling. PD evolved independently in several lineages of brown algae and green algae (depicted as cellulosic cell walls, brown, with cytosolic channels, white). Land plant PD contain a tightly compressed strand of ER called the 'desmotubule' (shown in blue). Some closely related algae may have 'PD' (some Charales and Coleochaetales), although these PD lack the desmotubule. Other close relatives of land plants never have PD (Zygnematales). Filamentous fungi form septal pores that allow cytoplasm to move between cells (cytoplasm, yellow; chitinous cell wall, black lines). Animal cells use a variety of mechanisms for cell–cell signaling, including signal exchange at the cellular surface (as in a chemical synapse, depicted in green; receptors in purple), gap junctions (as in an electrical synapse, depicted in blue; gap junction proteins in yellow), and cytonemes (cells in pink, cytonemes black extensions from the plasma membrane).

Chapter Two: Chloroplasts extend stromules independently and in response to internal redox signals

This following chapter is a modified version of an article published in *Proceedings of the National Academy of Science USA* (Brunkard et al., 2015b).

Abstract: A fundamental mystery of plant cell biology is the occurrence of “stromules”, stroma-filled tubular extensions from plastids (such as chloroplasts) that are universally observed in plants but whose functions are, in effect, completely unknown. One of the most prevalent hypotheses is that stromules exchange signals or metabolites between plastids and other subcellular compartments and that stromules are induced during stress. Until now, however, no signaling mechanisms originating within the plastid have been identified that regulate stromule activity, a critical missing link in this hypothesis. Using confocal and superresolution three-dimensional microscopy, we show that stromules form in response to light-sensitive redox signals within the chloroplast. Stromule frequency increased during the day or after treatment with chemicals that produce reactive oxygen species specifically in the chloroplast. Silencing expression of the chloroplast NADPH-thioredoxin reductase (*NTRC*), a central hub in chloroplast redox signaling pathways, increased chloroplast stromule frequency, while silencing expression of nuclear genes related to plastid genome expression and tetrapyrrole biosynthesis had no impact on stromules. Leucoplasts, which are not photosynthetic, also make more stromules in the day. Leucoplasts do not respond to the same redox signaling pathway, but instead increase stromule formation when exposed to sucrose, a major product of photosynthesis, although sucrose had no impact on chloroplast stromule frequency. Thus, different types of plastids make stromules in response to distinct signals. Finally, isolated chloroplasts can make stromules independently after extraction from the cytoplasm, suggesting that chloroplast-associated factors are sufficient to generate stromules. These discoveries demonstrate that chloroplasts are remarkably autonomous organelles that alter their stromule frequency in reaction to internal signal transduction pathways.

INTRODUCTION

Chloroplasts, the descendants of ancient bacterial endosymbionts, exert impressive influence over processes that are not directly related to their metabolic roles. In recent years, forward genetic screens have led to the discoveries that chloroplasts are critical regulators of leaf shape, cell-cell signaling through plasmodesmata, pathogen defense, and even alternative splicing in the nucleus (Avendaño-Vázquez et al., 2014; Burch-Smith et al., 2011b; Estavillo et al., 2011; Koussevitzky et al., 2007; Nomura et al., 2012; Petrillo et al., 2014; Stonebloom et al., 2012; Xiao et al., 2012). In almost all of these pathways, however, the signaling route between the chloroplast and the nucleus is unknown. This is a pressing question for plant biology and cell biology in general: how do organelles communicate with the nucleus to coordinate genetic programs and cellular function? One possible route for this communication is stromules, which are stroma-filled tubular extensions of unknown function from plastids (Hanson and Sattarzadeh, 2011; Köhler et al., 1997; Schattat et al., 2012a).

Stromules were first observed in spinach cells (Wildman et al., 1962), and have since been observed in every cell type and land plant species investigated to date (Natesan et al., 2005). Several studies have identified conditions that can induce or decrease stromule formation (Erickson et al., 2014; Gray et al., 2012; Holzinger et al., 2007; Natesan et al., 2009; Schattat and Klösgen, 2011), concluding that stromule frequency can change in response to abiotic stress, phytohormone signaling, and massive disruption of cellular function (such as strong inhibition of cytosolic translation or of actin microfilament dynamics). Almost nothing is known about the genetics of stromules; some mutants with strong morphological defects in plastids, such as mutants with improper plastid division or lacking plastid mechanosensitive channels, cannot form stromules at normal frequencies, but these plastids are so severely misshapen that their stromule frequencies cannot be directly compared to wild-type plastids (Holzinger et al., 2008; Veley et al., 2012). Few experiments have tested whether signals inside plastids can affect stromule frequency, and to date, these experiments (for example, treatment with antibiotics that interfere with plastid genome expression(Gray et al., 2012)) have all suggested that stromule frequency is not regulated by internal plastid biology. Here, we test whether light-sensitive redox signaling pathways initiated within chloroplasts regulate stromule activity.

RESULTS AND DISCUSSION

Chloroplasts make more stromules during the day

We began our study by conducting a time course to determine the effects of light on chloroplast stromule formation. For all *in planta* experiments (except where noted otherwise), we observed stromules in the proximal abaxial epidermis of cotyledons of young *Nicotiana benthamiana* or *Arabidopsis thaliana* plants, or in the proximal abaxial epidermis of young leaves two weeks after silencing gene expression with virus-induced gene silencing (VIGS). We collected a single *z*-stack of confocal images of only one leaf of each plant, and considered plants as independent samples (the number of plants observed for each treatment for an experiment is listed throughout as *n*). Thus, each experiment considers the stromule frequency determined from hundreds, thousands, or even tens of thousands of plastids.

Over the course of two days, we measured stromule frequency in cotyedons from young *N. benthamiana* seedlings every four hours, and found significantly more stromules during the day than during the night (Figure 2.1, S2.6). In the day, 20.8% ± 1.8% of chloroplasts had stromules, but only 12.8% ± 0.9% of chloroplasts had stromules at night ($n \geq 22$, $p < 0.0005$; throughout, stromule frequencies are reported as percentages ± standard errors). There was no significant difference in stromule frequency between the first and second day or between the first and second night, indicating that the observed changes were reactions to the changing light environment rather than a progressive developmental change over 48 hours. Past studies investigating the relationship between chloroplast stromule frequency and light reported that light decreases stromule frequency in seedling hypocotyls during de-etiolation after skotomorphogenesis, and that constant darkness or only blue light increase stromule frequency after photomorphogenesis (Gray et al., 2012). The apparent discrepancy between these conclusions and our results showing that light promotes chloroplast

stromule formation is explained by the different plastid types used in the de-etiolation experiment (etioplasts transitioning to become chloroplasts) and the dramatic developmental and physiological transitions used in both experiments (constant darkness to constant light, or vice-versa) that are not reflective of typical chloroplast stromule behavior in normal, healthy plants. We conclude that light promotes chloroplast stromule formation during the day.

ROS inside chloroplasts promote stromule formation

Plants sense light with the pigments of the photosynthetic electron transport chain (pETC) in the chloroplast or with photoreceptors elsewhere in the cell (Hughes, 2013). We tested whether stromule frequency responds specifically to light sensed by the chloroplast itself by chemically inhibiting pETC activity. We used two pETC inhibitors: DCMU (3-(3,4-dichlorophenyl)-1,1-dimethylurea) and DBMIB (2,5-dibromo-6-isopropyl-3-methyl-1,4-benzoquinone). DCMU prevents reduction of plastoquinone (PQ) at photosystem II and generates singlet oxygen, whereas DBMIB prevents plastoquinols (PQH_2) from reducing the cytochrome b_6f complex and generates superoxide (Petrillo et al., 2014). We measured the effects of DCMU and DBMIB on the chloroplast stromal redox status as monitored by a stromal redox-sensitive transgenic GFP biosensor, pt-roGFP2 (Stonebloom et al., 2012), to find very low active concentrations of each compound with our treatment technique, and found that 10 µM DCMU or 12 µM DBMIB are sufficient to strongly oxidize redox buffers in the chloroplast stroma, with the normalized proportion of oxidized pt-roGFP2 rising from 20.0% ± 3.5% in control conditions to 68.9% ± 3.0% after 10 µM DCMU treatment or 41.5% ± 7.1% after 12 µM DBMIB treatment ($n \geq 28$, $p < 0.01$) (Figure S2.7).

We assessed the stromule frequency two hours after treating *N. benthamiana* cotyledons with either of the photosynthesis inhibitors (Figure 2.2A–C, S2.7A–C). In the epidermal chloroplasts of mock treated cotyledons, the average chloroplast stromule frequency was 9.2% ± 1.4%. After treatment with DCMU or DBMIB, stromule frequency increased by more than half, to 15.5% ± 2.6% with DCMU or 16.8% ± 2.9% with DBMIB ($n \geq 20$, $p < 0.05$). This suggests that stromule formation responds to light-sensitive redox signals inside the chloroplast, the first demonstration that internal chloroplast pathways may regulate stromules.

Unlike *N. benthamiana*, the epidermis of *A. thaliana* has two distinct types of plastids: chloroplasts in the guard cells and leucoplasts in the pavement cells (Figure S2.8). Leucoplasts are not photosynthetic, but like chloroplasts, they have many other roles in metabolism and storage. As in *N. benthamiana* epidermal chloroplasts, DCMU and DBMIB promote stromule formation in guard cell chloroplasts of *A. thaliana* cotyledons, raising the stromule frequency from 15.7% ± 3.8% to 28.1% ± 4.0% (DCMU, $n \geq 16$, $p < 0.05$) and 48.1% ± 6.3% (DBMIB, $n \geq 10$, $p < 0.0005$) (Figure 2.2D). This demonstrates that the induction of chloroplast stromules by DCMU and DBMIB is conserved in evolutionarily divergent plants (*N. benthamiana* is an asterid and *A. thaliana* is a rosid, with the last common ancestor of the two species living over 100 million years ago (Bell et al., 2010)). Leucoplasts in the epidermis of *A. thaliana*, on the other hand, were unaffected by DCMU and DBMIB treatment (14.6% ± 3.4% in control conditions versus 14.6% ± 2.8% with DCMU, $n \geq 16$, $p = 0.98$, and 13.5% ± 4.3% with DBMIB, $n \geq 10$, $p = 0.84$), showing that the effects of DCMU and DBMIB are specific

responses to their roles interfering with the pETC (Figure 2.2E). To further test whether stromules form in response to the chloroplast redox status specifically, as opposed to any oxidative stress in the cell, we also treated *A. thaliana* cotyledons with SHAM. SHAM inhibits the mitochondrial alternative oxidase, which leads to rapid and strong oxidation of mitochondrial redox buffers (Stonebloom et al., 2012). SHAM did not impact chloroplast stromule formation in *A. thaliana* (15.7% ± 3.8% in control versus 12.8% ± 3.3% with SHAM, $n \geq 13$, $p = 0.57$), supporting the hypothesis that chloroplast stromule frequency is specifically regulated by the redox status of the chloroplast (Figure 2.2F, S2.9).

In summary, low concentrations of DCMU or DBMIB are sufficient to induce significant increases in stromule frequency within only two hours. This is apparently not a secondary effect of broad disruption of cellular metabolism or redox homeostasis, since leucoplasts, which are not photosynthetic, are unaffected by the treatments, and disrupting mitochondrial function and generating ROS in mitochondria by SHAM treatment does not affect chloroplast stromule frequency. Thus, light-sensitive redox cues inside chloroplasts specifically affect stromule frequency.

NADPH-dependent thioredoxin c regulates chloroplast stromule frequency

Signaling from chloroplasts to other organelles within the plant cell is critical for plant survival and development (Chi et al., 2013; Woodson and Chory, 2008). Chloroplast-to-nucleus signaling is transduced through several pathways, some of which are light sensitive. We used VIGS in *N. benthamiana* as a reverse genetic approach (Brunkard et al., 2015c) to determine whether disrupting the light-sensitive chloroplast-to-nucleus signal transduction pathways impacts stromule formation. VIGS strongly reduces gene expression in young leaves within one to two weeks of infection by generating small RNAs that specifically target a gene for post-transcriptional silencing (Brunkard et al., 2015c).

Chloroplasts contain their own genomes encoding about 80 proteins (mostly related to photosynthesis or transcription and translation), and light exerts control over plastid genome expression (PGE) at transcriptional and post-transcriptional levels (Barkan, 2011). Thus, we first focused on NbISE2, an essential plastid RNA helicase required for healthy chloroplast biogenesis and PGE (Burch-Smith et al., 2011b). Without *ISE2*, hundreds of nuclear genes involved in photosynthesis are strongly downregulated (Burch-Smith et al., 2011b). Silencing *NbISE2* gene expression had no impact on stromule frequency, however (6.8% ± 1.0% in controls versus 6.6% ± 0.9% after silencing *NbISE2*, $n = 8$, $p = 0.85$) (Figure 2.2J, S2.10), which agrees with past reports that antibiotics directly interfering with PGE, such as lincomycin, have no effect on stromule frequency (Gray et al., 2012).

PGE coordinates the expression of photosynthesis-associated nuclear genes through a signal transduction pathway mediated by tetrapyrrole metabolism (Chi et al., 2013; Terry and Smith, 2013; Woodson and Chory, 2008). Genetic disruptions to tetrapyrrole metabolism, specifically defects in the branch point between heme and chlorophyll biosynthesis, interfere with chloroplast biogenesis and photosynthesis (Terry and Smith, 2013). We next tested whether loss of NbGUN2, a chloroplast heme oxygenase that participates in chloroplast-to-nucleus communication, impacts stromule formation. As with *NbISE2*, silencing *NbGUN2* gene expression had no impact on

chloroplast stromule frequency (7.2% ± 1.3% after silencing *NbGUN2*, $n = 8$, $p = 0.82$) despite causing clear physiological stress and chlorosis (Figure 2.2J, S2.10–S2.12).

We then silenced the expression of the chloroplast NADPH-dependent thioredoxin reductase (*NbNTRC*) (Figure S2.13, S2.14), which regulates the redox status and activity of myriad chloroplast proteins and is a critical hub in chloroplast redox signal transduction (Michalska et al., 2009). Silencing *NbNTRC* more than doubles stromule frequency (13.7% ± 1.7%, $n = 8$, $p < 0.01$), providing genetic evidence that redox signaling within the chloroplast regulates stromule formation (Figure 2.2J–L, S2.10, S2.13, S2.14). Moreover, *NbNTRC* is now the first gene identified that regulates stromule frequency without other apparent effects on chloroplast shape.

Sucrose promotes stromule formation in epidermal leucoplasts, but not in chloroplasts

Schattat *et al.* reported that stromule frequency increases during the day in the epidermal leucoplasts of *A. thaliana* (Schattat et al., 2012b). Since leucoplasts do not contain pigments and do not respond to DCMU or DBMIB, we sought another hypothesis to explain why leucoplast stromule frequency is light responsive. Physiologically, one of the major impacts of light on epidermal pavement cells is an increase in sucrose imported from underlying cells that contain photosynthesizing chloroplasts. Previous reports had indicated that stromule frequency is sensitive to sugar levels, but with inconsistent conclusions (Schattat et al., 2011). We found that epidermal leucoplast stromule frequency rises remarkably following sucrose treatments in *A. thaliana* (33.9% ± 3.8% with sucrose versus 11.8% ± 3.9% without sucrose, $n \geq 8$, $p < 0.001$) (Figure 2.2H, S2.15). Chloroplast stromule frequency, on the other hand, did not respond to sucrose treatments in either the epidermal guard cells or mesophyll of *A. thaliana* (in the epidermis, 15.4% ± 3.9% with sucrose versus 15.7% ± 3.8% without, $n \geq 8$, $p = 0.96$; in the mesophyll, 5.0% ± 0.9% with sucrose, 6.3% ± 1.7% without sucrose, $n \geq 8$, $p = 0.52$) (Figure 2.2G, 2.2I, S2.15). These results imply that different plastid types employ separate signaling pathways to induce stromule formation.

Isolated chloroplasts can form stromules

With the finding that signals originating within the chloroplast can trigger stromule formation, we then explored whether stromule formation is dependent on cytosolic structures (e.g., the cytoskeleton) as has been previously suggested (Hanson and Sattarzadeh, 2011; Natesan et al., 2009), or if chloroplasts can make stromules on their own. Past studies have argued that stromule formation is guided and supported by the cytoskeleton and endoplasmic reticulum, but it is unknown whether stromules require these external factors to form (Hanson and Sattarzadeh, 2011; Schattat et al., 2011). To address this question, we extracted chloroplasts from leaves of *N. benthamiana*, *A. thaliana*, and *Spinacia oleracea* using well-established methods for isolating functional, undamaged chloroplasts (Joly and Carpentier, 2011). We visualized chloroplast stroma either with GFP by extracting chloroplasts from leaves expressing plastid-targeted GFP or with a supravital stain, carboxyfluorescein diacetate (CFDA), which only fluoresces after hydrolysis by carboxylesterases in the chloroplast stroma (Schulz et al., 2004). We easily found isolated chloroplasts with intact stromules in all three species and regardless of staining technique (Figure 2.3, S2.16). The stromules were dynamic and could grow very long, sometimes extending more than 150 μm from chloroplasts only 4

to 6 μm in diameter (Figure S2.16). As in plant cells, stromules were often bent and curved along their lengths, while some stromules were instead very long and straight (Figure 2.3, S2.16). Using time-lapse microscopy, we repeatedly observed isolated chloroplasts form apparently new stromules, validation that chloroplasts can generate stromules independently; stromules are absent in the first frames of chloroplasts visualized in Figure 2.3D, 2.3E, but they appear and lengthen over the course of 8 minutes (see also Movies S1 and S2).

Superresolution microscopy illuminates stromule ultrastructure

Since stromules can form in isolation after extracting chloroplasts from their cellular context, we decided to further investigate stromules using superresolution microscopy to gain new insight into their ultrastructure, which will inform future efforts to discover the chloroplast-associated structural components responsible for stromule formation. The diameter of stromules is postulated to be less than 200 nm, but this size is below the diffraction limit of conventional light microscopy (Schattat et al., 2012b), even under optimal conditions. Stromules are challenging to visualize by transmission electron microscopy, since stromule membranes are not easily distinguished from other membranes in thin sections required for conventional electron microscopy. We used three-dimensional structured illumination microscopy (3D-SIM) to obtain the highest resolution images of wild-type stromules to date, and show some representative examples here (Figure 2.4, Movie S3) (Schulz et al., 2004). The improved resolution of 3D-SIM is illustrated by the well-defined thylakoid grana in 3D-SIM images (Figure 2.4B–E) compared to thylakoids visualized by more conventional confocal scanning laser microscopy (Figure 2.4A).

At their smallest, we observed stromules less than 150 nm in diameter (Figure 2.4E), and since this is approximately the resolution of 3D-SIM, stromules could be even narrower. 3D-SIM also revealed striking variability in stromule diameter along the length of an individual stromule. Stromules often were narrowest near the chloroplast body, and then typically varied between about 200 nm to about 600 nm wide at different positions along their lengths, as shown in an example here (Figure 2.4E). The variability in stromule width was apparent whether we observed chloroplasts *in planta* or after isolation, suggesting that structural factors inside the chloroplast could be responsible for the heterogeneous diameter of stromules.

CONCLUSIONS

Chloroplasts are extraordinarily independent organelles, with their own genomes, as many as three thousand different proteins, and an array of biochemical activities ranging from photosynthesis and carbon fixation to the synthesis of amino acids, fatty acids, hormones, and pigments. Here, we have shown that chloroplasts are even more independent, generating stromules in response to changes in the internal chloroplast redox status in a pathway regulated by the chloroplast NADPH-dependent thioredoxin reductase NTRC. Leucoplasts, non-photosynthetic plastids, do not make stromules in response to the same redox cues as chloroplasts, but are instead responsive to sucrose concentrations, demonstrating that different types of plastids form stromules in response to different signals. We propose a model consistent with these findings that light promotes stromule formation in leaves by increasing ROS in chloroplasts (Lai et

al., 2012) and by increasing sucrose levels in cells with leucoplasts (Figure 2.5). Previous reports have investigated stromules using a variety of plastid types in a broad range of species and tissues, generally assuming that stromules act similarly in all cells (Erickson et al., 2014; Gray et al., 2012; Hanson and Sattarzadeh, 2011; Holzinger et al., 2007, 2008; Köhler et al., 1997; Natesan et al., 2005, 2009; Schattat and Klösgen, 2011; Schattat et al., 2012a; Wildman et al., 1962). In light of the clear differences in signals that influence leucoplast and chloroplast stromule formation (Figure 2.2, 2.5), future work will need to carefully consider the biological context of stromule activity. With the discovery that stromules extend from chloroplasts independently of external structures, analogies to cytonemes could help reveal the roles of stromules, since cytonemes are comparable thin, tubular projections that extend from animal cells to facilitate intercellular communication during development (Bischoff et al., 2013; Roy et al., 2014). While the function of stromules remains unknown, it is worth speculating that they similarly facilitate signal transduction between organelles, since stromules have been observed associating with the nucleus, plasma membrane, endoplasmic reticulum, and other plastids (Hanson and Sattarzadeh, 2011; Schattat et al., 2011, 2012a).

Numerous studies in just the past few years have demonstrated the vital importance of chloroplast-to-nucleus signaling in plant growth and responses to stress (Avendaño-Vázquez et al., 2014; Burch-Smith et al., 2011b; Chi et al., 2013; Estavillo et al., 2011; Koussevitzky et al., 2007; Nomura et al., 2012; Petrillo et al., 2014; Stonebloom et al., 2012; Terry and Smith, 2013; Woodson and Chory, 2008; Xiao et al., 2012), with critical agricultural implications, but the structural pathways underlying this signal transduction remain largely uncharacterized. Stromules may contribute to these pathways, since they dynamically respond to physiological signals inside the chloroplast, and continued study of stromules may illuminate how chloroplasts physically interact with their environment to coordinate cellular function.

Acknowledgments: J.O.B. and A.M.R. were supported by pre-doctoral fellowships from the National Science Foundation. We thank J. Mathur for the generous gift of pt-GFP *N. benthamiana* seeds. We also acknowledge M.A. Ahern for corroborating stromule counts and S.E. Ruzin and D. Schichnes for microscopy support.

METHODS

Plant and chemical materials

For most *Nicotiana benthamiana* studies, we used a stable transgenic stromal fluorescent marker line, *35S$_{PRO}$:FNRtp:EGFP*, elsewhere called “pt-GFP” (Schattat et al., 2011). We also used the *N. benthamiana* wild-type accession Nb-1 for isolation of wild-type chloroplasts. For *Arabidopsis thaliana* studies, we used a stable transgenic stromal fluorescent marker line (Stonebloom et al., 2012), *35S$_{PRO}$:RbcStp:roGFP2*, elsewhere called “pt-roGFP2”. pt-roGFP2 was also used for measuring stromal redox status.

We obtained DCMU (3-(3,4-dichlorophenyl)-1,1-dimethylurea, also known as Diuron, product number D2425), DBMIB (2,5-dibromo-6-isopropyl-3-methyl-1,4-benzoquinone, product number 271993), and SHAM (salicylhydroxamic acid, product number S607) from Sigma-Aldrich. Concentrated stock solutions were prepared in DMSO (dimethyl sulfoxide).

Microscopy

For all standard stromule visualization experiments, we used a Zeiss LSM 710 confocal microscope equipped with an acousto-optical tunable filter to tightly control laser power. GFP was excited with a 488 nm laser with less than 0.25mW original power and emissions from 500 nm to 530 nm were detected.

For three-dimensional structured illumination microscopy, we used a Zeiss Elyra PS.1 microscope equipped with standard GFP and Cy5 filter sets.

Diurnal time course experiment

N. benthamiana stably expressing pt-GFP were grown for 5 days under 100 µmol of photons $m^{-2}s^{-1}$ (measured with a LI-COR 250A light meter with a LI-190R quantum sensor that detects photosynthetically active radiation, 400nm to 700nm) with 12 hour day length. Epidermal chloroplasts of cotyledons of intact plants were observed every 4 hours over the course of 48 hours. A green light-emitting diode was used during night time-points to prevent exposure to photosynthetically active radiation.

pETC inhibitor treatments

The redox status of pt-roGFP2 in *A. thaliana* cotyledons (grown as for pETC inhibitor treatments) was measured following treatment with 10 µM DCMU, 12 µM DBMIB, or 0.1% DMSO (mock treatment), following the same protocol as in Stonebloom *et al.* but using a Zeiss LSM 710 confocal microscope with 405 nm and 488 nm lasers, collecting emissions ranging from 500 nm to 530 nm (Stonebloom et al., 2012).

N. benthamiana stably expressing pt-GFP were grown for 14 days under 100 µmol of photons $m^{-2}s^{-1}$ of light with 16 hour day length. Cotyledons were painted with DCMU (10 µM from 10 mM stock solution in DMSO), DBMIB (12 µM from 12 mM stock solution in DMSO), or control (0.1% DMSO) two hours prior to observing epidermal chloroplasts.

A. thaliana pt-roGFP2 plants were stratified for 3 days at 4°C and then grown for 14 days under 100 µmol of photons $m^{-2}s^{-1}$ of light with 16 hour day length. Cotyledons

were removed and placed on 0.5x Murashige and Skoog plates (0.8% agar, pH 5.6) with DCMU (10 μM from 10 mM stock solution in DMSO), DBMIB (12 μM from 12 mM stock solution in DMSO), SHAM (200 μM in DMSO), sucrose (30 mM, or 1% w/v), or control (0.1% DMSO) two hours prior to imaging cotyledon epidermal leucoplasts (of pavement cells) and chloroplasts (of guard cells).

Virus-induced gene silencing

pt-GFP plants were grown for 3 weeks under 100 μmol of photons $m^{-2}s^{-1}$ of light with 16 hour day length before agroinfiltrating with the appropriate VIGS vectors (for details on VIGS vector construction, see following paragraph). Two weeks later, young leaves with silenced gene expression were cut and the epidermal chloroplasts of the basal region of the leaf were visualized immediately.

GUN2 (TAIR ID At2g26670) and *NTRC* (TAIR ID At2g41680) orthologues in *N. benthamiana* were identified from gene trees generated by BLAST searches using *A. thaliana* protein sequence queries (Figure S2.11, S2.13). *N. benthamiana* is an allotetraploid resulting from the hybridization of two *Nicotiana* species, and therefore often has two homeologues of genes that are single-copy in *A. thaliana*. Moreover, both *GUN2* and *NTRC* are members of larger gene families: in *A. thaliana*, there are three NADPH-dependent thioredoxin reductases (NTRA and NTRB are in the cytosol and mitochondria, while NTRC is in plastids) and four heme oxygenases (HO1, HO3, and HO4 are closely related and partially redundant, while HO2 serves a distinct function) (Gisk et al., 2010; Reichheld et al., 2007). To identify all true orthologues of *GUN2* and *HO1* and design silencing constructs targeting these genes, but not orthologues of *NTRA/NTRB* or *HO2*, *A. thaliana* protein sequences were used in a BLAST search against the *N. benthamiana* genome (v0.4.4 predicted cDNAs) from the Sol Genomics Network (http://solgenomicsl.net) and also against the land plant genomes available at Phytozome (http://www.phytozome.net). Amino acid sequences of these putative homologues were aligned with MAFFT (http://mafft.cbrc.jp) using the highly accurate L-INS-i algorithm. Aligned residues were used to generate a gene tree with the Neighbor-Joining method using 100 samples for bootstrapping. Silencing triggers were then designed to silence all copies of the target genes but no other genes in the *N. benthamiana* genome, using BLAST searches to confirm that no genomic sequence between 20 and 24 nucleotides long matched the silencing trigger with less than 3 mismatches.

NbISE2, *NbGUN2*, and *NbNTRC* were silenced using virus-induced gene silencing (VIGS) as described by Brunkard *et al.* alongside a viral negative control, pYC1 (*Tobacco rattle virus* with a mock silencing trigger against β-glucoronidase) (Brunkard et al., 2015c). Briefly, to prepare the silencing constructs, RNA was extracted from *N. benthamiana* genotype Nb-1 (Spectrum Plant Total RNA Kit, Sigma-Aldrich) and treated with DNase I (New England Biolabs). This RNA was used to synthesize cDNA with SuperScript III Reverse Transcriptase (Invitrogen) and oligo$(dT)_{20}$ primers. Silencing triggers were then amplified and inserted into the TRV-derived VIGS vector, pYL156, using standard restriction enzyme-based methods (Brunkard et al., 2015c).

Chloroplast extraction

Intact chloroplasts were extracted from mature leaves of pt-GFP (*N. benthamiana*), Nb-1 (wild-type *N. benthamiana*), pt-roGFP2 (*A. thaliana*), and spinach by grinding leaves in extraction buffer (50 mM Hepes NaOH, 330 mM sorbitol, 2 mM EDTA, 1 mM $MgCl_2$, 1 mM $MnCl_2$, pH 6.9), filtering the homogenate through several layers of cheesecloth, and then pelleting by centrifugation and resuspending in isolation buffer (50 mM Hepes NaOH, 330 mM sorbitol, 2 mM EDTA, 1 mM $MgCl_2$, 1 mM $MnCl_2$, 10 mM KCl, 1 mM NaCl, pH 7.6) as previously described (Joly and Carpentier, 2011). More complex protocols, such as inclusion of a Percoll gradient for purification (35% v/v), had no discernable effect on chloroplast stromule formation. Isolated spinach or wild-type *N. benthamiana* chloroplasts were incubated with an equal volume of 25 mg/L 5(6)-carboxyfluorescein diacetate (Sigma-Aldrich, product number 21879) for five minutes, centrifuged at 700 x *g* for another 60 seconds, and resuspended in isolation buffer (Schulz et al., 2004). Chloroplasts were immediately visualized by confocal or structured illumination microscopy after isolation.

Data analysis

Stromule frequencies were counted using ImageJ software (http://imagej.nih.gov/ij/) to scan through *z*-stacks of confocal images using a focal depth of one airy unit, which allowed us to visualize stromules extended in any axis from the plastid. Stromules were counted regardless of length but only if less than 1 μm in diameter, as described by Hanson and Sattarzadeh (Hanson and Sattarzadeh, 2011). Most past studies have reported stromule frequencies per cell, considering multiple cells from a single leaf as independent samples. Schattat and Klösgen, for example, found little variation in stromule frequencies within an individual leaf, but dramatic variation in stromule frequencies between different leaves (Schattat and Klösgen, 2011). This led them to treat separate fields of view within a single leaf as distinct samples, reducing the apparent variation and effectively increasing statistical power. We also found that stromule frequency varied very little among cells within a leaf, but varied notably among leaves of the same age and condition from different plants. Therefore, we considered one leaf per plant as an individual sample (*n*), and observed many plants for each experiment. Throughout an experiment, the leaves analyzed experienced the same growth conditions, and were observed when they were the same age and size.

We conducted power analysis ($\alpha=0.05$, $\beta=0.20$) on pilot studies under our growth conditions to determine the sufficient sample size to confidently assert whether or not a treatment caused changes in stromule frequency, and found an approximate minimal $n \geq 16$ for *N. benthamiana* time course and chemical treatment experiments, or $n \geq 8$ for all other experiments. Per treatment, we counted more than 5,000 plastids, at least 100 cells, and approximately 20 plants (for each chemical treatment) or 8 plants (for each silencing experiment). Mean stromule frequencies were compared with the Student's *t* test, with significance indicated when $p < 0.05$. We also analyzed all data using angular transformations to account for differences in variation in data sets with very high or low stromule frequencies, but the transformation had no impact on the statistical significance of our results, so we present the data as raw frequencies for the purpose of clear presentation. Standard errors are presented throughout to describe stromule frequencies. R (http://www.r-project.org) was used for all statistical analyses.

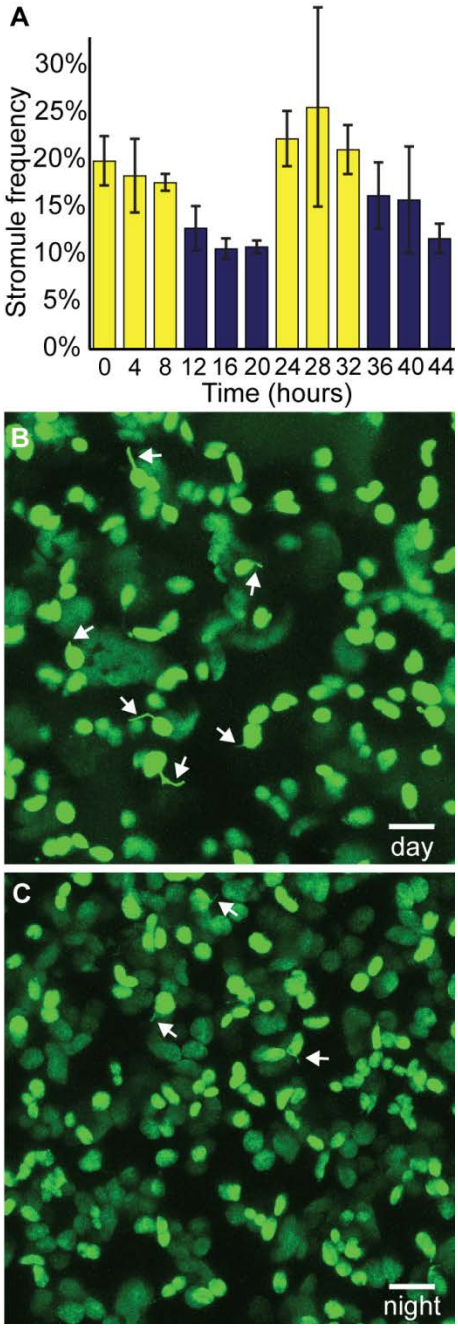

Figure 2.1. Chloroplast stromule frequency varies with diurnal cycles. (**A**)Stromule frequency rises in the day (yellow bars) and decreases at night (blue bars) in chloroplasts of *N. benthamiana* seedlings ($n \geq 22$, $p < 0.0005$). (**B,C**) Representative images of *N. benthamiana* epidermal chloroplasts labeled with stromal GFP (green) in the day (**B**) or at night (**C**). Some stromules are indicated by white arrows (as a visual aid, here and in other figures; not all stromules are indicated, and the indicated stromules were selected at random); scale bars, 10 μm; error bars, standard error of the mean (SE).

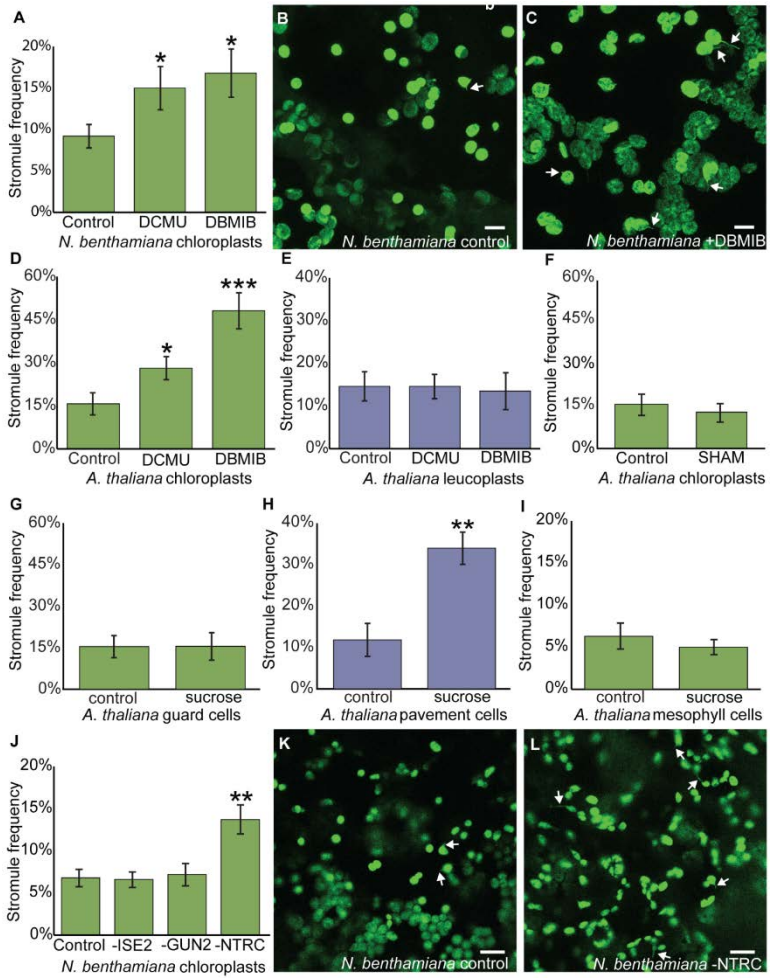

Figure 2.2. ROS in the chloroplast induce stromules. (**A**) DCMU and DBMIB treatments both increase stromule frequency in chloroplasts of *N. benthamiana* seedlings (n ≥ 20, p < 0.05). (**B,C**) Representative images of *N. benthamiana* chloroplasts treated with control (**B**) or with DBMIB (**C**). (**D**) *A. thaliana* epidermal chloroplast stromule frequency increases after DCMU or DBMIB treatment (DCMU, $n \geq 16$, $p < 0.05$; DBMIB, $n \geq 10$, $p < 0.0005$). (**E**) Stromule frequency in *A. thaliana* epidermal leucoplasts is unaffected by DCMU or DBMIB treatment (DCMU, n ≥ 16, p = 0.98; DBMIB, $n \geq 10$, $p = 0.84$). (**F**) *A. thaliana* epidermal chloroplast stromule frequency is unaffected by SHAM ($n \geq 13$, $p = 0.57$). (**G**) *A. thaliana* epidermal chloroplast frequency is similar in chloroplasts with or without sucrose treatment ($n \geq 8$, $p = 0.96$). (**H**) *A. thaliana* epidermal leucoplast stromule frequency increases after sucrose treatment ($n \geq 8$, $p < 0.01$). (**I**) Stromule frequency is not affected by sucrose treatment in *A. thaliana* mesophyll chloroplasts ($n \geq 8$, $p = 0.52$). (**J**) Silencing *NbNTRC* increases stromule frequency in *N. benthamiana* leaves ($n = 8$, $p < 0.01$) but silencing *NbISE2* or *NbGUN2* does not affect stromule frequency ($n = 8$, $p > 0.82$). (**K,L**) Representative images of *N. benthamiana* chloroplasts in control (**K**) or after silencing *NbNTRC* (**L**). Chloroplasts and stromules in are labeled with GFP. Some stromules are indicated by white arrows; scale bars, 10 μm; *$p < 0.05$, **$p < 0.01$, ***$p < 0.0005$; error bars, SE.

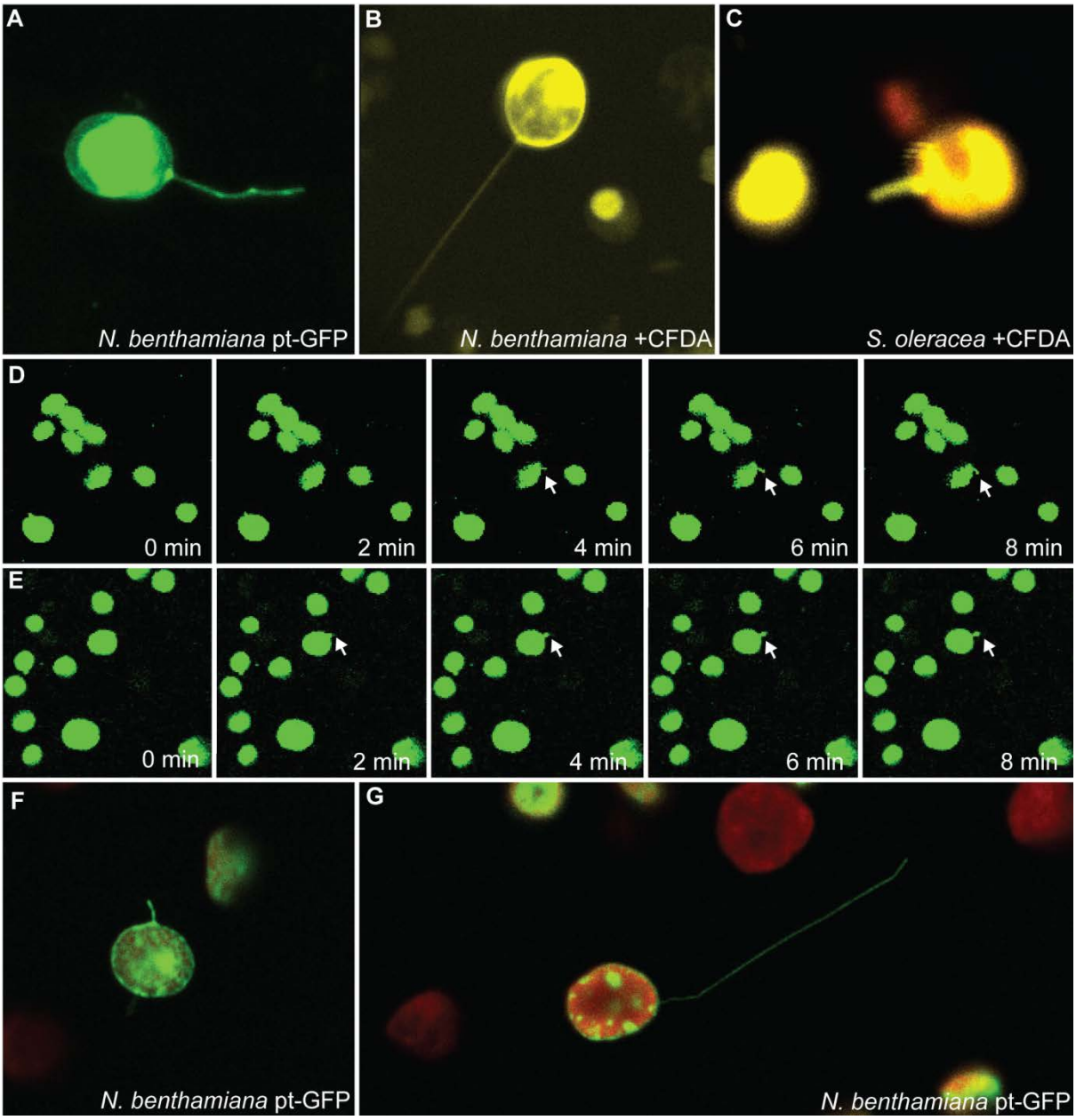

Figure 2.3. Isolated chloroplasts form stromules. *N. benthamiana* chloroplasts labeled with stromal GFP (**A**, green) or CFDA staining (**B**, yellow) show stromules after isolation from their cellular environment. (**C**) Chloroplasts isolated from *S. oleracea* and stained with CFDA (yellow; chlorophyll autofluorescence, red) also have stromules. (**D,E**) Isolated *N. benthamiana* chloroplasts labeled with stromal GFP form new stromules over time. Newly forming stromules are indicated by white arrows. (**F,G**) *N. benthamiana* chloroplasts isolated with a Percoll purification step and labeled with stromal GFP (green; chlorophyll autofluorescence, red) also have stromules.

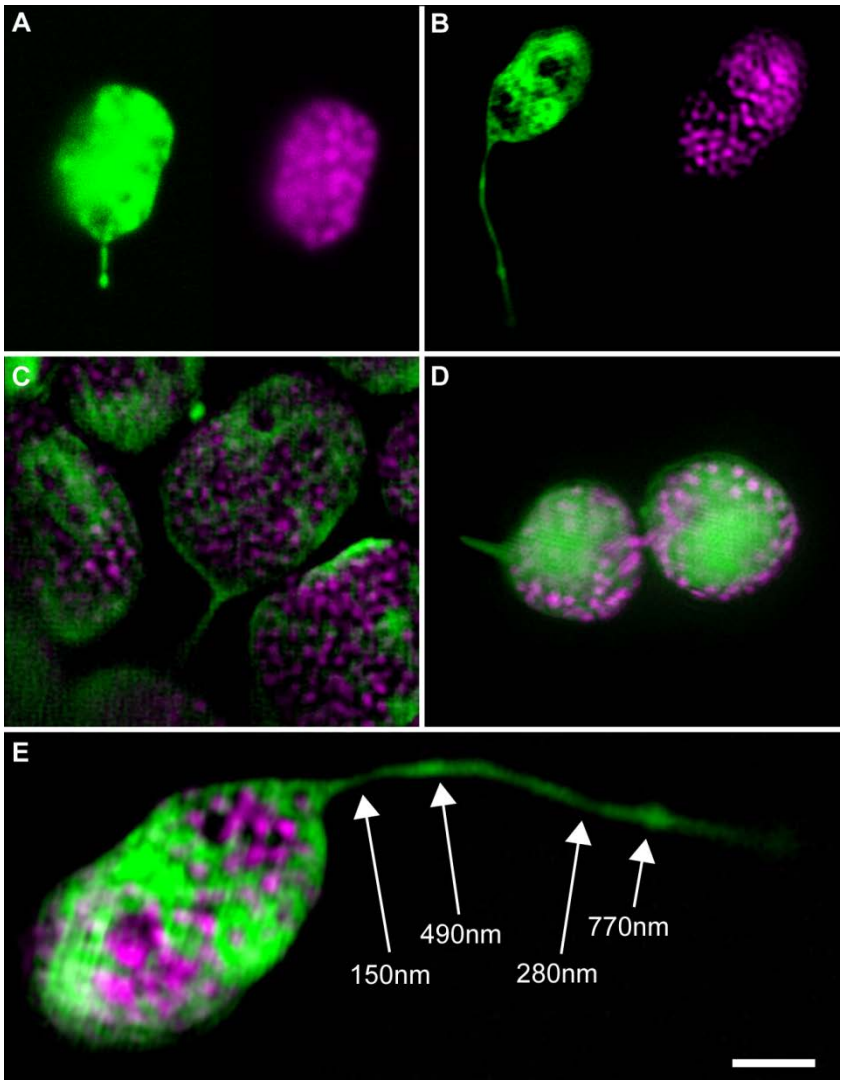

Figure 2.4. Examples of fluorescent stromules in *N. benthamiana* chloroplasts visualized by three-dimensional structured illumination microscopy (3D-SIM). (**A,B**) Comparison of confocal laser scanning microscopy (**A**, also shown in Figure S2.16) and 3D-SIM (**B**, also shown in Supplementary Video 3) to visualize chloroplast structure (stromal GFP, green, left; thylakoid chlorophyll, magenta, right). In particular, note the improved resolution of stromule width and the clarity of the thylakoid grana in the 3D-SIM *z*-slice (**B**). (**C**) 3D-SIM *z*-slice image of mesophyll chloroplasts with stromules. (**D**) An epidermal chloroplast connected by a thin bridge that contains both stroma and thylakoids also has a stromule (on left), as shown by SIM. (**E**) 3D-SIM reveals variability in stromule width (stromal GFP, green; chlorophyll autofluorescence, magenta; white scale bar, 2 μm). One *z*-slice from a 3D-SIM reconstruction is shown here, with measured stromule diameters labeled at indicated positions (white arrows).

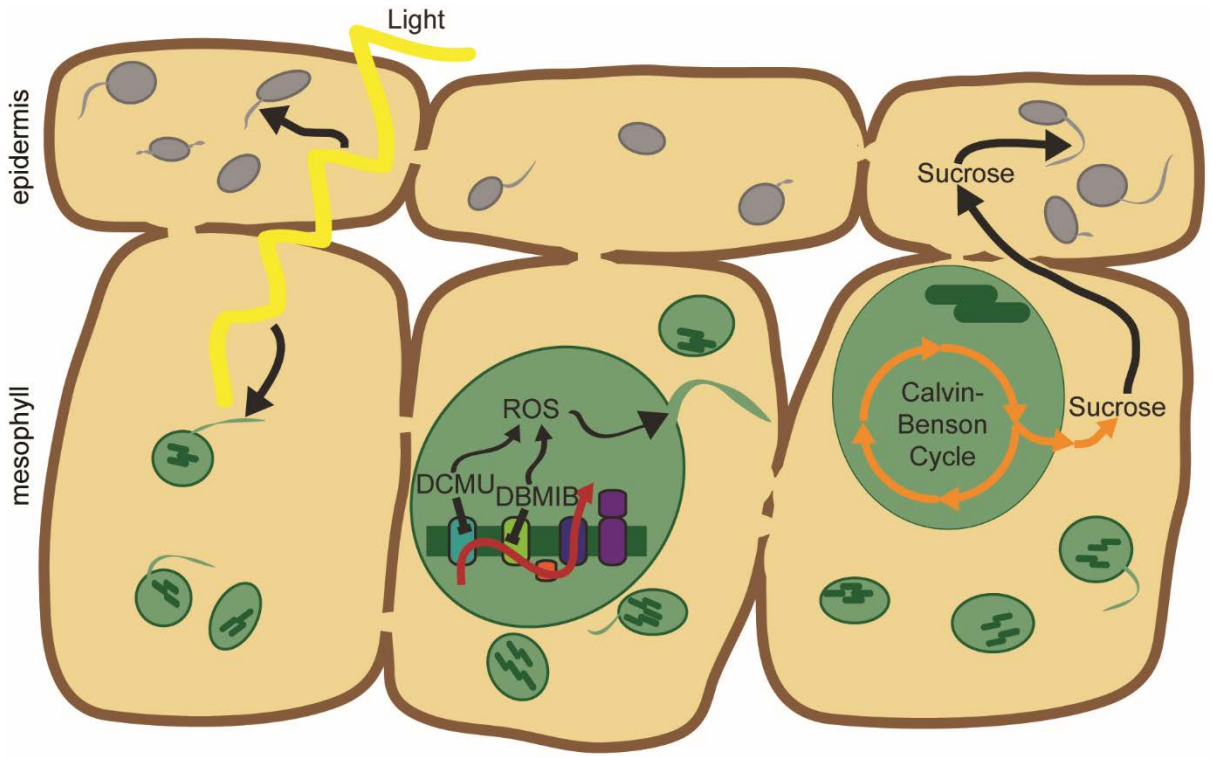

Figure 2.5. Stromules are initiated by signals within the chloroplast. Stromule frequency increases in the light (daytime) in both chloroplasts and leucoplasts (left). ROS generated from the pETC trigger stromule formation in chloroplasts (middle). Sucrose promotes stromule formation in leucoplasts, but not chloroplasts (right). Sucrose is synthesized in the cytosol from products of the Calvin-Benson cycle in chloroplasts and then moves into neighboring heterotrophic pavement cells via plasmodesmata. For simplicity of presentation, we only include photosynthetic mesophyll cells (and not photosynthetic guard cells) in this diagram, because there is no evidence to suggest that stromules in these cell types behave differently.

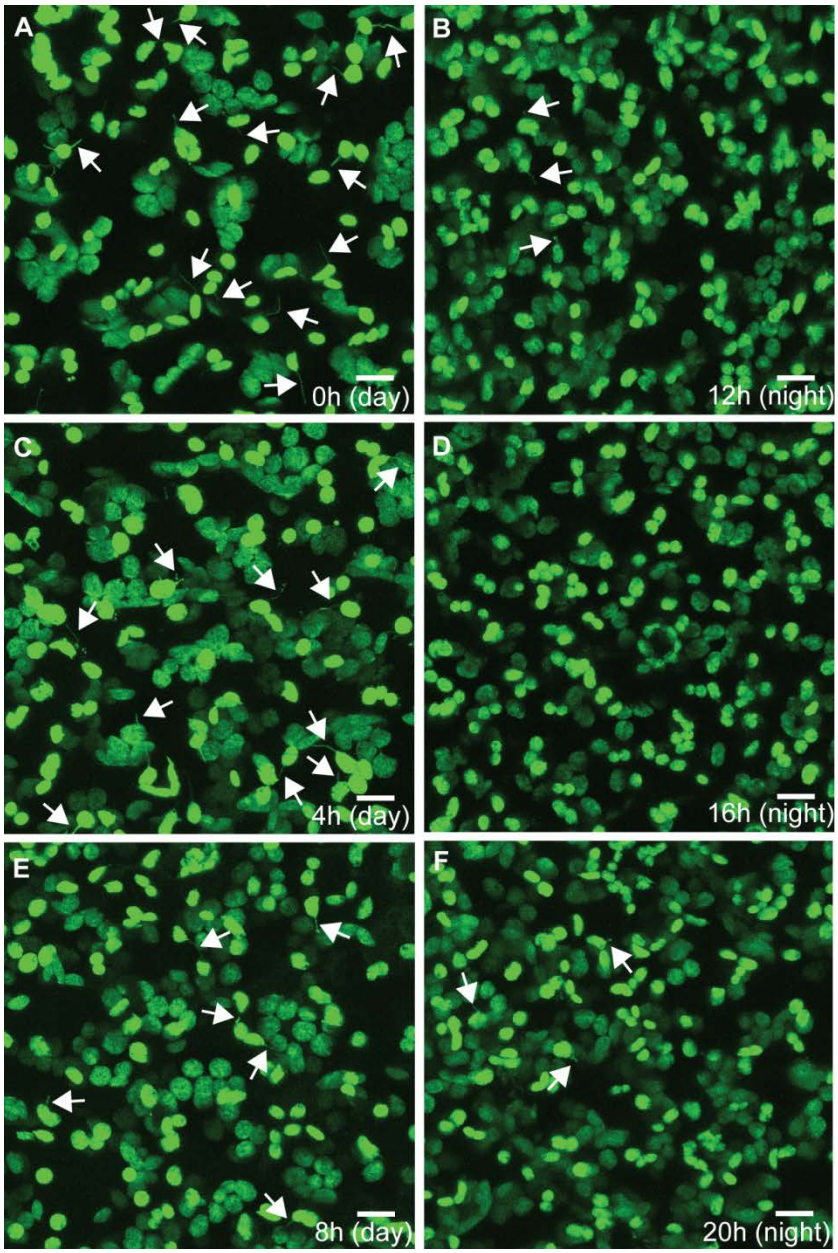

Supporting Figure 2.6. Representative images of stromule frequency over the course of 48 hours during a 12 hour light / 12 hour dark cycle. *N. benthamiana* chloroplast stromule frequency is high throughout the day (**A**, dawn; **C**, 4h after dawn; **E**, 8h after dawn) and low throughout the night (**B**, dusk; **D**, 4h after dusk; **F**, 8h after dusk). Chloroplasts and stromules are labeled with stromal GFP. Some stromules are indicated by white arrows; scale bars, 10 μm.

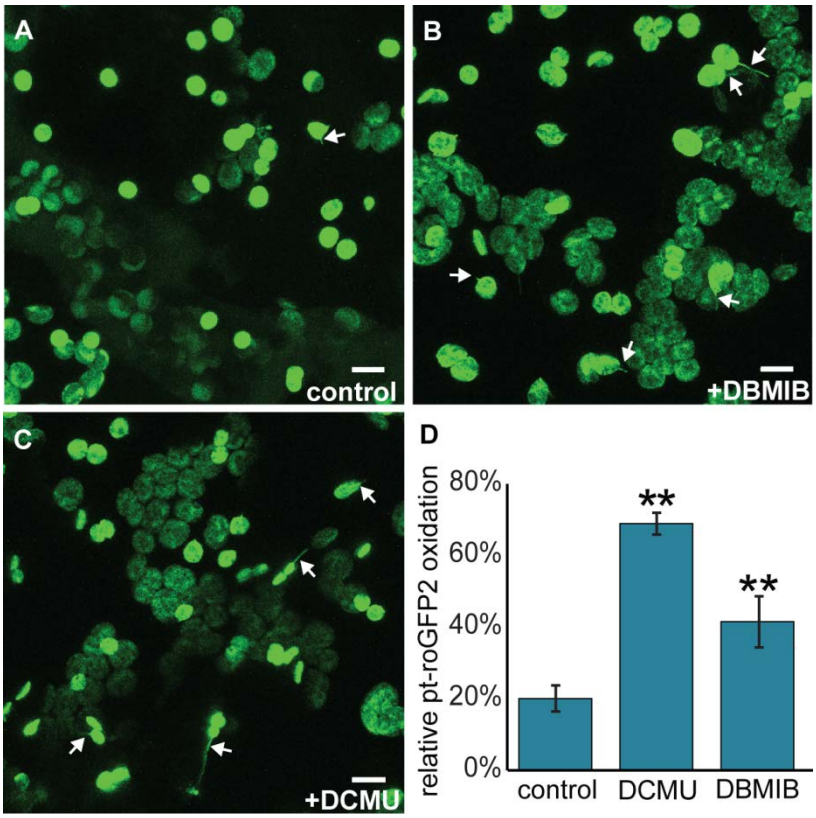

Supporting Figure 2.7. Oxidation of stromal redox buffers by ROS from photosynthesis induces stromules in chloroplasts. Representative images of stromule formation with control (**A**), DBMIB (**B**) and DCMU (**C**) treatments in *N. benthamiana* chloroplasts. (**D**) DBMIB and DCMU both cause strong oxidation of chloroplast redox buffers as measured by pt-roGFP2 in *A. thaliana* cotyledons. $n \geq 28$, $^{**}p < 0.01$. Chloroplasts and stromules are labeled with stromal GFP. Some stromules are indicated by white arrows; scale bars, 10 μm; error bars, SE.

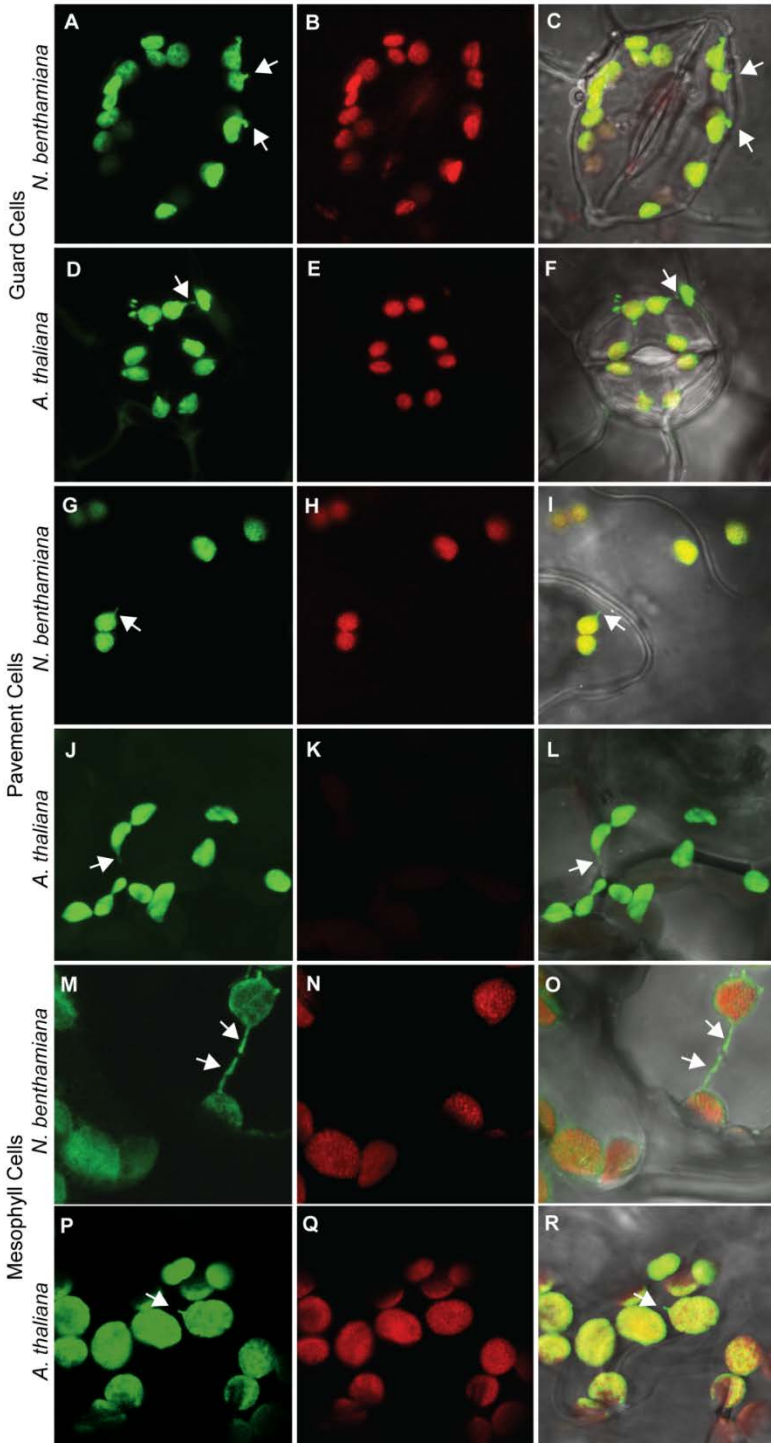

Supporting Figure 2.8. Representative images of chloroplasts and leucoplasts in *N. benthamiana* and *A. thaliana* visualized with confocal laser scanning microscopy. Guard cells (**A–C** and **D–F**), pavement cells (**G–I** and **J–L**), and mesophyll cells (**M–O** and **P–R**) all contain chloroplasts in *N. benthamiana*, as do *A. thaliana* guard cells (**B**) and mesophyll cells (**F**). *A. thaliana* pavement cells (**J–L**), however, have leucoplasts that lack chlorophyll (**K**). Green, stromal GFP; red, chlorophyll autofluorescence; gray, transmitted light. Some stromules are indicated by white arrows; error bars, SE.

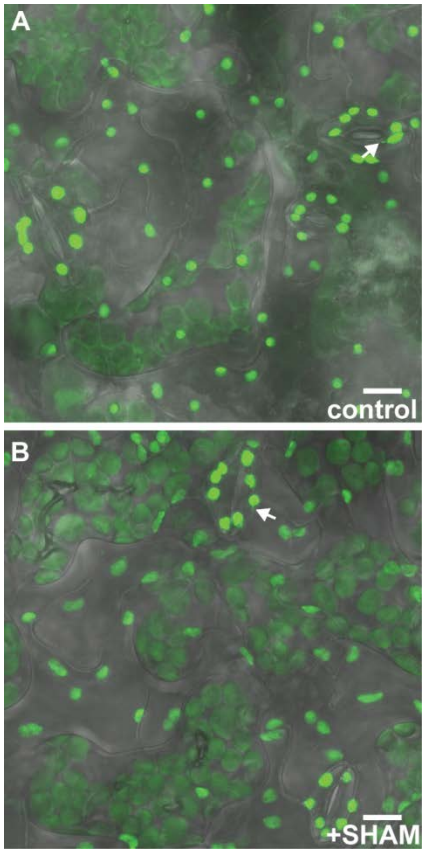

Supporting Figure 2.9. SHAM does not impact stromule frequency in *A. thaliana* guard cells. Stromule frequency is similar in guard cells with control treatment (**A**) or SHAM treatment (**B**). Green, stromal GFP; gray, transmitted light. Some stromules are indicated by white arrows; scale bars, 10 μm.

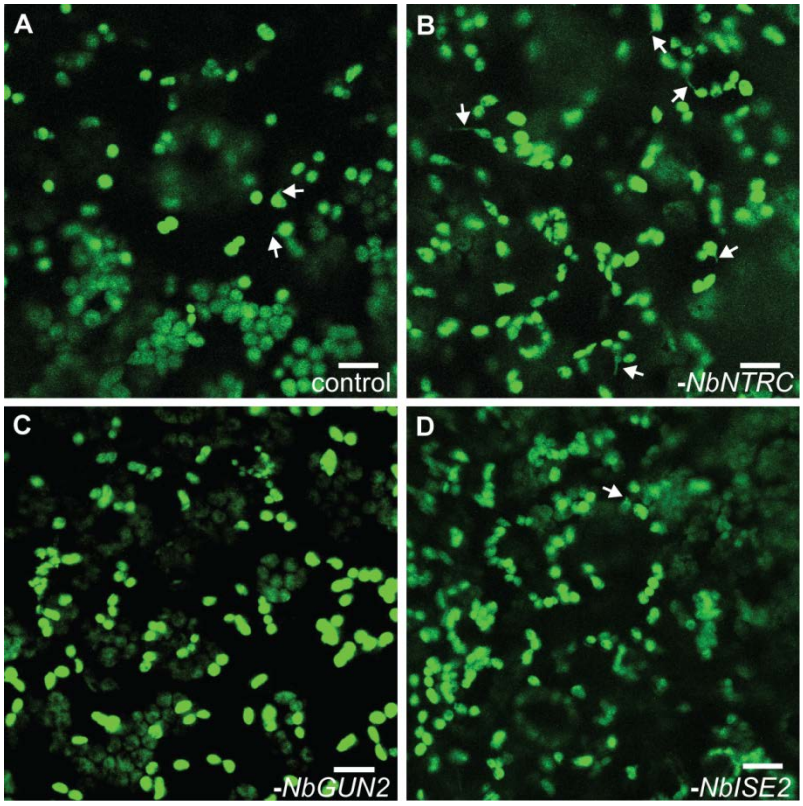

Supporting Figure 2.10. Representative images of stromule frequency in *N. benthamiana* after silencing *NbNTRC* (**B**)*, NbGUN2* (**C**)*,* or *NbISE2* (**D**), versus control (**A**). Green, stromal GFP. Some stromules are indicated by white arrows; scale bars, 10 µm.

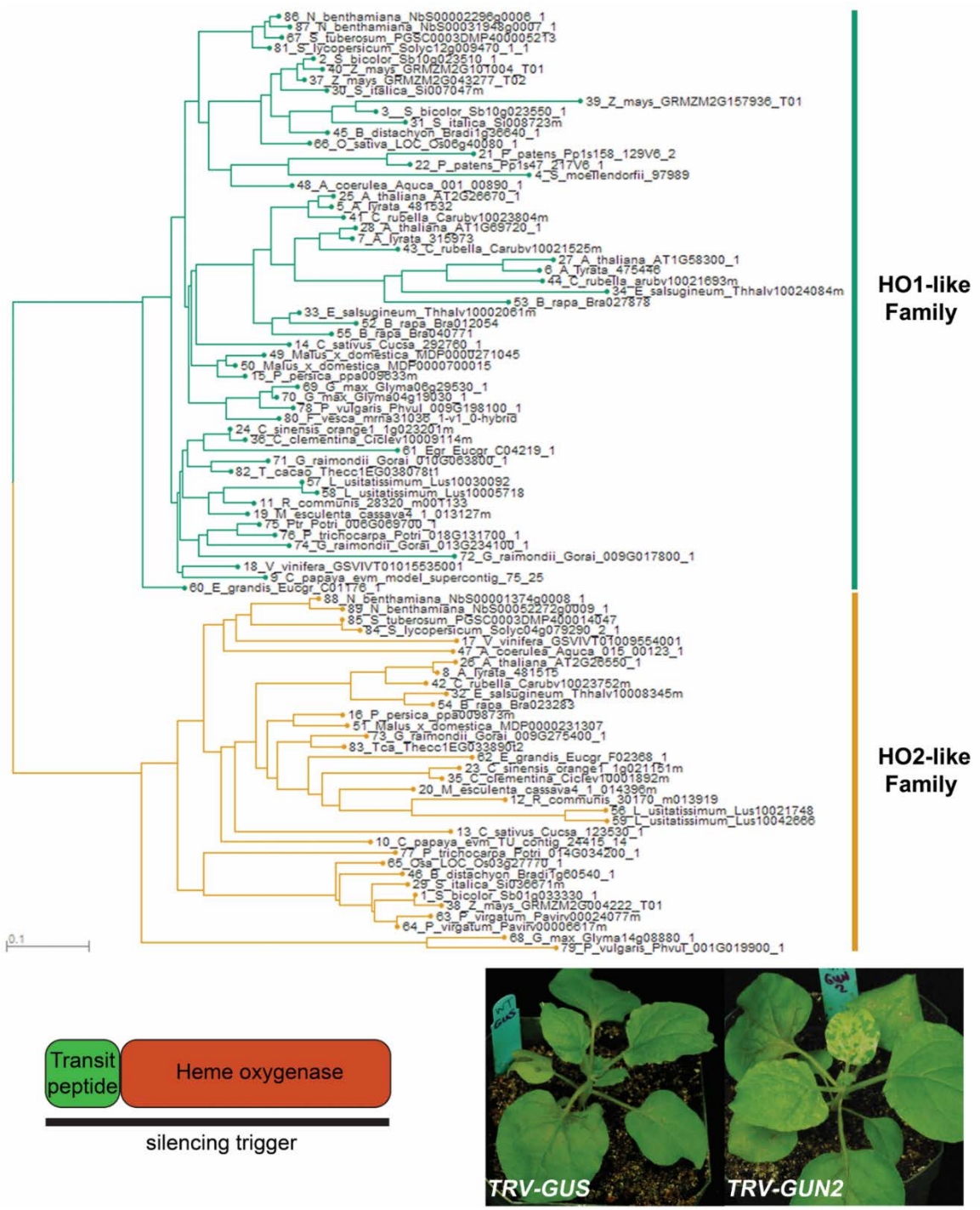

Supporting Figure 2.11. Identification of *GUN2* orthologues in *N. benthamiana*. A gene tree of heme oxygenases arranged homologues into two clades: *HO1* (a.k.a. *GUN2*)-like and *HO2*-like. *N. benthamiana* has two *HO1* homeologues (top). The silencing trigger against *NbGUN2* was designed to cover the entire gene sequence (837 bp, lower left). Silencing *NbGUN2* caused expected phenotypes, such as chlorosis (lower right).

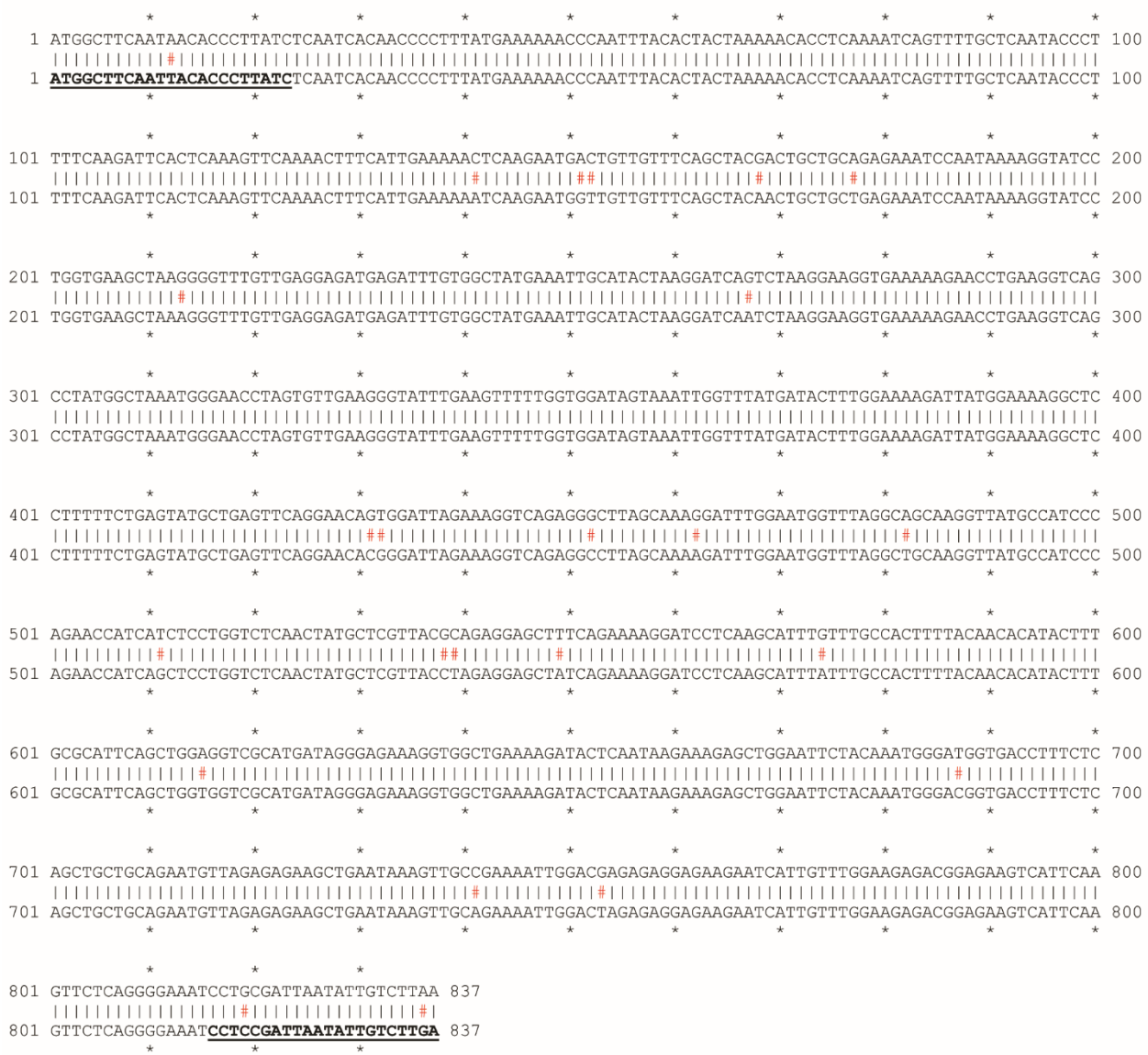

Supporting Figure 2.12. The silencing trigger for *NbGUN2* (bottom line) was cloned using primers specific to *NbGUN2a* (NbS00031948g0007). Here, the silencing trigger is aligned against the homeologous gene, *NbGUN2b* (NbS00002296g0006). Mismatches are indicated with red hashtags, aligned primer sequences are in bold and underlined.

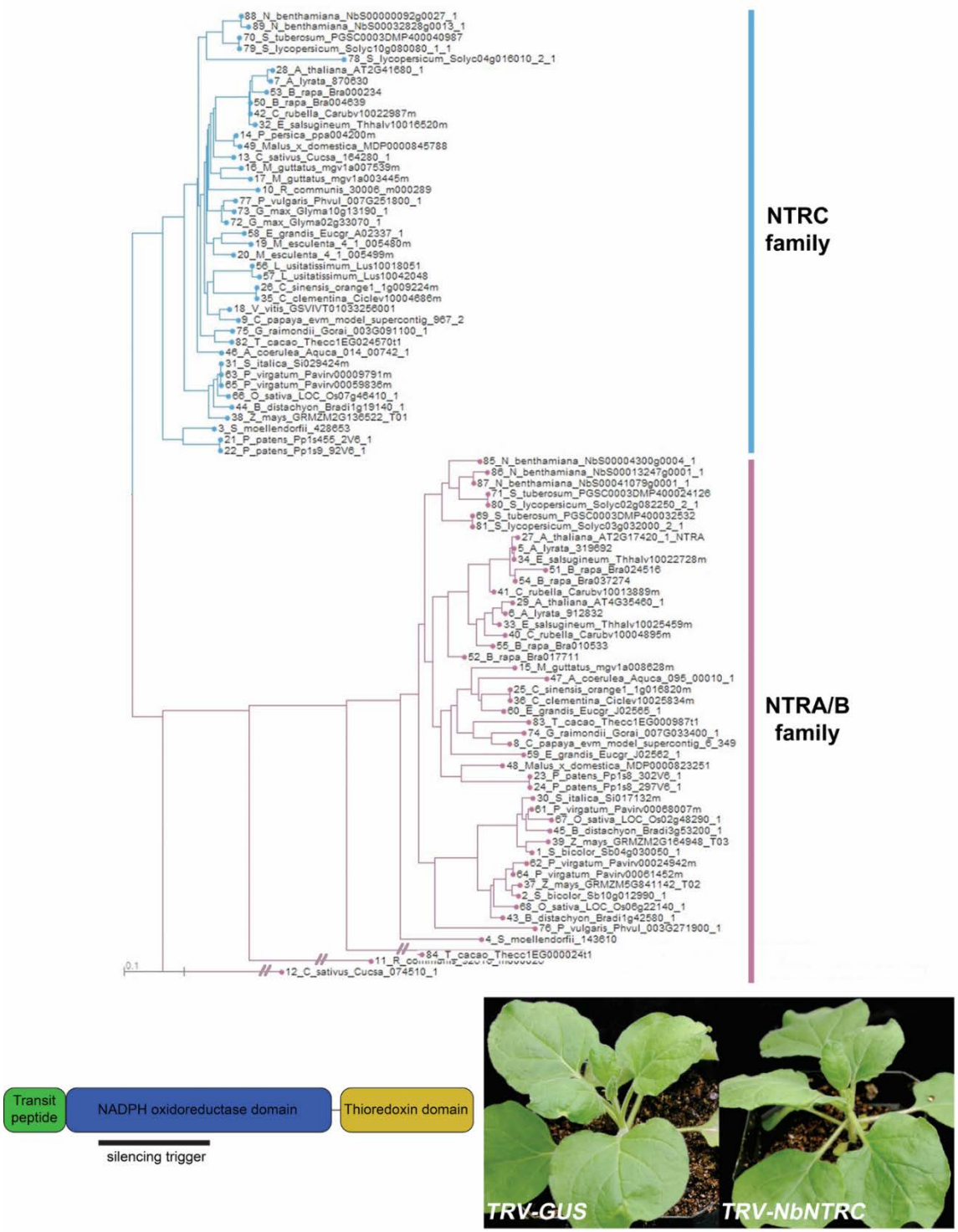

Supporting Figure 2.13 Identification of *NTRC* orthologues in *N. benthamiana*. A gene tree based on *AtNTRC* arranged homologues into two clades: *NTRA/NTRB*-like and *NTRC*-like. *N. benthamiana* has two *NTRC* homeologues (top). The silencing trigger against *NbNTRC* was designed against a sequence that encodes part of the NADPH oxidoreductase domain (lower left). Plants without gene silencing (*TRV-GUS*) appeared similar to plants silencing *NbNTRC* expression (*TRV-NbNTRC*, lower right).

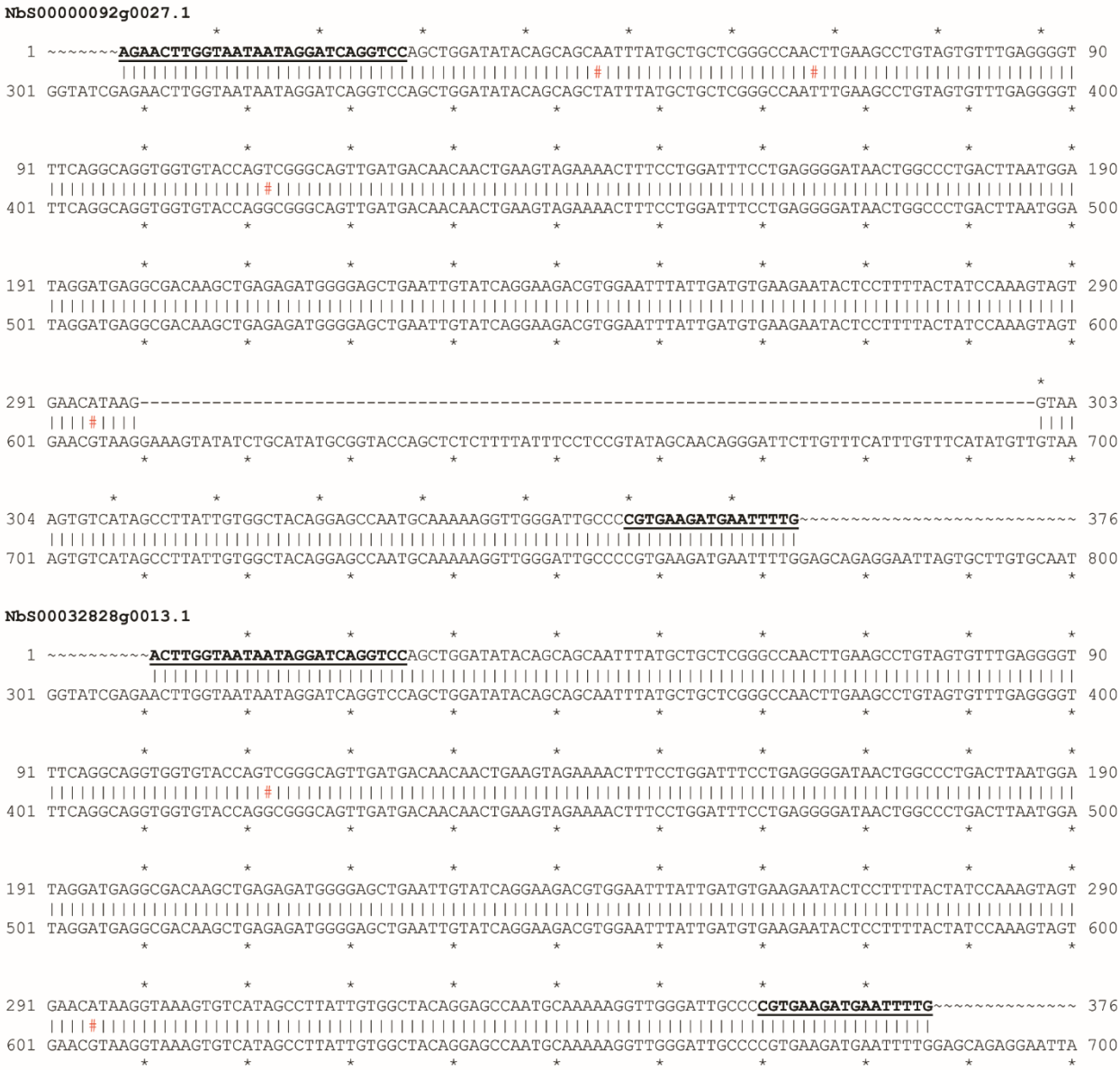

Supporting Figure 2.14. The silencing trigger for *NbNTRC* (top line) was cloned using primers specific to either *NbNTRC* homeologue. The predicted cDNA sequence of Nb00000092g0027.1 is likely misannotated to include an intron (numbered here as nucleotides 610 to 696, bottom row, top alignment). Accounting for this discrepancy, the silencing trigger is ~99% identical to both *NbNTRC* homeologues. Mismatches are indicated with red hashtags, aligned primer sequences are in bold and underlined.

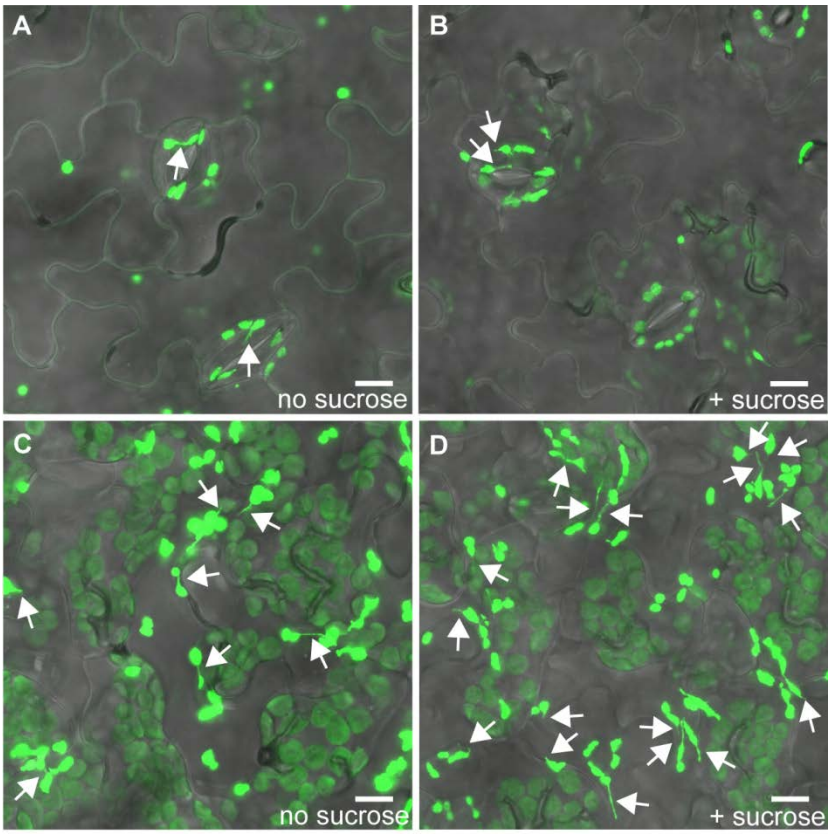

Supporting Figure 2.15. Sucrose increases leucoplast but not chloroplast stromule frequency. Representative images of stromule frequency with and without sucrose treatment in *A. thaliana* epidermal cells. Stromule frequency is similar in chloroplasts without sucrose treatment (**A**) or with sucrose treatment (**B**). Sucrose treatment increases stromule frequency in leucoplasts (**D**) compared to control (**C**). Plastids and stromules are labeled with stromal GFP (green). Some stromules are indicated by white arrows; scale bars, 10 μm.

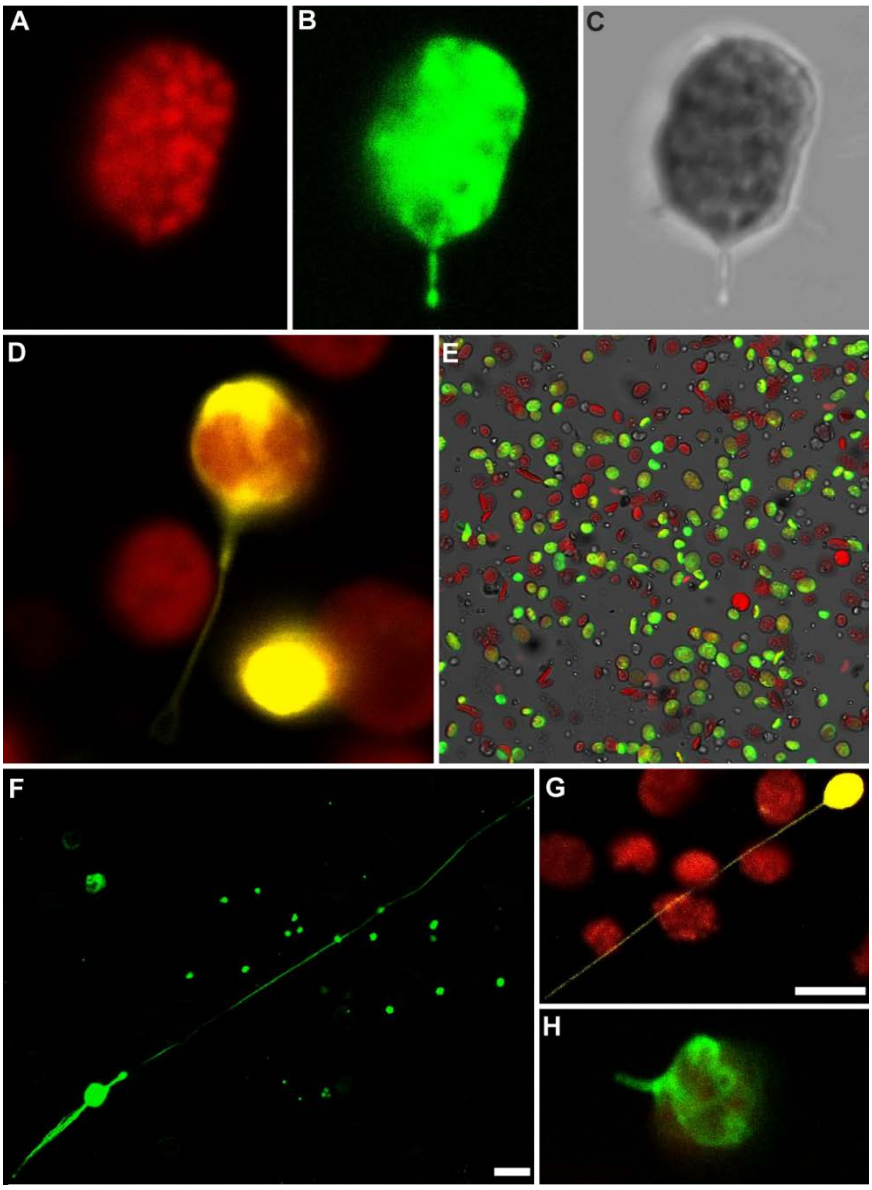

Supporting Figure 2.16. Stromules of isolated chloroplasts visualized by confocal microscopy and 3D-SIM. (**A–C**) After extraction from cells, isolated chloroplasts of *N. benthamiana* have stromules, as visualized by either stromal GFP fluorescence (**B**) or transmitted light (**C**), while chlorophyll autofluorescence remains restricted to the thylakoids (**A**). (**D**) CFDA also labels stromules in isolated *N. benthamiana* chloroplasts (CFDA, yellow; chlorophyll, red). (**E**) Representative example of sample purity after chloroplast isolation protocol. Many chloroplasts are fully intact, with stromal GFP (green); some were damaged during extraction and have lost stromal GFP, but retain the thylakoid membranes (chlorophyll autofluorescence, red); and very small quantitites of nonfluorescent materials remain with the sample (transmitted light, gray). (**F,G**) After isolation, some *N. benthamiana* chloroplasts have stromules that are very long, as visualized by GFP (**F**, in green) or CFDA staining (**G**, in yellow; chlorophyll autofluorescence, red). (**H**) Isolated *A. thaliana* chloroplasts expressing stromal roGFP2 (green) also have stromules after extraction from cells. Scale bars, 5 μm.

Chapter Three: Plasmodesmatal transport is regulated by light and the circadian clock

Jacob O. Brunkard, Anne M. Runkel, Patricia C. Zambryski

INTRODUCTION

PD transport changes over the course of plant development. In young embryos, small molecules can move between cells rapidly, and very large molecules, such as proteins, also move from cell-to-cell (Kim and Zambryski, 2005; Kim et al., 2002, 2005a, 2005b). As embryos mature, the rate of PD transport decreases, and large proteins (such as 3xGFP, which is 81 kDa) are restricted to the cell in which they are translated (Kim and Zambryski, 2005; Kim et al., 2002, 2005a, 2005b). Similarly, PD transport is much greater in young leaves than in mature leaves (Crawford and Zambryski, 2001a; Oparka et al., 1999a; Roberts et al., 1997b, 2001; Stadler et al., 2005). The precise mechanisms of these changes in PD transport remain unknown, but several groups have independently discovered that chloroplasts influence PD transport by affecting both PD function and the number of PD in cell walls (Benitez-Alfonso et al., 2009; Brunkard et al., 2013; Burch-Smith and Zambryski, 2010, 2012; Burch-Smith et al., 2011b; Provencher et al., 2001; Stonebloom et al., 2012). PD transport is not restricted in embryos or leaves of plants defective in chloroplast biogenesis (including the mutants *ise1*, *ise2*, and *clpr2*) (Burch-Smith and Zambryski, 2010; Burch-Smith et al., 2011b; Carlotto et al., 2015; Kobayashi et al., 2007; Stonebloom et al., 2009). On the other hand, plants with strong plastid oxidative stress (including the mutants *gat1/trx-m3* and likely *sxd1*, as well as plants treated with methyl viologen, an herbicide that causes chloroplast oxidative stress) exhibit decreased PD transport in leaves(Benitez-Alfonso et al., 2009; Provencher et al., 2001; Stonebloom et al., 2012). The finding that PD function and formation responds to signals from chloroplasts implies that PD transport is coordinated with chloroplast-related physiology, inviting speculation that PD could be regulated by light.

A handful of studies have previously explored whether PD transport is affected by light. An early study in maize found that PD transport appears to decrease if etiolated seedlings are treated with 60 minutes of white light (Epel and Erlanger, 1991). When that treatment is followed by a 10 minute pulse of far-red light, PD transport instead remains high; if followed by a 10 minute pulse of far-red light and then a 10 minute pulse of red light, PD transport decreases. Phytochromes react to red and far-red light to promote de-etiolation and photomorphogenesis in response to red (or white) light, but far-red light can reverse this signaling pathway (Hughes, 2013). Thus, the demonstration that PD transport decreases in response to white light and red light, but not far-red light, implies that PD transport decreases during photomorphogenesis.

A later report argued that light also downregulates PD transport in leaves. *Nicotiana benthamiana* leaves were severed from plants grown under 16 hour (h) light / 8 h dark photoperiods and placed on nutrient-free agarose gels (Liarzi and Epel, 2005). Detached leaves were bombarded with transgenes to express GFP and then transferred to either constant darkness or back to the16 h light / 8 h dark cycle; GFP movement from transformed cells was measured after 48 h. PD transport was reported

to be higher under constant dark conditions than under normal light/dark cycles in young leaves, but no strong difference was observed in mature leaves. Given that young leaves rely on imported carbohydrates from older leaves, that no nutrients were provided to the leaves after detachment, and that PD transport was only assayed in constant darkness, the results of this assay could be a starvation response rather than representative of how PD transport is affected by light in natural settings.

Indeed, another report suggested that PD frequency in C4 grasses increases when seedlings are grown under high light conditions, which implies that PD transport increases with light intensity (Sowiński et al., 2007). Four grass species were grown under low light (50 µE m^{-2} s^{-1}), medium light (200 µE m^{-2} s^{-1}), or high light (1000 µE m^{-2} s^{-1}) with 14 h light / 10 h dark cycles. The density of PD between cell types bordering the vasculature significantly increased with higher light intensity, and the increase in PD frequency correlated with increased movement of carbohydrates fixed by photosynthesis and labeled with radioactive ^{14}C.

To resolve these conflicting reports, and to enhance our understanding of the relationship between PD and chloroplast physiology, here we perform detailed studies to explore whether PD transport is affected by light and the circadian clock.

RESULTS AND DISCUSSION

PD transport is higher during the day

We used a GFP movement assay in *N. benthamiana* leaves to determine if intercellular transport is different during the day than during the night. Plants were grown in a 12 h light / 12 h dark light cycle under otherwise constant conditions. *Agrobacterium* carrying *$35S_{PRO}$:GFP* T-DNA was infiltrated into leaves with very low inoculum ($OD_{600nm} < 10^{-4}$) at either dusk or dawn, after which GFP movement away from distinct, individual transformed cells in the leaves was visualized with confocal scanning laser microscopy (Brunkard et al., 2015c). For consistency, only similar plants and leaves of comparable size and age were used for these assays, and GFP movement was only visualized in the proximal 25% of the leaf.

Whether leaves were infiltrated at dawn or dusk, GFP moved the same distance after 48 h (Figure 3.1, Table 3.1, $n \geq 106$, $p = 0.26$), confirming that the time of infiltration had no impact on the observed rates of PD transport. When observed after 36 h or after 60 h, however, GFP moved signif-icantly less in leaves infiltrated at dusk than in leaves infiltrated at dawn (36 h: $n \geq 117$, $p < 10^{-7}$, 60 h: $n \geq 102$, $p < 10^{-10}$). Thus, PD transport is higher during the day than at night, since GFP moves more in leaves that have experienced two days and one night (versus one day and two nights), and GFP moves the most in leaves that have experienced 3 days.

Remarkably, an additional night has little to no impact on GFP movement, suggesting that PD transport at night is relatively negligible. PD transport was not significantly different in leaves observed 60 h after infiltration at dusk (2 days, 3 nights) than in leaves 48 h after infiltration at dusk (Figure 3.1, Table 3.1, $n \geq 111$, $p = 0.20$) or 48 h after infiltration at dawn (Figure 3.1, Table 3.1, $n \geq 106$, $p = 0.91$). Similarly, GFP movement is only slightly lower in leaves 36 h after infiltration at dawn (2 days, 1 night)

than in leaves 48 h after infiltration. This implies that PD transport is dramatically lower at night than during the day.

To verify the conclusion that PD transport is higher during the day than at night using an independent technique, we assayed PD transport using fluorescent dye loading techniques in Arabidopsis (Figure 3.2). We germinated Arabidopsis seeds on nutrient plates and loaded a fluorescent symplastic tracer, HPTS, into young seedlings by cutting the plant at the base of the shoot and applying a small amount of HPTS (Gisel et al., 1999, 2002). After several minutes, the cotyledons of seedlings were visualized using confocal scanning laser microscopy. We found that HPTS rapidly moved from the base of the shoot into the cotyledon through PD when HPTS was applied during the day, but not when HPTS was applied at night (Figure 3.2). In a second set of experiments using the same growth conditions, we cut a single cotyledon off of a young seedling and applied a small amount of FITC bound to dextrans of various sizes (4 kDa, 10 kDa, 40 kDa, or 70 kDa) to the seedling at the cut surface. After 30 minutes, we observed the roots of plants near the root tip to determine if the FITC-Dextrans could move from the phloem into the surrounding root cells through PD. Again, we consistently observed more transport through PD during the day than at night, supporting the hypothesis that PD transport is higher during the day than during the night.

The circadian clock regulates PD transport

High rates of PD transport during the day could be directly caused by light or could be under the control of light-entrained pathways controlled by the circadian clock. To distinguish between these possibilities, we first tested whether transferring plants grown in 16 h light / 8 h dark cycles to constant light or constant dark impacted PD transport. After 48 h, there was no significant difference in GFP movement between plants under constant light or the 16 h light / 8 h dark cycle, with GFP moving either 2 or 3 cells in more than 73.3% of observations (Figure 3.3). GFP movement was severely lower in plants under constant dark conditions: GFP had not spread from the transformed cell in 22.8% of cells observed, and had moved less than 2 cells in 75.4% of observations (Figure 3.3). Light is therefore required for PD transport during the day, but constant light is insufficient to significantly promote PD transport.

In plants, the circadian clock serves primarily to anticipate environmental changes and to gate responses to irregular or fluctuating stimuli. For example, the circadian clock prevents the induction of photosynthesis-associated nuclear genes by brief bursts of light at night, preventing wasteful protein synthesis. Gating can be observed by entraining plants under regular day/night cycles, moving them into constant conditions, and then applying a stimulus (e.g., light) at either “day” or “night”; ungated responses will be observed in both cases, but gated responses will differ depending on when the stimulus is applied. We tested whether PD transport is gated by the circadian clock by agroinfiltrating plants and transferring them to constant darkness at dawn, and applying 12 h of light either during the second subjective night or third subjective day, and then observing GFP movement at 72 h post infiltration. Light was sufficient to somewhat induce PD transport when applied during subjective night (Figure 3.3). When light was applied during subjective day, however, PD transport dramatically increased by approximately 2-fold in comparison to PD transport in plants under constant

darkness. This demonstrates that the stimulation of PD transport by light is gated by the circadian clock.

PD transport declines gradually as leaves age and compensates for shorter days

We next sought to determine whether PD transport is lower in plants grown with shorter daylengths, since PD transport is strongly regulated by light. We grew *N. benthamiana* plants under 12 h or 16 h daylengths and observed their growth rates and morphological phenotypes throughout their development, and then assayed PD transport in multiple leaves in 6 week old plants. Since plants grow more slowly under shorter daylengths, there were no *a priori* means to determine two physiologically similar leaves to use for comparison between the two sets of plants. Instead, we assayed PD transport in several leaves from each plant that we predicted would include both sink and source leaves. As the plant shoot develops, leaves transition from heterotrophic "sinks" for carbohydrates, nitrogen, and other resources to photoautotrophic "sources" of carbohydrates for the rest of the plant (Masclaux et al., 2000). The sink-to-source physiological transition is supported by the restriction of PD transport in source leaves, which can then actively load sugars into the phloem without allowing the sugars to move back into the leaf through PD. In this way, regulation of PD transport permits the formation of a carbohydrate concentration gradient that drives plant growth and development.

We found that PD transport, as measured by the GFP movement assay, decreases in an approximately linear pattern with respect to leaf age, regardless of photoperiod conditions (Figure 3.4). Previous studies often used qualitative measurements to define the sink-to-source transition in PD transport (specifically, fluorescent constructs that either do or do not move from the phloem into the ground tissue), and have therefore emphasized the sink-to-source transition within leaves: PD transport is restricted first in the distal region of the leaves, and then this restriction moves proximally until PD transport is low throughout the entire leaf. The data presented here demonstrate that PD transport decreases gradually and quantitatively as a leaf ages. Remarkably, there is no significant difference in the rate of PD transport of plants grown under 12 h or 16 h photoperiods, as tested by an analysis of covariance with respect to leaf age (ANCOVA $p = 0.27$; homogeneity of regressions $p = 0.25$). Thus, leaves in plants grown under shorter photoperiods appear to compensate for the decrease in daily light by increasing the rate of PD transport during the day.

CONCLUSION

In this report, we have shown that PD transport occurs primarily during the day, regulated by light and the circadian clock. High rates of PD transport can only occur in the presence of light, but light is not sufficient to induce these high rates of PD transport at subjective night, indicating that PD transport is under the control of the circadian clock. None of the genes that are currently known to encode PD-localized proteins are under the transcriptional control of the circadian clock, according to publicly available transcriptome data (including the eight *PD-LOCALIZED PROTEIN1* homologues, the three *PD CALLOSE BINDING PROTEIN1* homologues, the PD-targeted *CALLOSE SYNTHASEs*, and the *PD BETA-GLUCANASEs* that degrade callose at PD),

suggesting that some uncharacterized light-sensitive pathway gated by the circadian clock coordinates PD transport. PD transport impacts a broad range of biological processes in plants, including redistribution of resources, the formation of hormone gradients, the exchange of protein and small RNA signals, and viral trafficking. All of these diverse processes are likely affected by the circadian regulation of PD transport and, therefore, cell-cell signaling in plants.

METHODS

Plant growth conditions

N. benthamiana accession Nb-1 plants were grown as described (Brunkard et al., 2015c) on light carts under ~100 µE m^{-2} s^{-1} photosynthetically active radiation with either 12 h or 16 h daylengths, as indicated in the text. Plants were photographed every day after germination in order to accurately record leaf ages.

Assaying PD transport in single leaves

Except for the photoperiod experiment (described in detail below), all movement assays were conducted using the fourth expanded leaf of 5 week old plants. GFP movement assays were conducted as previously described (Brunkard et al., 2015c), observing GFP movement in only the proximal 25% of the leaf. For each experiment, either two or three plants were assayed for each condition per replicate (observing GFP movement from up to 50 transformed cells), and the entire experiment was replicated three times.

Assaying PD transport in multiple leaves

For the photoperiod experiment, GFP movement assays were performed as previously described (Brunkard et al., 2015c), but *Agrobacterium* carrying the *$35S_{PRO}$:GFP* T-DNA binary vector was infiltrated into every leaf of the plant in 6 week old plants. GFP movement was observed in all leaves in the proximal 25% region of the leaf using three biological replicates. Data were not included if the total number of transformed cells observed in a given leaf age across all three biological replicates was less than 10. Leaves beyond 30 days old were also not included, because GFP was generally unable to move beyond the transformed cell, and thus the GFP movement assay is not sufficiently sensitive to assay changes in PD transport in these leaves.

Assaying PD transport with fluorescent tracers

HPTS (8-hydroxypyrene-1,3,6-trisulfonic acid) was dissolved in 0.5X Murashige and Skoog (MS) media at 1 mg / mL. A small amount of HPTS was applied to the root immediately after cutting the root near the root-shoot connection in 4 day old Arabidopsis seedlings grown on 0.5X MS, 0.8% agar plates. Cotyledons were then observed approximately 10 minutes after application of the dye. FITC-Dextrans (fluorescein isothiocyanate-dextran) were also dissolved at 1 mg / mL in 0.5X MS. Any FITC-Dextrans smaller than the indicated molecular weight were removed by centrifugation with a size exclusion column (Amicon). FITC-Dextrans were applied to the cut surface of the seedling immediately after cutting the cotyledon, and dye unloading in the root was observed 30 minutes later.

Microscopy

GFP was observed in the epidermis of *N. benthamiana* leaves using a Zeiss 710 confocal scanning laser microscope. Identical settings (such as laser strength and gain) were used for all GFP experiments. HPTS was also observed with a Zeiss 710 confocal scanning laser microscope. FITC-Dextran unloading in roots was observed with epifluorescence illumination using a Zeiss AxioImager M2.

Statistical analysis

Each cell transformed to express GFP was considered an independent sample for the movement assay. Movement assay results are presented as the average movement of GFP and standard error of the mean. For most experiments, GFP movement between conditions were compared using unpaired heteroscedastic *t* tests in Excel.

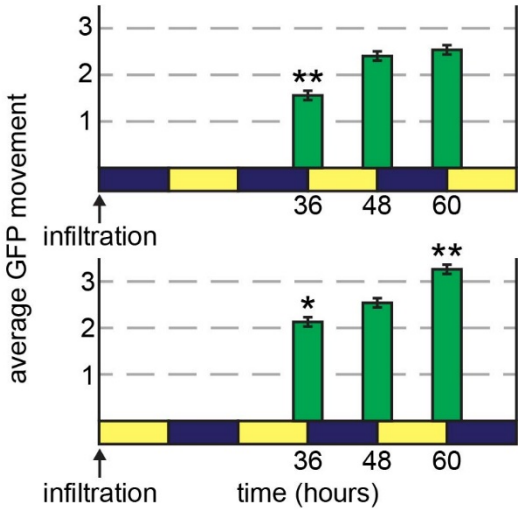

Figure 3.1. PD transport is higher during the day than at night. *N. benthamiana* leaves were agroinfiltrated to express GFP at either dusk (top) or dawn (bottom) in 5 week old plants grown under 12 h light (yellow) / 12 h dark (blue) cycles. In leaves infiltrated at dusk (top), GFP movement significantly increased during the second day, but did not change during the second night. In leaves infiltrated at dawn (bottom), GFP movement somewhat increased during the second night, but dramatically increased during the third day. *$p < 10^{-3}$, ** $p < 10^{—5}$. For more details, see Table 1.

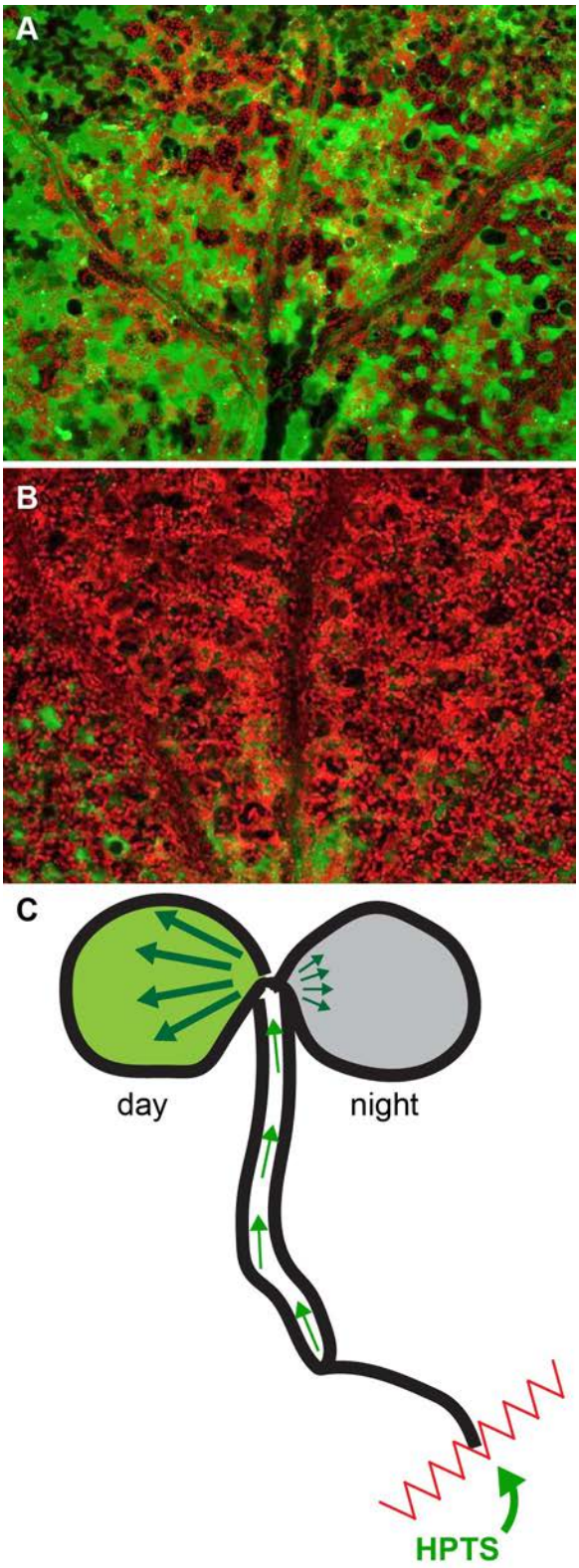

Figure 3.2. A small fluorescent tracer, HPTS, moves rapidly through PD in the shoot during the day, but not during the night. Seedlings were loaded with HPTS at a cut surface of the root close to the shoot-root axis, and then cotyledons were observed

using confocal scanning laser microscopy after 30 minutes. (**A**) The proximal region of this cotyledon has loaded with HPTS (green) during the day; chloroplasts are shown in red. (**B**) The proximal region of this cotyldeon has not loaded with HPTS (green) during the night; chloroplasts are shown in red. (**C**) Schematic of technique: HPTS is loaded at a cut surface of the root and then moves through PD in the shoot and unloads into cotyledons rapidly during the day (left) or slowly at night (right).

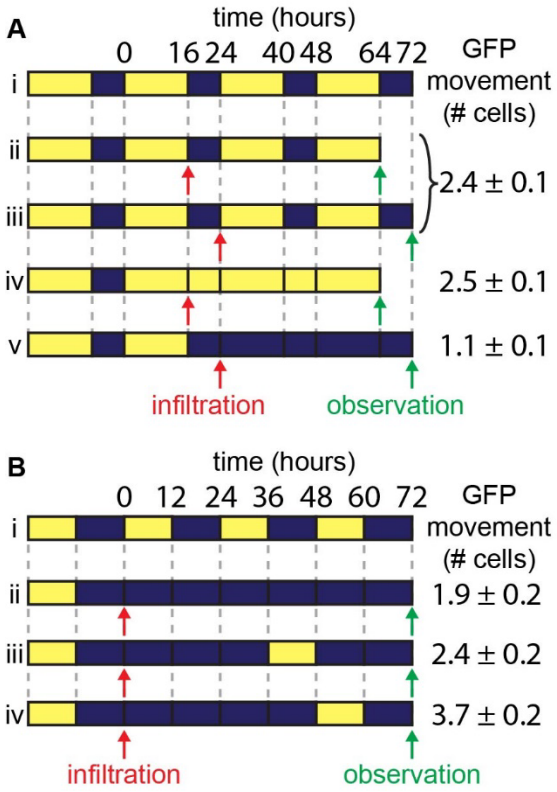

Figure 3.3. PD transport is regulated by the circadian clock. Light treatment is represented by yellow, dark treatment is represented by blue. Line (i) of both (**A**) and (**B**) shows the day/night cycles that would be experienced by plants if they were not transferred to new light regimes. (**A**) After growing in 16 h light / 8 h dark cycles, *N. benthamiana* leaves were agroinfiltrated at dawn or dusk (as indicated by red "infiltration" arrows) to express GFP. GFP movement was then assayed after 48 h (as indicated by green "observation" arrows) of continued light/dark cycles (lines (ii) and (iii)) or 48 h of constant light starting at the end of the day (line (iv)), or constant darkness starting at the end of the night (line (v)). Constant light did not affect PD transport, but constant darkness significantly decreased PD transport (p). (**B**) PD transport was assayed in plants that had been growing in 12 h light / 12 h dark cycles and then transferred to constant dark conditions; GFP movement was assayed 72 h after agroinfiltration. Treatment with 12 h of light during the second subjective night after agroinfiltration (line (iii)) somewhat increased PD transport compared to PD transport in constant dark (line (ii)), but treatment with 12 h of light during the third subjective day (line (iv)) dramatically increased PD transport, suggesting that PD responds to light in a pathway gated by the circadian clock.

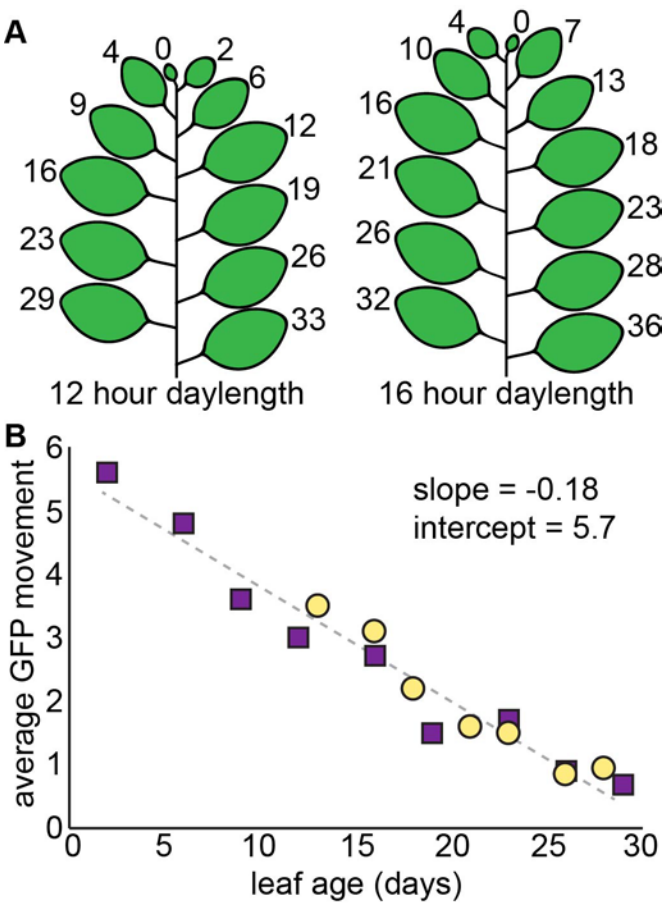

Figure 3.4. (**A**) The age of leaves (in number of days) 6 weeks after germination is shown in these schemes of *N. benthamiana* plants grown with 12 hour daylengths or 16 hour daylengths. Cotyledons are not including in this cartoon because they have typically senesced within the first 6 weeks of growth. (**B**) Average GFP movement in leaves of different ages is shown for plants grown with 12 hour daylengths (purple boxes) or 16 hour daylengths (yellow boxes). PD transport declines in the same linear relationship with leaf age in both sets of plants (ANCOVA p = … homogeneity …). The linear relationship is depicted with a gray dashed line with slope -0.18 and y-intercept 5.7.

Table 3.1. Time course of GFP movement in *N. benthamiana* leaf epidermis.

Time of infiltration	Hours after infiltration	Average GFP movement	Standard error	Sample size (*n*)	Significance group
Infiltrated at dusk	36 hours	1.56	0.08	117	a
	48 hours	2.41	0.07	124	c
	60 hours	2.54	0.07	111	c
Infiltrated at dawn	36 hours	2.13	0.07	124	b
	48 hours	2.53	0.08	106	c
	60 hours	3.26	0.08	102	d

CHAPTER FOUR: Glucose-TOR signaling coordinates the sink-to-source transition and leaf aging

Jacob O. Brunkard, Min Xu, Elena A. Shemyakina, Howard M. Goodman, Patricia C. Zambryski

ABSTRACT

As leaves age, they transition from heterotrophic “sinks” for carbohydrates to photoautotrophic “sources” of carbohydrates. During the sink-to-source transition, transport through plasmodesmata (PD), nanoscopic channels that connect plant cells across the cell wall, is restricted. This change in PD transport allows leaves to passively import sugars through PD when they are young sinks and then actively export sugars across the plasma membrane when they are mature sources. Little is known about how plants regulate the sink-to-source transition. We identified a mutant defective in the restriction of PD transport, *ise4*, that is a recessive allele of *AtReptin*, which encodes a subunit of the R2TP chaperone complex. We demonstrate that *ise4* is specifically defective in activating the glucose-TOR signaling pathway that coordinates sugar availability with cellular physiology, and that glucose-TOR signaling causes restricted PD transport in embryos and in leaves. This leads to a new model of how plants allocate resources across the shoot through dynamic signaling pathways that sense how much excess sugar is available for export, which allows the plant to fine-tune the sink-to-source transition in response to changing physiological conditions.

Plasmodesmatal transport is restricted during development

Unique among the major multicellular lineages, plants undergo regular transitions from heterotrophy to photoautotrophy. Young, growing leaves are heterotrophic “sinks” for carbohydrates, nitrogen, and other resources, while older, mature leaves are photoautotrophic “sources” of carbohydrates for the rest of the shoot and root. Developmentally, the sink-to-source transition is driven by the restriction of plasmodesmatal (PD) transport in source leaves (Aoki and Hirose, 2012; Bihmidine et al., 2013; Masclaux et al., 2000; Turgeon, 1989). Although the sink-to-source restriction of PD transport has been thoroughly characterized, little is known about how this transition is regulated by the plant.

PD are nanoscopic channels that connect the cytosol of adjacent plant cells across the cell wall, permitting transport of molecules including water, nutrients, sugars, small RNA, and cytosolic proteins (up to ~70kDa, depending on the cell type and physiological conditions) (Brunkard et al., 2015a; Sager and Lee, 2014; Sevilem et al., 2015). In sink leaves, high rates of PD transport allow for rapid unloading of sugars from the phloem. In source leaves, restricted PD transport prevents sugars from flowing back into the ground tissue once sugars are loaded into the phloem by plasma membrane transporters. Thus, the sink-to-source transition in PD transport is critical for establishing the concentration gradient that drives carbohydrate redistribution

throughout the shoot (Crawford and Zambryski, 2001b; Oparka et al., 1999b; Roberts et al., 1997a, 1997b; Turgeon, 1989).

During embryogenesis, Arabidopsis undergoes a similar restriction in PD transport at the mid-torpedo morphological stage (Kim and Zambryski, 2005; Kim et al., 2005a, 2005b). Wild-type embryos are able to rapidly transport 10kDa FITC-Dextran throughout the embryo until the mid-torpedo stage, when PD transport decreases (Kim et al., 2002). We conducted a forward genetic screen to identify essential genes that are required for this decrease in PD transport by isolating embryo-defective mutants that continue to rapidly transport 10kDa FITC-Dextran dyes throughout the embryo at the mid-torpedo stage (Figure 4.1A). Out of thousands of mutants, we identified five lines with increased PD transport, which we call *ise1–ise5*. We have previously characterized *ISE1* and *ISE2*, which are mitochondrial and plastid RNA helicases, respectively (Burch-Smith et al., 2011b; Kobayashi et al., 2007; Stonebloom et al., 2009). Here, we show that *ISE4* encodes a chaperone complex subunit that is required for TOR (TARGET OF RAPAMYCIN) signaling. TOR is a kinase that responds to nutritional status to regulate a range of biological processes, including the transcription and translation of thousands of genes (Wullschleger et al., 2006; Xiong et al., 2013). We demonstrate that TOR restricts PD transport in embryos and leaves, and that TOR therefore coordinates the sink-to-source transition in response to carbohydrate availability.

ISE4 encodes *AtREPTIN*

We mapped *ise4* to a single nucleotide mutation in At5g67630, which encodes the Arabidopsis orthologue of Reptin (also known as RVB2, RuvBL2, and Tip49b, among other names) (Nano and Houry, 2013; Rosenbaum et al., 2013). The *ise4* phenotype was complemented with the genomic sequence driven by the full native promoter (which includes the full ORF of a small gene of unknown function, At5g67640), a genomic sequence driven by a truncated native promoter (which lacks the start codon for At5g67640), or the At5g67630 coding sequence driven by the full native promoter, confirming that *ise4* is allelic to *AtReptin* (Figure 4.1B). Reptin is an essential and promiscuous AAA+ ATPase found in all eukaryotes that acts as a chaperone for various multiprotein complexes and has conserved roles in chromatin remodeling, telomerase assembly, transcription, translation, and phosphatidylinositol 3-kinase related kinase (PIKK) assembly (Nano and Houry, 2013; Rosenbaum et al., 2013). Homozygous null alleles of *AtReptin* are female gametophyte lethal, but *ise4* is a weak allele that causes development to arrest much later, at the mid-torpedo stage of embryogenesis. AtReptin-GFP localizes to the nucleus and cytoplasm (Figure 4.1C), as in other model organisms. For many of its functions, Reptin forms a multiheteromeric complex with Pontin (also known as RIN1, RVB1, RuvBL1, and Tip49a, among other names), a related AAA+ ATPase (AtReptin and AtPontin are 40% identical). We used a yeast two-hybrid assay to confirm that AtReptin and AtPontin interact, as expected (Figure 4.1D, Figure 4.2).

In most species, *Reptin* and *Pontin* are single copy genes, but the Arabidopsis genome contains a second annotated *Reptin* orthologue previously named *AtTip49b1* (At3g49830) (Holt et al., 2002). At3g49830 is likely a pseudogene, however: no expressed sequence tags for this locus have been detected, microarray analyses have

not found conditions in which this gene is expressed [citation], and we were unable to amplify At3g49830 cDNA by RT-PCR from RNA extracted from whole plants. Moreover, an exonic T-DNA insertion (SALK_036848) in At3g49830 causes no clear phenotypes, whereas a T-DNA insertion (GK-543F01) in At5g67630 is female gametophyte lethal, which demonstrates that At3g49830 cannot complement loss of At5g67630 despite their high amino acid sequence similarity. Finally, At3g49830 contains several polymorphisms at key residues that are conserved in *Reptin* orthologues throughout eukaryotes, including T80I at the conserved Walker A motif, which would severely impair the ability of At3g49830 to bind nucleotides (Figure 1E) (Deyrup et al., 1998). Thus, we conclude that At5g67630 is the only functional Arabidopsis orthologue of *Reptin*.

The *ise4* mutation, A81V, occurs at a conserved residue adjacent to the Walker A motif that presumably interferes with Reptin ATP-binding or ATPase activity (Figure 1E). In other model systems, many of Reptin's functions do not require ATP hydrolysis, such as its role as a chaperone for chromatin remodeling complexes (Etard et al., 2005; Jónsson et al., 2004), but Reptin's ATPase activity is required for the R2TP (RVB1-RVB2-Tah1-Pih1) chaperone complex that contributes to the assembly of small nucleolar ribonucleoproteins (snoRNPs), RNA polymerase II, and PIKK complexes in yeast and mammals (Izumi et al., 2010; Kakihara and Houry, 2012; Kakihara et al., 2014; Nano and Houry, 2013; Venteicher et al., 2008).

Less than 5% of *ise4* seeds germinate on plant culture media (0.5X MS, 0.5% sucrose, 0.8% agar), but the germination rate can be partially rescued by the addition of 10μM gibberellic acid (GA_3), which causes up to ~80% of seeds to germinate. Homozygous *ise4* plants germinated on GA_3 grow slowly, form small leaves, and are chlorotic (Figure 4.3A). Their roots display gravitropic defects, growing 29.1° ± 4.5° from the gravitational axis, versus wild-type roots that grow 10.0° ± 1.0° degrees from the gravitational axis (Figure 4.3A, $p < 0.001$, $n \geq 6$). We used virus-induced gene silencing (VIGS) to compare the effects of acutely knocking down *Reptin* expression with the phenotypes of the weak, potentially ATPase-deficient *ise4* allele (Brunkard et al., 2015c). Plants were infected with *Tobacco rattle virus* (TRV) modified to contain silencing triggers against *Reptin*, *Pontin*, or a negative control (*GUS*). Silencing *Reptin* expression in either *Nicotiana benthamiana* or Arabidopsis, we observed a range of vegetative phenotypes, including chlorosis, smaller and sometimes misshapen leaves, reduced or delayed formation of new leaves, decreased internode length, and increased axillary growth (Figure 4.3B,C). Floral development was also disrupted after silencing *Reptin*: some flowers lacked identifiable petals or sepals, stamens were often green and sterile, and many Arabidopsis siliques were bent or otherwise misshapen (Figure 4.3C). We observed identical phenotypes after using VIGS to knock down expression of Reptin's interacting partner, *Pontin*, in both *N. benthamiana* and Arabidopsis.

The *ise4* transcriptome reveals acceleration of ABI3-regulated seed maturation

To further investigate the effect of *ise4* on *A. thaliana* development, we used RNA-Seq to quantify changes in gene expression between *ise4* and wild-type seeds at the mid-torpedo morphological stage of embryogenesis, when PD transport is restricted in wild-type plants but remains high in *ise4*. 607 genes were upregulated and 627 genes were downregulated in *ise4* compared to its wild-type siblings ($p < 0.05$, $q <$

0.05). The expression of three genes that encode PD proteins were altered, but the pattern of gene expression is not predicted to cause increased PD transport (Table 4.1), suggesting that PD transport is altered by undescribed mechanisms in *ise4*.

Using MapMan gene ontology tools (Thimm et al., 2004), we identified several significantly affected processes in *ise4* ($p < 0.05$ after Benjamini-Hochberg correction): photosynthesis, abiotic stress response, and RNA processing. Dozens of photosynthesis genes are down-regulated in *ise4*, including genes that encode components of both photosystems, RuBisCO and associated proteins involved in carbon fixation, and several enzymes of the Calvin-Benson cycle (Table 4.2). Repression of photosynthesis genes was expected, since *ise4* mutant embryos are chlorotic. The pattern of altered gene expression is distinct from the *ise1* and *ise2* transcriptomes, where many more photosynthesis genes are down-regulated, including most of the genes that encode subunits of light harvesting complex II (Table 4.2). Several abiotic stress response genes are upregulated in *ise4*, mostly related to osmotic stress and drought tolerance, likely due to increased ABA response in *ise4* mutants (see below). Lastly, several small nucleolar RNAs (snoRNAs), which are involved in rRNA processing, do not accumulate in *ise4*, indicating that the R2TP chaperone complex requires Reptin activity (Table 4.3; see below) (Kakihara and Houry, 2012; Kakihara et al., 2014; King et al., 2001; Nano and Houry, 2013).

In addition to the *ise* mutants, our lab also identified a mutant, *dse1*, with extremely reduced PD transport at the mid-torpedo stage of embryogenesis (Xu et al., 2012b). We recently conducted an analysis of the *dse1* transcriptome, which will be described in depth in a forthcoming manuscript. Briefly, the expression of 767 genes was altered in *dse1* mutants compared to wild-type seeds. Photosynthesis-associated nuclear gene expression is repressed in *dse1* (Table 4.2), while expression of genes associated with seed maturation and ABA response are induced in *dse1*.

Despite their opposite PD phenotypes, the *ise4* and *dse1* transcriptomes significantly overlap and are strongly co-regulated (most genes are activated or repressed in both transciptomes) (Figure 4.4A). The *ise1* and *ise2* transcriptomes, on the other hand, are extremely similar to each other but have no significant overlap with *ise4* or *dse1* (Burch-Smith et al., 2011b). Many of the commonly affected genes in the *ise4*/*dse1* transcriptomes are predicted targets of ABI3, a transcription factor that is a master regulator of seed maturation during embryogenesis (Mönke et al., 2012; Yamamoto et al., 2014). ABI3 promotes expression of genes that encode proteins involved in amino acid storage, lipid storage/oleosome genesis, and desiccation tolerance, among other functions (Mönke et al., 2012). Of the 98 genes conservatively identified as the core target regulon of ABI3, 46 are induced in *ise4* and 34 are induced in *dse1*; none of the ABI3 regulon genes are down-regulated *ise4*, and only 3 are repressed in *dse1* (Figure 4.4B, Table 4.4) (Mönke et al., 2012). In contrast, *ise1* and *ise2* both induce only 1 of the ABI3-regulated genes, but each represses 18 ABI3-regulated genes (Figure 4.4B). Genes affected in the *ise4* transcriptome significantly overlap with the transcriptome of *abi3-6* (a null allele of *ABI3*), but as expected, most are not co-regulated (Figure 4.4A) (Nambara et al., 1994; Yamamoto et al., 2014).

Corroborating the transcriptome results, cells in *ise4* embryos more closely resemble older embryonic cells than WT mid-torpedo stage cells (Figure 4.4C). Most conspicuously, *ise4* cells are packed with oleosomes (Figure 4.4C), storage bodies that

are filled with triacylglycerols and surrounded by phospholipids and oleosin proteins (Huang, 1992); *OLEOSIN* genes are induced by ABI3 and strongly upregulated in *ise4* (Table 4.4). In concert, the data from the four transcriptomes indicate that *ise1* and *ise2* embryos are transcriptionally immature compared to wild-type siblings at the same mid-torpedo morphological stage, whereas *dse1* and *ise4* have entered late seed maturation before completing morphological embryogenesis. These results also imply that the ABI3-regulated seed maturation program is not responsible for the transition to restricted PD transport during embryogenesis, since *ise4* and *dse1* have different PD phenotypes but similar early activation of the ABI3 regulon, and *ise1*, *ise2*, and *ise4* have the same increase PD transport phenotype, but opposite ABI3 activity.

The precocious activation of ABI3 may be explained by an increase in ABA synthesis in *ise4* mutants. A crucial regulatory step in ABA synthesis is the irreversible cleavage of epoxycarotenoids from ABA precursors by 9-cis-epoxycarotenoid dioxygenases (NCEDs) (Lefebvre et al., 2006; Nambara and Marion-Poll, 2005). Three *NCED* genes are expressed during seed development, and all three are significantly upregulated in *ise4* mutants (Table 4.5). *NCED6* is also upregulated in *dse1* and *ise2*; in both *ise1* and *ise2*, however, a UDP-glucosyl transferase gene that biochemically inactivates ABA (*UGT71B6*) is induced, which would counteract ABA synthesis (Dong et al., 2014; Priest et al., 2006). The induction of *NCED* expression in *ise4* and *dse1* support the hypothesis that the similarities between the *dse1* and *ise4* transcriptomes, and the differences between *dse1*/*ise4* and *ise1*/*ise2*, are partially due to increased ABA synthesis, ABA signaling, and ABI3 activity. Indeed, increased ABA response is likely responsible for the significant upregulation of abiotic stress-related genes in *ise4*, most of which are involved in osmotic stress or drought response.

ise4 is defective in R2TP activity, but not in Reptin-dependent chromatin remodeling complexes

We next used the *ise4* transcriptome to explore whether any or all of Reptin's functions discovered in other model systems are also affected in *ise4* mutants. Reptin is a crucial component of several chromatin remodeling complexes, including the ATPase-type remodeling complexes, INO80 and SWR1/SWR-C (Nano and Houry, 2013; Rosenbaum et al., 2013). Both INO80 and SWR1 depend on the ATPase activity of their eponymous protein subunits, Ino80 and Swr1, but do not appear to require Reptin or Pontin ATPase activity (Jónsson et al., 2004). We first compared the *ise4* transcriptome directly with the transcriptomes of *ino80* and *swr1* (known as *pie1* in Arabidopsis) null mutants, and found no significant overlap in the affected genes (March-Díaz et al., 2008; Zhang et al., 2015). INO80 and SWR1 catalyze the removal and deposition of the H2A.Z histone variant, so we next compared *ise4* to the list of H2A.Z-enriched gene bodies in Arabidopsis (Coleman-Derr and Zilberman, 2012), and again, there was no significant overlap between these gene lists. For comparison, both the *ino80* and *swr1* transcriptomes did significantly overlap with the list of H2A.Z-enriched genes, as expected. The absence of co-regulated genes in *ise4* versus *ino80*, *swr1*, or the H2A.Z-enriched gene set demonstrates that neither INO80 nor SWR1 function is impaired in *ise4*. This supports the hypothesis that only ATPase activity is disrupted in the ise4 A81V variant of AtReptin, and that ATPase-independent functions

of AtReptin, including participation in INO80 and SWR1 chromatin remodeling, continue in *ise4* seeds.

Reptin is also a component of the TIP60 histone acetyltransferase (HAT) complex. Arabidopsis encodes two redundant orthologues of the core HAT enzyme (the eponymous Tip60), called *HAM1* and *HAM2*. *ham1*;*ham2* double null mutants are female gametophyte lethal (Latrasse et al., 2008), as are null alleles of *reptin* or *pontin* (Holt et al., 2002). *ise4* is not gametophyte lethal, however, and can even survive to form adult plants when treated with GA_3, implying that TIP60 must continue to function in *ise4*. These results also suggest that Reptin ATPase activity is not required for participation in TIP60 histone acetyltransferase activity in Arabidopsis, which has not been tested in other model systems, to our knowledge.

There are significantly lower levels of small nucleolar RNAs (snoRNAs) in *ise4* compared to wild-type (Table 4.3), suggesting that either snoRNAs are transcribed at lower levels, or that snoRNAs are unstable in *ise4*. In animals and yeast, a complex that contains Reptin, called R2TP, promotes snoRNA accumulation and snoRNP stability (Kakihara and Houry, 2012; Kakihara et al., 2014; King et al., 2001; Nano and Houry, 2013). Since snoRNA levels are low in *ise4* mutants, we decided to investigate whether other R2TP-associated functions are disrupted in *ise4*. In animals and yeast, the R2TP complex participates in snoRNP assembly, RNA polymerase II assembly, and phosphatidylinositol-3 kinase-related protein kinase (PIKK) complex assembly. The four components of R2TP are Reptin and Pontin, which are highly conserved across eukaryotes; Tah1/hSpagh (TPR-containing protein associated with HSP90, also known as hSpaghetti), a tetratricopeptide-repeat containing protein that is less well-conserved than Reptin and Pontin; and Pih1 (Protein interacting with HSP90), which is highly divergent in different clades (Kakihara and Houry, 2012). We identified a clear Arabidopsis orthologue of *Spaghetti*, *AtSpagh*, with BLAST searches using human hSpagh as a query; *Spaghetti* orthologues are found throughout plants. Pih1, on the other hand, has no clear orthologues in *Arabidopsis*, and no Pih1 domain-containing proteins are found in seed plants, although bryophytes and seedless vascular plants do have genes predicted to encode Pih1 domain-containing proteins.

The R2TP complex is believed to mediate interactions between the promiscuous HSP90 chaperone and various protein substrates, stabilizing snoRNPs, RNA polymerase II, and PIKK complexes (Izumi et al., 2010; Kakihara and Houry, 2012; Nano and Houry, 2013; Takai et al., 2010). PIKKs are a small family of related kinases that are highly conserved across eukaryotes. Four PIKKs are present in the Arabidopsis genome: ATM and ATR (ATAXIA-TELANGIECTASIA MUTATED, At3g48190, and ATM AND RAD3-RELATED, At5g40820) are both involved in DNA damage response, TRRAP (TRANSFORMATION/TRANSCRIPTION DOMAIN-ASSOCIATED PROTEIN, encoded by two paralogues, At2g17930 and At4g36080) interacts with TIP60 and is involved in histone acetyltransferase activity, and TOR (TARGET OF RAPAMYCIN, At1g50030) is a critical regulator of growth in response to nutritional status (Templeton and Moorhead, 2005). Of the PIKKs in Arabidopsis, only TOR is known to be required for embryogenesis (Menand et al., 2002), so we next pursued whether TOR signaling is disrupted in *ise4*.

In other model systems, a TOR complex (TORC1) is activated through several pathways that sense the availability of free amino acids and glucose (Dibble and

Manning, 2013; Jewell and Guan, 2013; Wullschleger et al., 2006). Orthologues for subunits of a second TOR complex (TORC2) are not found in plants, and so TORC2 will not be discussed here. Like other PIKK complexes, TORC1 assembly is dependent on R2TP. A recent, elegant study of TOR signaling in Arabidopsis showed that TOR is activated by glucose (or sucrose) in a pathway dependent on glycolysis and the mitochondrial electron transport chain, and that glucose-activated TOR promotes root meristem activity (Xiong et al., 2013). In young seedlings grown under low light conditions (depleting endogenous sugar levels), TOR is inactivated and the root meristem becomes quiescent until glucose or sucrose are supplied (whether externally or from photosynthetic tissue). When glucose is added, the expression of 2,368 genes is affected. When *TOR* expression is knocked down by inducible RNAi (Xiong and Sheen, 2012), glucose no longer impacts the expression of these genes, demonstrating that the effects of glucose on quiescent seedlings act through a TOR-dependent pathway. We will refer to this set of 2,368 genes as the glucose-TOR transcriptome.

Glucose-TOR signaling is disrupted in *ise4*

We compared the *ise4* and glucose-TOR transcriptomes, and found significant overlap between the two ($p < 10^{-39}$). Of the 1,234 genes affected in *ise4*, 213 are also affected in the glucose-TOR transcriptome, and 76.5% of these are co-regulated, implying that *ise4* is defective in glucose-TOR signaling (Figure 4.5). Neither the *ise1* nor the *ise2* transcriptomes show any significant overlap with the glucose-TOR transcriptome. The *dse1* transcriptome, however, shows significant overlap ($p < 10^{-3}$), but with opposite effects on gene expression: of the 767 genes affected in *dse1*, 111 are affected in the glucose-TOR transcriptome, but only 21.6% of these are co-regulated. As discussed above, although the *ise4* trancriptome is not significantly similar to the *ise1* or *ise2* transcriptomes, *ise4* is significantly similar to the *dse1* transcriptome; strikingly, one of the most clear transcriptomic difference between *dse1* and *ise4* mutants is the set of genes regulated by glucose-TOR signaling. This supports the hypothesis that TOR signaling is required for the restriction of PD transport during embryogenesis, and encourages speculation that *dse1* may be precociously decreasing PD transport by hyperactivating the glucose-TOR signaling pathway.

tor mutants cannot be directly assayed for a PD phenotype because they are embryo-defective and arrest at the globular stage of embryogenesis, before the transition to restricted PD transport should occur (Wullschleger et al., 2006). Instead, we tested whether TOR activity impacts PD transport in adult *Nicotiana benthamiana* plants by treating leaves with a highly selective inhibitor of TOR kinase activity, AZD-8055, previously shown to inhibit TOR signaling in plants at lower concentrations and with higher specificity than rapamycin (Montané and Menand, 2013). We assayed PD transport in leaves by transiently expressing GFP through agroinfiltration, and then measuring how far GFP moved from a transformed epidermal cell 48 hours after infiltration (Brunkard et al., 2015c). After treatment with 1 µM AZD-8055, an approximately minimal effective concentration (Montané and Menand, 2013), PD transport dramatically increases ($p < 10^{-5}$, $n \geq 90$). In mock treated leaves, GFP moved an average of 1.9 ± 0.1 cells, and in 99% of cells observed, GFP did not move more than 3 cells from the intial transformed cell. In AZD-8055 treated leaves, GFP moved 2.5 ± 0.1 cells on average, and moved 4 or more cells away in 19% of observations.

Thus, TOR signaling negatively regulates PD transport, and the loss of TOR activity in *ise4* mutants could directly explain the *ise* phenotype.

TOR signaling dynamically regulates leaf aging and the sink-to-source transition

TOR is a master regulator of growth and aging in other model systems (Kapahi et al., 2010). We used publicly available transcriptomes of different rosette leaves from 17 day old Arabidopsis plants (Schmid et al., 2005) to determine whether TOR signaling might contribute more broadly to leaf aging in plants, which would support the hypothesis that TOR coordinates the sink-to-source transition. First, we compared gene expression between a very young and a very mature rosette leaf (leaves #2 and #12), which we will call the "young versus old" transcriptome. As predicted, the set of "young versus old" genes significantly overlaps with the glucose-TOR transcriptome ($p < 10^{-193}$), and 86.5% are co-regulated. We then compared changes in gene expression between leaves of similar ages (leaf #2 with leaf #4, leaf #4 with leaf #6, and leaf #6 with leaf #8) to identify genes that continually change in expression during the sink-to-source transition. This "aging" transcriptome also significantly overlaps with the glucose-TOR transcriptome, and 82.5% of the overlapping genes are co-regulated. Thus, activation of TOR by sugars may broadly contribute to regulating leaf aging.

These results suggest a new mechanistic model for how plants partition resources between sinks and sources in plant shoots. In very young, heterotrophic sink leaves, imported sugars and the downstream products of their catabolism (such as ATP) are rapidly consumed as the leaf grows, leaving TOR in an inactive state. As leaves expand and begin to photosynthesize, older sink leaves generate some excess sugars through photosynthesis, which activate glucose-TOR signaling and cause PD transport to decrease. Ultimately, mature source leaves consume a much smaller proportion of the sugars they photosynthesize, causing strong activation of TOR and highly restricted PD transport, which permits older leaves to actively load phloem with their excess sugars for translocation to sink tissues. This model of a measured, fine-tuned system to regulate PD transport agrees with a recent demonstration that PD transport decreases gradually as leaves age, rather than suddenly switching from sink to source status (see previous chapter).

To test this model, we used the GFP movement assay to quantify PD transport in plants after removing sink leaves or after removing source leaves (Figure 4.7) (Mason et al., 2014). In the unaltered plants, GFP moved 2.6 ± 0.1 cells after 48 hours in older sink leaves. In plants without young sink leaves, PD transport was significantly lower, with GFP moving only 2.1 ± 0.1 cells. Conversely, in plants lacking source leaves, PD transport was significantly higher, with GFP moving 3.3 ± 0.1 cells in the older sink leaves. These results agree with the model that TOR coordinates the sink-to-source transition in response to carbohydrate availability. After removing sink tissues, more sugars are available for the older sink leaf, activating TOR and causing decreased PD transport; after removing source tissues, less sugars are available for the older sink leaf, deactivating TOR and causing increased PD transport.

CONCLUSIONS

We propose that glucose-TOR signaling is required for the restriction of PD transport during embryogenesis and during the sink-to-source transition in leaves. This model leads to several new conclusions about the coordination of plant growth and development. More broadly, the combined results of our screen for *ise* and *dse* mutants show that PD transport during embryogenesis is controlled by physiological, rather than strictly developmental, pathways. The decrease in PD transport at the mid-torpedo stage is not caused by initiation of the ABI3 program and ABA responses, since mutants with increased or decreased PD transport show strong activation of ABI3-regulated genes (*ise4* and *dse1*). Instead, PD transport at this stage of embryogenesis is regulated by chloroplast function (as revealed by the *ise1*/*ise2* mutants) and sugar availability (as revealed by the *ise4* mutant).

Current efforts to improve crop yield focus primarily on maximizing nutrient (i.e., fertilizer) use efficiency, increasing overall carbon fixation, and optimizing carbohydrate partitioning across the plant (for example, devoting more resources to seeds in cereal crops, or more resources to vegetative tissue in biofuel crops) (Bihmidine et al., 2013). Modifications to the glucose-TOR signaling pathway hold promise for engineering crops that more efficiently partition resources according to agricultural needs.

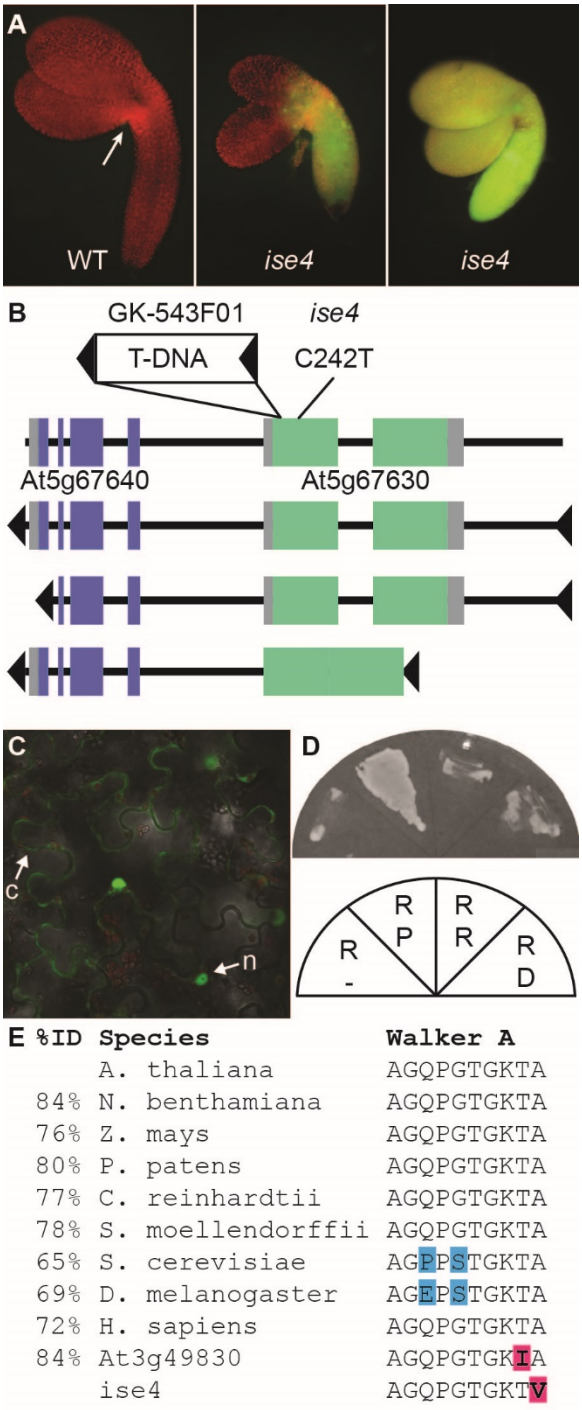

E

%ID	Species	Walker A
	A. thaliana	AGQPGTGKTA
84%	N. benthamiana	AGQPGTGKTA
76%	Z. mays	AGQPGTGKTA
80%	P. patens	AGQPGTGKTA
77%	C. reinhardtii	AGQPGTGKTA
78%	S. moellendorffii	AGQPGTGKTA
65%	S. cerevisiae	AGPPSTGKTA
69%	D. melanogaster	AGEPSTGKTA
72%	H. sapiens	AGQPGTGKTA
84%	At3g49830	AGQPGTGKIA
	ise4	AGQPGTGKTV

Figure 4.1. *ISE4* encodes the Arabidopsis orthologue of Reptin. (A) 10kDa FITC-Dextran does not move beyond the loading site (indicated by white arrow) in wild-type (WT) mid-torpedo stage embryos. In *ise4* mutants, 10kDa FITC-Dextran can rapidly move throughout the shoot-root axis (middle panel) or the entire embryo (right panel), indicating much higher rates of PD transport. (B) *ise4* is a point mutation at nucleotide 242 (C242T) in the coding sequence of At5g67630. A null allele of At5g67630 (GK-543F01) is caused by a T-DNA insertion near the translation start site of the gene.

Three constructs that complemented *ise4* are shown, including the full genomic sequence and promoter (top), the genomic sequence and truncated promoter (middle, missing the start site of At5g67640), and the At5g67630 coding sequence with the full genomic promoter. Open reading frames are shown in color (green or blue), untranslated regions are shown in gray, and T-DNA left and right borders are shown with black arrowheads. (C) AtReptin-GFP localizes to the nucleus (bright circles; one nucleus is labeled “n”) and cytosol (fluorescence near the cell wall; some cytosolic AtReptin-GFP is labeled “c”) in *N. benthamiana* epidermal cells. Green, GFP; red, chlorophyll autofluorescence. (D) Yeast two-hybrid assay confirms that AtReptin and AtPontin interact. Letters indicate bait (top letter) and prey (bottom letter) constructs. -, empty vector; R, AtReptin; P, AtPontin; D, DSE1 (a protein not predicted to interact with AtReptin or AtPontin). (E) Amino acid sequences of Reptin orthologues are highly identical between distantly related eukaryotes (left, %ID). The Walker A or P-loop motif is conserved in Reptin orthologues (exceptions highlighted in cyan), but the Walker A motif is mutated at key residues in the pseudogene paralogue of *AtReptin*, At3g49830, and in *ise4* (residues bold and highlighted in magenta).

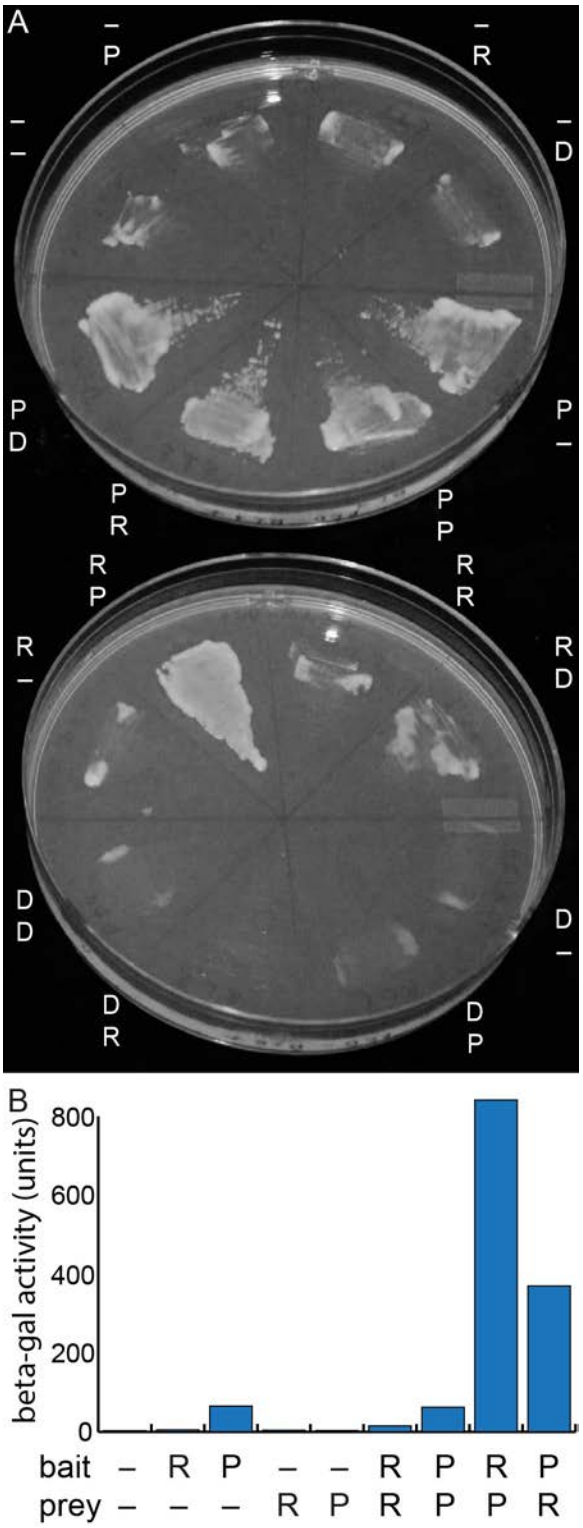

Figure 4.2. Quantitative yeast two-hybrid demonstrates that AtReptin and AtPontin interact. (**A**) Yeast grown on selective media (-Trp –Leu –Ura) containing indicated plasmids. (**B**) Quantification of interaction strength assayed spectrophotometrically by

beta-galactosidase activity of liquid cultures. Top line, bait (pCD); bottom line, prey (pC-ACT); –, no insert; R, AtReptin; P, AtPontin; D, DSE1 (a protein not predicted to interact with AtReptin or AtPontin).

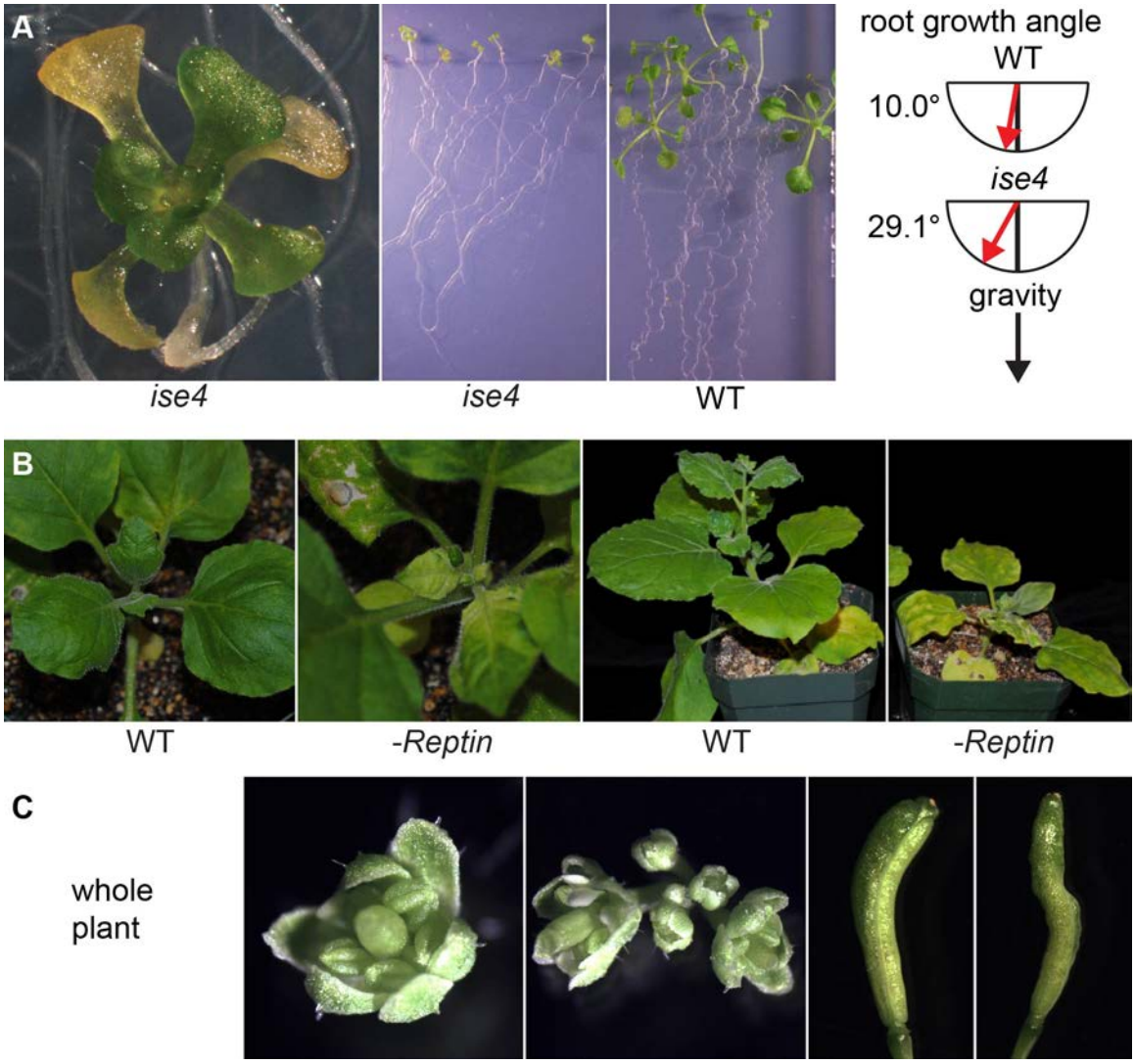

Figure 4.3. *Reptin* regulates root, shoot, and floral plant development. (A) *ise4* seeds germinate after treatment with gibberellic acid (left). *ise4* plants are smaller and more chlorotic than wild-type plants grown under identical conditions (center). *ise4* roots display gravitropic defects. (B) Silencing *NbReptin* in *N. benthamiana* causes chlorosis 14 days post infection (left panels). Over time, silencing *NbReptin* causes delayed development (right panels, 35 days post infection). (C) Silencing *AtReptin* disrupts plant development (left). Some flowers lack petals and/or sepals and have sterile, underdeveloped stamens (center panels). Siliques are curved or misshapen (right panels).

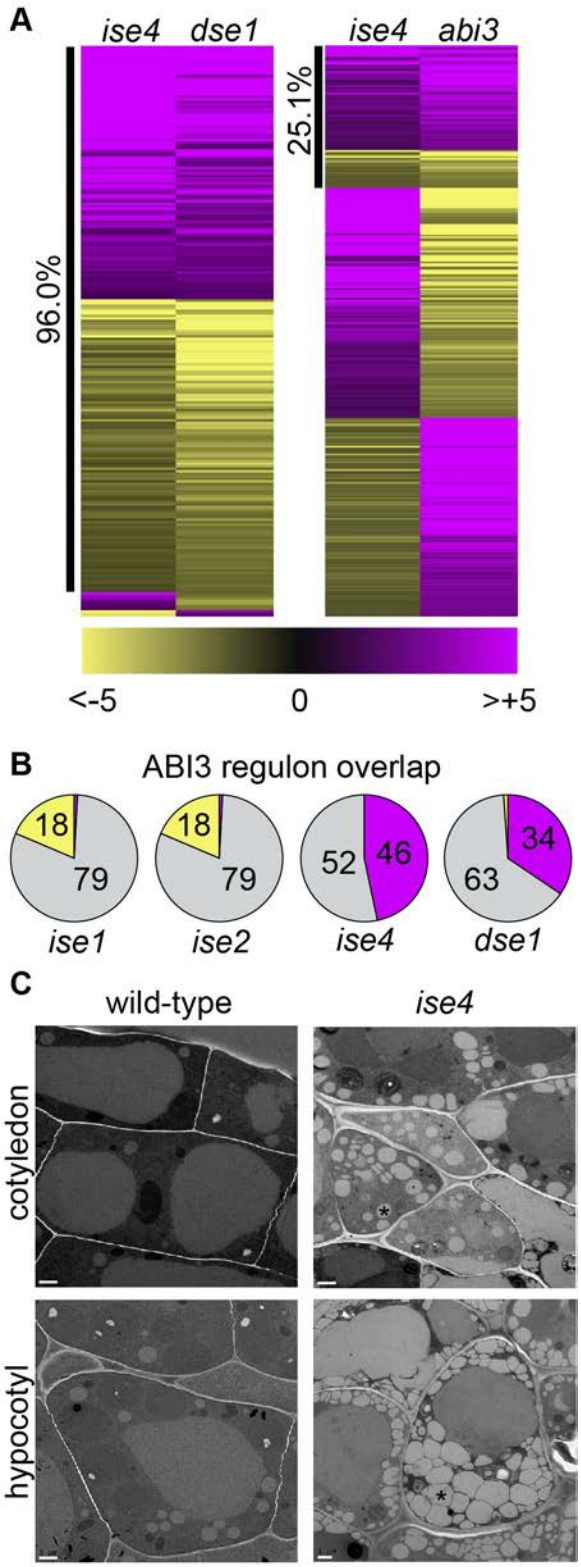

Figure 4.4. (A) The transcriptomes of *ise4* and *dse1* are co-regulated (left), and the transcriptomes of *ise4* and *abi3* are significantly opposite. Each line in the heatmap represents a single gene whose expression is altered in both *ise4* and *dse1*; purple

indicates up-regulation in the mutant and yellow indicates down-regulation in the mutant. (B) Genes in the ABI3 core regulon are down-regulated in *ise1* and *ise2* mutants, but up-regulated in *ise4* and *dse1* mutants (yellow, up-regulated; purple, down-regulated; gray, no significant change in expression). 98 genes are in the ABI3 core regulon; the number of affected genes are indicated in the pie graphs except when ≤ 3. (C) Mid-torpedo stage WT and *ise4* embryos visualized by transmission electron microscopy (TEM). Sections were prepared from either the cotyledons (top) or hypocotyl (bottom) of the embryos. Select oleosomes in *ise4* are labelled with asterisks; oleosomes are unstained and appear pale. White scale bar represents 1 µm.

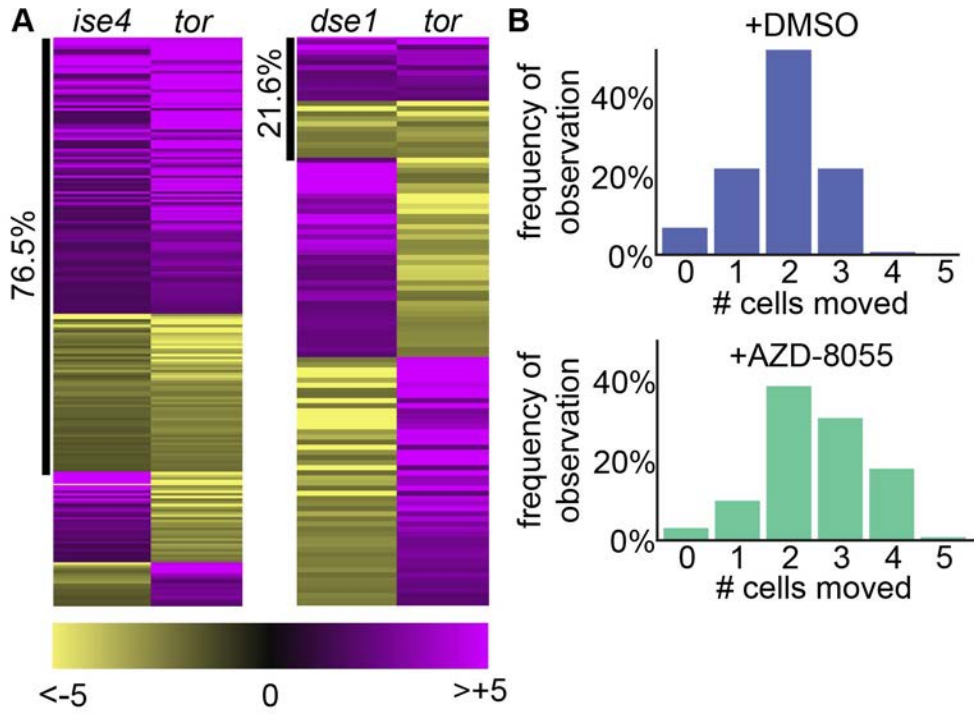

Figure 4.5. TOR signaling regulates PD transport. (A) The *ise4* and glucose-TOR transcriptomes are co-regulated, indicating that *ise4* is defective in TOR signaling. The *dse1* and glucose-TOR transcriptomes signicantly overlap, but have opposite patterns of gene expression. (B) Treating leaves with 1µM AZD-8055, a chemical inhibitor of TOR signaling, causes increased movement of GFP from transformed cells in the epidermis of *N. benthamiana* leaves relative to controls (DMSO). The histograms indicate the frequency of GFP moving the distance indicated.

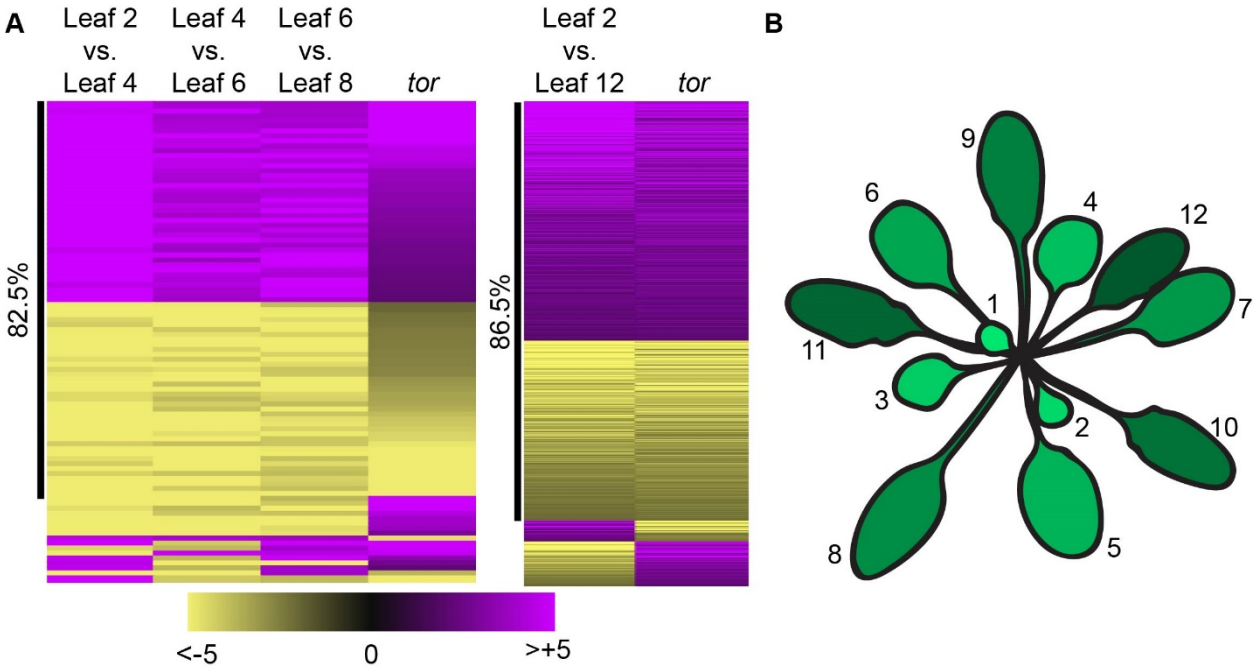

Figure 4.6. Genes regulated by glucose-TOR signaling are differentially expressed as leaves age. (A) The "aging" transcriptome, genes that are differentially expressed as leaves transition from sinks to sources, is co-regulated with the glucose-TOR transcriptome (left). The "young versus old" transcriptome, genes that are differentially expressed between a very young sink leaf and a very mature source leaf, is also co-regulated with the glucose-TOR transcriptome (right). These results imply that glucose-TOR signaling regulates gene expression as leaves age. (B) Illustration of a 17 day old Arabidopsis rosette used to quantify gene expression during leaf development. Leaves are labeled sequentially from youngest (#1) to oldest (#12).

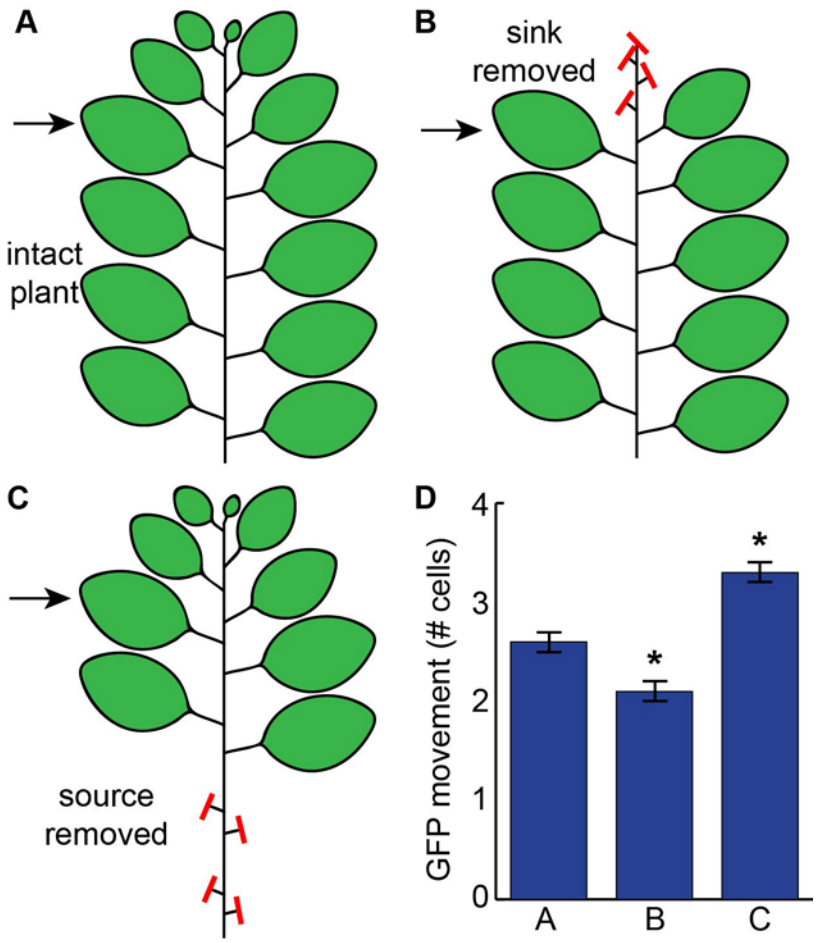

Figure 4.7. PD transport is regulated by sink/source dynamics. (**A–C**) Schematic cartoon of *N. benthamiana* plants used for this experiment. The leaf used for movement assays (leaf #5) is labeled with a black arrow. Leaves removed are indicated by red lines. (**A**) An intact plant. (**B**) A plant with apical sink tissues removed. (**C**) A plant with source leaves removed. (**D**) Average GFP movement away from individual transformed cells in the leaf.

Table 4.1. Changes in expression of genes that encode characterized PD proteins.

TAIR Locus ID	Gene name	Loss-of-function phenotype	Overexpression phenotype	Fold-change in abundance		
				ise4	*ise1*	*ise2*
At1g18650	*PD CALLOSE BINDING PROTEIN 3 (PDCB3)*	No phenotype (redundancy with *PDCB1*, *PDCB2*)	Decreased PD transport (predicted)	-1.8	-3.3	-3.3
At1g70690	*PD LOCALIZED PROTEIN 5 (PDLP5)*	Increased PD transport	Decreased PD transport	6.7		5.5
At2g01660	*PD LOCALIZED PROTEIN 6 (PDLP6)*	Increased PD transport (predicted)	Decreased PD transport (predicted)	2.0		2.2

Table 4.2. Altered expression of photosynthesis-associated nuclear genes.

Biological Function	TAIR Locus ID	Gene Name	Fold-change in expression			
			ise4	*dse1*	*ise1*	*ise2*
Light Harvesting Complex II	At3g27690	Lhcb2.3	-1.8	-7.6		
	At2g34420	Lhcb1.5	1.6			
	At2g40100	Lhcb4.3		-2.1		
	At3g08940	Lhcb4.2		-3.5	-6.9	-8.3
	At1g15820	Lhcb6		-3.3	-5.5	-3.9
	At5g01530	Lhcb4		-2.0	-6.0	-3.4
	At1g29910	Lhcb1.2			-29.4	-4.0
	At4g10340	Lhcb5			-13.1	-5.5
	At2g05100	Lhcb2.1			-4.4	-8.9
	At1g29920	Lhcb1.1			-3.4	-3.5
	At2g05070	Lhcb2.2			-3.3	-9.5
	At2g34430	Lhcb1.4			4.1	
Photosystem II	At1g44575	NPQ4	-1.6			
	At3g55330	PPL1	-3.9	-3.9		
	At1g03600	Psb27	-1.5	-3.4		
	At3g50820	PsbO2	-1.5	-4.1		
	At4g28660	Psb28	-1.5	-2.6		-2.9
	At4g21280	PsbQ1	-1.5	-3.3	-3.2	-3.0
	At3g56650	thylakoid lumenal 20 kDa protein		-4.1		
	At2g28605	PsbP-like protein		-3.0		
	At2g39470	PPL2		-4.6	2.8	
	At3g01440	PsbQ		-3.0		-3.7
	At3g21055	PsbTN		-2.2	-2.8	-3.8
	At5g66570	PsbO1			-6.2	-9.4
	At4g15510	PsbP family protein			-4.7	-2.3
	At4g05180	PsbQ2			-3.7	-6.4
	At1g06680	PsbP-1			-3.2	-4.0
	At2g06520	PsbX			-2.7	-2.9
	At4g37230	33 kDa subunit of PS II				-6.2
Light Harvesting Complex I	At1g19150	Lhca6	-3.0	-3.1	-4.6	
	At3g61470	Lhca2	-1.8			
	At1g61520	Lhca3		-2.1		
	At5g28450	Lhca2-like protein			-2.6	-2.8
	At1g34000	OHP2			-2.7	
	At3g47470	Lhca4			-2.1	
Photosystem I	At1g55670	PsaG	-1.6			
	At1g52230	PsaH2	-1.7	-3.6		
	At4g28750	PsaE1	-1.5		-5.7	-5.7
	At1g31330	PsaF	-1.5		-3.0	-3.2
	At1g03130	PsaD2		-2.8	-3.1	-10.4
	At2g20260	PsaE2		-2.5	-2.8	
	At2g46820	PsiP		-2.2		
	At4g12800	PsaL			-8.2	-2.6
	At3g16140	PsaH1			-7.3	-11.5
	At1g08380	PsaO			-5.1	-6.6
	At4g02770	PsaD1			-2.7	-3.5
	At1g30380	PsaK			-2.1	-2.2

Table 4.2, continued.

Biological Function	TAIR Locus ID	Gene Name	Fold-change in expression			
			ise4	*dse1*	*ise1*	*ise2*
State Transition	At4g01330	protein kinase				-5.4
ATP synthase	At4g04640	AtpC1	-1.5	-2.3	-2.4	-2.7
	At4g09650	AtpD			-3.4	-3.4
	At2g31040	ATP synthase family			2.2	
	At4g32260	ATP synthase family				-2.6
Cyclic e- Transport	At2g05620	PGR5	-3.0	-3.9	-2.4	
Plastocyanin	At1g20340	PETE2	-1.6	-2.3	-15.7	-6.4
	At1g76100	PETE1		-4.2		
Ferredoxin / Ferredoxin reductase	At4g32590	Ferredoxin-related	-2.0			
	At5g66190	FNR1	-1.8	-2.0		
	At1g20020	FNR2	-3.1	-4.6	-3.2	-2.9
	At3g16250	NDF4		-4.4		
	At1g74880	NdhO		-3.6		
	At2g01590	CRR3		-3.1		
	At4g32360	Ferredoxin reductase			-2.8	-3.2
	At1g10960	AtFD1			-2.3	-2.1
	At1g02180	Ferredoxin-related			-2.6	
	At1g15140	Oxidoreductase family protein			4.7	
Photorespiration	At1g12550	Oxidoreductase family protein	-1.7			
	At2g35370	GDCH	-2.8	-5.8		
	At1g68010	HPR	-1.9	-3.4		
	At2g13360	AGT1	-1.7	-2.5		
	At3g14420	GOX1	-1.7	-3.7	-2.2	-2.2
	At1g11860	Aminomethyltransferase	-1.6		-4.0	-3.7
	At1g32470	Gly cleavage system H protein		-11.4	-4.3	-3.2
	At3g14415	GOX2		-3.7	-2.1	-2.2
	At4g33010	AtGLDP1			-2.4	-5.7
	At3g14130	HAOX1			-2.2	
	At1g79870	Oxidoreductase family protein			2.4	3.1
Calvin-Benson Cycle	At3g55800	SBPASE	-1.5			
	At5g38420	RbcS-2B	-3.2			
	At3g54050	FBPase	-2.8	-7.5		
	At5g38410	RbcS-3B	-2.8	-4.3		
	At2g39730	RCA	-1.8	-2.2		
	At1g42970	GAPB	-1.7	-2.8		
	At1g55490	Cpn60B	-2.1			-2.6
	At4g20130	PTAC14	-2.0			-3.5
	At1g32060	PRK	-2.1	-2.4	-3.1	-6.4
	At3g26650	GAPA-1	-1.6	-2.5	-2.4	-4.7
	At1g12900	GAPA-2	-1.5	-3.2	-2.8	-13.3
	At4g38970	FBPase	-2.3	-3.0	2.5	-3.7
	At5g38430	RbcS-1B		-5.7		
	At3g04790	Ribose 5-phosphate isomerase		-2.3		
	At2g21330	FBPase		-2.3		
	At3g12780	PGK1			-2.9	
	At2g28000	Cpn60A			2.3	6.6
	At1g79530	GAPCP-1			2.9	2.3
	At1g56190	PGK				4.5

Table 4.3. Small nucleolar RNA (snoRNA) abundance in wild-type versus *ise4* seeds for all snoRNA loci annotated by TAIR and detected in both wild-type and *ise4* transcriptomes. FPKM, **f**ragments **p**er **k**b transcript per **m**illion mapped reads.

TAIR Locus ID	FPKM		Fold-change in abundance	Statistical Signficance		
	WT	*ise4*		*p* value	*q* value	significant?
At2g20721	118.5	3.1	-37.86	0.00	0.01	yes
At5g44286	687.6	25.4	-27.03	0.21	0.56	-
At2g43138	281.2	16.4	-17.14	0.42	0.74	-
At4g02555	2877.4	178.0	-16.16	0.02	0.14	-
At1g12015	754.3	63.2	-11.94	0.07	0.34	-
At5g66562	728.0	69.4	-10.48	0.07	0.34	-
At1g03743	198.8	19.7	-10.09	0.38	0.72	-
At1g29071	402.7	42.9	-9.38	0.06	0.31	-
At3g01316	4445.2	493.6	-9.01	0.00	0.05	yes
At3g01313	185.5	28.7	-6.46	0.23	0.58	-
At1g03746	297.9	56.7	-5.25	0.16	0.50	-
At1g75163	4580.2	1059.6	-4.32	0.18	0.52	-
At1g03935	397.6	95.7	-4.15	0.12	0.44	-
At2g35387	5212.9	1359.6	-3.83	0.00	0.03	yes
At4g03295	3587.6	960.4	-3.74	0.01	0.09	-
At3g47342	10243.1	2748.6	-3.73	0.00	0.00	yes
At5g10572	156.0	46.0	-3.39	0.08	0.35	-
At5g51174	2905.9	934.7	-3.11	0.00	0.01	yes
At5g66564	615.0	206.9	-2.97	0.13	0.46	-
At4g25631	1463.4	502.8	-2.91	0.47	0.78	-
At4g39361	14658.5	4550.7	-2.73	0.00	0.05	-
At5g41471	422.7	157.8	-2.68	0.08	0.36	-
At3g27865	343.8	137.9	-2.49	0.22	0.57	-
At5g13225	4697.0	2021.9	-2.32	0.01	0.11	-
At1g12013	8066.8	3556.0	-2.27	0.00	0.00	yes
At1g74453	78.7	35.8	-2.20	0.14	0.48	-
At1g20015	250.8	115.6	-2.17	0.34	0.68	-
At3g24612	27379.8	13228.9	-2.07	0.00	0.01	yes
At1g19376	432.4	210.0	-2.06	0.27	0.62	-
At3g47347	32.7	16.0	-2.04	0.36	0.70	-
At1g19373	113.5	58.3	-1.95	0.65	0.88	-
At4g15258	900.6	491.4	-1.83	0.05	0.29	-
At3g58193	179.9	102.6	-1.75	0.60	0.86	-
At3g13525	142.0	87.7	-1.62	0.63	0.87	-
At3g21805	12806.4	8214.2	-1.56	0.16	0.50	-
At4g39363	2587.6	1917.1	-1.45	0.57	0.84	-
At3g58196	163.4	125.7	-1.30	0.85	0.96	-
At4g05048	123.2	101.8	-1.21	0.72	0.91	-
At5g53902	683.2	621.0	-1.10	0.42	0.75	-
At5g54075	1146.1	1269.3	1.11	0.39	0.73	-
At3g50825	67.0	83.3	1.24	0.84	0.95	-
At5g52471	20.8	133.7	6.44	0.51	0.81	-

Table 4.4. Altered expression of genes identified in the ABI3 conservative core regulon.

TAIR Locus ID	Gene Name	Fold-Change in Expression			
		ise4	*dse1*	*ise1*	*ise2*
At2g21490	LEA family	1046.9	8.1		
At1g04560	AWPM 19	1038.1	31.4	-14.0	-3.3
At2g19320	Unknown	1008.8			
At5g45690	Unknown	1008.7			
At1g54870	Oxidoreductase	1003.3	7.3		-7.0
At2g23640	Reticulan like protein B13	1002.9			
At2g42000	Metallothionein 4	1001.8			
At4g18920	Unknown	1001.6			
At4g39130	LEA family	1001.5			
At5g18450	AP2-domain transcription factor	1001.1			
At3g21380	Mannose-binding lectin family	1000.8			
At4g28520	Cruciferin 3	510.6			
At1g03880	Cruciferin 2	268.8	2.9	-2.5	-2.3
At5g54740	Seed storage albumin 5	74.6			
At2g28420	Glyoxylase I family protein	56.5	10.8		
At4g27150	Seed storage albumin 2	55.1			
At5g22470	NAD+ ADP-ribosyltransferase	39.2	3.6	-6.4	-3.2
At5g07190	Seed gene 3	28.3		-2.7	-3.6
At4g26740	Seed gene 1	21.3		-4.7	
At3g15670	LEA family	17.9	108.9		
At5g55240	Peroxygenase 2	15.5			
At1g73190	Aquaporin-like superfamily	14.1			
At1g27990	Unknown	13.3	6.8		-4.1
At5g44120	RmlC-like cupins superfamily protein	12.8			
At4g16160	AtOEP16-2	12.3	2.2		-2.1
At3g22640	Cupin family	12.0		-3.7	-3.7
At2g31980	Phytocystatin 2	11.2			
At1g48130	1-cysteine peroxiredoxin 1	10.7			
At2g28490	RmlC-like cupins superfamily protein	9.3			
At1g32560	LEA family	8.0	4.7	-16.5	
At1g72100	LEA family	7.7	12.0		
At5g01300	PEBP family	6.8	2.2		
At1g17810	Beta-tonoplast intrinsic protein	6.5	-2.1	-5.3	-4.2
At3g63040	Unknown	5.5			
At2g25890	Oleosin family	5.2	2.5		
At1g27461	Unknown	4.6			
At4g25140	Oleosin 1	4.3			
At3g18570	Oleosin family	4.0			
At5g01670	NAD(P)-linked oxidoreductase family	3.4	3.4	-2.2	-2.5
At1g54860	Glycoprotein membrane precursor GPI-ar	3.4	-2.8		
At3g12203	Ser Carboxypeptidase-like 17	2.9		-4.9	-2.2
At5g40420	Oleosin 2	2.6			
At3g27660	Oleosin 4	2.6			
At3g54940	Papain family Cys protease	2.4			
At3g01570	Oleosin family	2.1			
At5g51210	Oleosin 3	1.8			

Table 4.4, continued.

TAIR Locus ID	Gene Name	Fold-Change in Expression			
		ise4	*dse1*	*ise1*	*ise2*
At3g51810	LEA family		213.4		
At5g06760	LEA family		87.6		
At2g35300	LEA family		24.4		
At2g42560	LEA family		19.7	2.3	
At3g53040	LEA family		18.8		
At2g15010	Plant thionin		12.3		
At5g44310	LEA family		10.7		-6.3
At4g21020	LEA family		9.5		
At2g21820	Unknown		8.9		
At4g27140	seed storage albumin 1		7.7		
At5g07330	Unknown		6.7		
At2g47770	Seed Trp-rich sensory protein		6.6		
At3g15280	Unknown		6.1	-2.9	
At2g36640	Embryonic cell protein 63		5.0	-7.3	-10.6
At2g18340	LEA family		4.1		
At3g50980	LEA family		3.8		8.9
At5g43770	Pro-rich family protein		3.3		
At1g05510	Unknown		3.1		
At5g04000	Unknown		3.0		
At3g58450	Adenine hydrolase-like family		2.7		
At5g09640	Ser Carboxypeptidase-like 19		-2.3	-2.9	-2.1
At5g16460	Seipin			-12.5	-2.4
At4g27530	Unknown			-6.1	-5.3
At1g03890	RmlC-like cupins family			-3.5	-5.7
At4g10020	Hydroxysteroid dehydrogenase 5			-3.4	-5.8
At5g24130	Unknown			-2.1	

Table 4.5. Genes encoding ABA metabolism enzymes with significantly altered expression in *ise1*, *ise2*, *ise4*, and *dse1* mutant seeds.

TAIR Locus ID	Gene Name	Enzyme Function	Fold-change in abundance			
			ise1	***ise2***	***ise4***	***dse1***
At3g21780	*UGT71B6*	ABA inactivation	2.3	2.1		
At3g14440	*NCED3*	ABA synthesis			6.4	
At3g24220	*NCED6*	ABA synthesis		2.2	3.8	2.3
At1g78390	*NCED9*	ABA synthesis			2.9	

Table 4.6. List of transcriptomes included in this study.

Transcriptome	Condition A	Condition B	Platform	Analysis	Citation
ise4	*ise4-1*/+ and +/+ mid-torpedo seed	*ise4-1* mid-torpedo seed	RNA-Seq (Ion Torrent Proton Chip)	Analyzed here	
ise1	*ise1-1*/+ and +/+ mid-torpedo seed	*ise1-1* mid-torpedo seed	Microarray (Affymetrix 1.0R Tiling Array)	Previously analyzed	
ise2	*ise2-1*/+ and +/+ mid-torpedo seed	*ise2-1* mid-torpedo seed	Microarray (Affymetrix 1.0R Tiling Array)	Previously analyzed	
dse1	*dse1-1*/+ and +/+ mid-torpedo seed	*dse1-1* mid-torpedo seed	Microarray (Affymetrix 1.0R Tiling Array)	Previously analyzed	
abi3	Col-0 bent-cotyledon seed	*abi3-6* bent-cotyledon seed	Microarray (Affymetrix ATH1 22k Genome Array)	Analyzed here	
ino80	Col-0 12 d old seedlings	*ino80-5* 12 d old seedlings	Microarray (Agilent Arabidopsis 4 x44k Array)	Previously analyzed	
swr1	Col-0 14 d old plants	*pie1-5* 14 d old plants	Microarray (Affymetrix ATH1 22k Genome Array)	Previously analyzed	
glucose-TOR	Glucose-treated quiescent seedlings (uninduced TOR-RNAi)	Glucose-treated quiescent seedlings, TOR-RNAi induced	Microarray (Affymetrix ATH1 22k Genome Array)	Previously analyzed	
"young vs. old"	Leaf #2, 17 d old Col-0 plant	Leaf #12, 17 d old Col-0 plant	Microarray (Affymetrix ATH1 22k Genome Array)	Analyzed here	
"aging"	Leaf #2, 17 d old Col-0 plant	Leaf #4, 17 d old Col-0 plant	Microarray (Affymetrix ATH1 22k Genome Array)	Analyzed here	
	Leaf #4, 17 d old Col-0 plant	Leaf #6, 17 d old Col-0 plant	Microarray (Affymetrix ATH1 22k Genome Array)	Analyzed here	
	Leaf #6, 17 d old Col-0 plant	Leaf #8, 17 d old Col-0 plant	Microarray (Affymetrix ATH1 22k Genome Array)	Analyzed here	

METHODS

Next-generation Mapping of *ise4*

ise4 was identified from a population embryo-defective ethyl methane sulfonate-mutagenized *A.thaliana* Landsberg *erecta* (L*er*) lines, as previously described (Kim et al., 2002; Kobayashi et al., 2007; Stonebloom et al., 2009). The mutated locus was mapped to a 120kbp region between the polymorphism PERL1125350 and the end of chromosome 5. Due to low recombination rates in this region, we used next-generation mapping to identify the causal mutation. 18 overlapping genomic fragments between 8 and 9 kbp long were amplified with iProof high-fidelity DNA polymerase (Bio-Rad Laboratories) from genomic DNA isolated from homozygous *ise4* mutants. The fragments were purified by gel extraction, and pooled in equal concentrations to …

ise4 was complemented with three different constructs. A long genomic sequence was composed of ~2.4kb upstream of At5g67630, the At5g67630 gene, and ~1kb downstream of At5g67630. A gene of unknown function, At5g67640, is within the ~2.4kb region upstream of At5g67630; no SNPs were identified in At5g67640 between WT and *ise4*, but to be sure that expression of At5g67640 did not affect the *ise4* phenotype, a short genomic sequence lacking the At5g67640 translation start site was also constructed, and this sequence complemented *ise4*. Finally, the ~2.4kb upstream sequence was used to drive expression of the coding sequence of At5g67630 cloned from Arabidopsis cDNA; this construct also complemented *ise4*. Complementation was performed by transforming *ise4*/+ heterozygotes with the floral dip method and testing for rescue of the embryo-defective phenotype.

RNA-Seq and transcriptome analysis

Homozygous *ise4* seeds at the mid-torpedo stage of embryogenesis and their wild-type or heterozygous mid-torpedo stage siblings were collected as previously described and stored at -80°C in RNAlater [ref]. For each pooled RNA sample, approximately 100-150 seeds were collected, and four replicates were collected (three replicates were used for RNA-Seq, the fourth replicate was used for RT-qPCR verification of RNA-Seq results). RNA was isolated with the Spectrum Plant Total RNA (Sigma-Aldrich) with on-column DNase I digestion (New England Biolabs). RNA was treated with RiboMinus (Life Technologies) to deplete 16S, 18S, 23S, and 25S rRNA, and then used to prepare Ion Torrent libraries with the Ion Total RNA-Seq Kit v2 (Life Technologies).

Libraries were sequenced with an Ion Proton I Chip. Torrent Suite Software was used to filter polyclonal reads, adapter dimers, reads of very low quality, and to trim 5' adapter and repetitive sequences. The remaining computational steps were completed using an instance of Galaxy. FASTQ Quality Trimmer was then used to remove low quality 3' ends (window size 10, step size 1, quality score ≥ 20) from reads, then reads were filtered with Filter FASTQ to remove reads less than 25 bp long.

To determine differences in gene expression between *ise4* and WT seeds, RNA-Seq results were compared using the Tuxedo Suite. Reads were mapped with TopHat2 to the L*er* genome and assembled into transcripts with Cufflinks. Cuffmerge was used to assemble the transcriptome with a L*er* reference transcriptome. Cuffdiff2 was used

to generate a list of differentially expressed genes comparing three replicates of *ise4* seeds with three replicates of WT seeds ($p < 0.05$, $q < 0.05$).

The *ise4* transcriptome was analyzed using MapMan software, which assigns genes to various categories based on their biological function and uses a Wilcoxon rank sum test, corrected with the Benjamini-Hochberg procedure to reduce the false positive rate, to identify categories that are significantly altered in gene expression. Gene lists from different transcriptomes were compared using a hypergeometric test for significant overlap using R software. Within the subset of overlapping genes, any genes that were up-regulated or down-regulated (regardless of the measured fold-change in expression) in all transcriptomes were considered “co-regulated”.

Transcriptomes included in this study are listed in Table 4.7. Several microarray experiments were reanalyzed here (as indicated Table 4.7) using the sensitive rank product method with MeV software.

REFERENCES

Amari, K., Boutant, E., Hofmann, C., Schmitt-Keichinger, C., Fernandez-Calvino, L., Didier, P., Lerich, A., Mutterer, J., Thomas, C.L., Heinlein, M., et al. (2010). A family of plasmodesmal proteins with receptor-like properties for plant viral movement proteins. PLoS Pathog. *6*, e1001119.

Aoki, N., and Hirose, T. (2012). Sucrose Transport in Higher Plants: From Source to Sink. In Photosynthesis, J. Eaton-Rye, B. Tripathy, and T. Sharkey, eds. (New York: Springer), pp. 703–729.

Avendaño-Vázquez, A.-O., Cordoba, E., Llamas, E., San Román, C., Nisar, N., De la Torre, S., Ramos-Vega, M., Gutiérrez-Nava, M.D.L.L., Cazzonelli, C.I., Pogson, B.J., et al. (2014). An Uncharacterized Apocarotenoid-Derived Signal Generated in ζ-Carotene Desaturase Mutants Regulates Leaf Development and the Expression of Chloroplast and Nuclear Genes in Arabidopsis. Plant Cell *26*, 2524–2537.

Balkunde, R., Bouyer, D., and Hulskamp, M. (2011). Nuclear trapping by GL3 controls intercellular transport and redistribution of TTG1 protein in Arabidopsis. Development *138*, 5039–5048.

Barkan, A. (2011). Expression of plastid genes: organelle-specific elaborations on a prokaryotic scaffold. Plant Physiol. *155*, 1520–1532.

Bell, C.D., Soltis, D.E., and Soltis, P.S. (2010). The age and diversification of the angiosperms re-revisited -- Bell et al. 97 (8): 1296 -- American Journal of Botany. Am. J. Bot. *97*, 1296–1303.

Benitez-Alfonso, Y., Cilia, M., San Roman, A., Thomas, C., Maule, A., Hearn, S., and Jackson, D. (2009). Control of Arabidopsis meristem development by thioredoxin-dependent regulation of intercellular transport. Proc. Natl. Acad. Sci. U. S. A. *106*, 3615–3620.

Benitez-Alfonso, Y., Faulkner, C., Pendle, A., Miyashima, S., Helariutta, Y., and Maule, A. (2013). Symplastic Intercellular Connectivity Regulates Lateral Root Patterning. Dev. Cell *26*, 136–147.

Benkovics, A.H., and Timmermans, M.C.P. (2014). Developmental patterning by gradients of mobile small RNAs. Curr. Opin. Genet. Dev. *27*, 83–91.

Bihmidine, S., Hunter, C.T., Johns, C.E., Koch, K.E., and Braun, D.M. (2013). Regulation of assimilate import into sink organs: update on molecular drivers of sink strength. Front. Plant Sci. *4*, 177.

Bischoff, M., Gradilla, A.-C., Seijo, I., Andrés, G., Rodríguez-Navas, C., González-Méndez, L., and Guerrero, I. (2013). Cytonemes are required for the establishment of a

normal Hedgehog morphogen gradient in Drosophila epithelia. Nat. Cell Biol. *15*, 1269–1281.

Bouyer, D., Geier, F., Kragler, F., Schnittger, A., Pesch, M., Wester, K., Balkunde, R., Timmer, J., Fleck, C., and Hülskamp, M. (2008). Two-dimensional patterning by a trapping/depletion mechanism: The role of TTG1 and GL3 in Arabidopsis trichome formation. PLoS Biol. *6*, 1166–1177.

Brocard-Gifford, I., Lynch, T.J., Garcia, M.E., Malhotra, B., and Finkelstein, R.R. (2004). The Arabidopsis thaliana ABSCISIC ACID-INSENSITIVE8 encodes a novel protein mediating abscisic acid and sugar responses essential for growth. Plant Cell *16*, 406–421.

Brunkard, J., Runkel, A., and Zambryski, P. (2015a). The cytosol must flow: intercellular transport through plasmodesmata. Curr. Opin. Cell Biol. *35*, 13–20.

Brunkard, J., Runkel, A., and Zambryski, P. (2015b). Chloroplasts extend stromules independently and in response to internal redox signals. Proc. Natl. Acad. Sci. USA.

Brunkard, J.O., Runkel, A.M., and Zambryski, P.C. (2013). Plasmodesmata dynamics are coordinated by intracellular signaling pathways. Curr. Opin. Plant Biol. *16*, 614–620.

Brunkard, J.O., Burch-Smith, T.M., Runkel, A.M., and Zambryski, P. (2015c). Investigating plasmodesmata genetics with virus-induced gene silencing and an agrobacterium-mediated GFP movement assay. Methods Mol. Biol. *1217*, 185–198.

Burch-Smith, T.M., and Zambryski, P.C. (2010). Loss of increased size exclusion limit (ise)1 or ise2 increases the formation of secondary plasmodesmata. Curr. Biol. *20*, 989–993.

Burch-Smith, T.M., and Zambryski, P.C. (2012). Plasmodesmata Paradigm Shift: Regulation from Without Versus Within. Annu. Rev. Plant Biol. *63*, 239–260.

Burch-Smith, T.M., Stonebloom, S., Xu, M., and Zambryski, P.C. (2011a). Plasmodesmata during development: Re-examination of the importance of primary, secondary, and branched plasmodesmata structure versus function. Protoplasma *248*, 61–74.

Burch-Smith, T.M., Brunkard, J.O., Choi, Y.G., and Zambryski, P.C. (2011b). PNAS Plus: Organelle-nucleus cross-talk regulates plant intercellular communication via plasmodesmata. Proc. Natl. Acad. Sci. *108*, E1451–E1460.

Carlotto, N., Wirth, S., Furman, N., Ferreyra Solari, N., Ariel, F., Crespi, M., and Kobayashi, K. (2015). The chloroplastic DEVH-box helicase ISE2 involved in plasmodesmata regulation is required for group II intron splicing. Plant. Cell Environ. n/a – n/a.

Chen, X.-Y., Liu, L., Lee, E., Han, X., Rim, Y., Chu, H., Kim, S.-W., Sack, F., and Kim, J.-Y. (2009). The Arabidopsis callose synthase gene GSL8 is required for cytokinesis and cell patterning. Plant Physiol. *150*, 105–113.

Chi, W., Sun, X., and Zhang, L. (2013). Intracellular signaling from plastid to nucleus. Annu. Rev. Plant Biol. *64*, 559–582.

Coleman-Derr, D., and Zilberman, D. (2012). Deposition of Histone Variant H2A.Z within Gene Bodies Regulates Responsive Genes. PLoS Genet. *8*.

Crawford, K.M., and Zambryski, P.C. (2000). Subcellular localization determines the availability of non-targeted proteins to plasmodesmatal transport. Curr. Biol. *10*, 1032–1040.

Crawford, K.M., and Zambryski, P.C. (2001a). Non-targeted and targeted protein movement through plasmodesmata in leaves in different developmental and physiological states. Plant Physiol. *125*, 1802–1812.

Crawford, K.M., and Zambryski, P.C. (2001b). Non-targeted and targeted protein movement through plasmodesmata in leaves in different developmental and physiological states. Plant Physiol. *125*, 1802–1812.

Cui, H., Levesque, M.P., Vernoux, T., Jung, J.W., Paquette, A.J., Gallagher, K.L., Wang, J.Y., Blilou, I., Scheres, B., and Benfey, P.N. (2007). An evolutionarily conserved mechanism delimiting SHR movement defines a single layer of endodermis in plants. Science *316*, 421–425.

Daum, G., Medzihradszky, A., Suzaki, T., and Lohmann, J.U. (2014). A mechanistic framework for noncell autonomous stem cell induction in Arabidopsis. Proc. Natl. Acad. Sci. U. S. A. *111*, 14619–14624.

Dettmer, J., Wu, S., Stierhof, Y., Miyashima, S., Yadav, S.R., Roberts, C.J., Campilho, A., Bulone, V., and Lichtenberger, R. (2011). Vate´ n A, D, : Callose biosynthesis regulates symplastic trafficking during root development. Dev Cell *21 SRC* - , 1144–1155.

Deyrup, A.T., Krishnan, S., Cockburn, B.N., and Schwartz, N.B. (1998). Deletion and site-directed mutagenesis of the ATP-binding motif (P- loop) in the bifunctional murine ATP-sulfurylase/adenosine 5'-phosphosulfate kinase enzyme. J. Biol. Chem. *273*, 9450–9456.

Dibble, C.C., and Manning, B.D. (2013). Signal integration by mTORC1 coordinates nutrient input with biosynthetic output. Nat. Cell Biol. *15*, 555–564.

Dong, T., Xu, Z.-Y., Park, Y., Kim, D.H., Lee, Y., and Hwang, I. (2014). Abscisic acid uridine diphosphate glucosyltransferases play a crucial role in abscisic acid homeostasis in Arabidopsis. Plant Physiol. *165*, 277–289.

Ehlers, K., and Große Westerloh, M. (2014). Developmental control of plasmodesmata frequency, structure, and function. In Symplasmic Transport in Vascular Plants, K. Sokołowska, and P. Sowiński, eds. (New York: Springer), pp. 41–82.

Epel, B.L., and Erlanger, M. a. (1991). Light regulates symplastic communication in etiolated corn seedlings. Physiol. Plant. *83*, 149–153.

Erickson, J.L., Ziegler, J., Guevara, D., Abel, S., Klösgen, R.B., Mathur, J., Rothstein, S.J., and Schattat, M.H. (2014). Agrobacterium-derived cytokinin influences plastid morphology and starch accumulation in Nicotiana benthamiana during transient assays. BMC Plant Biol. *14*, 127.

Estavillo, G.M., Crisp, P. a., Pornsiriwong, W., Wirtz, M., Collinge, D., Carrie, C., Giraud, E., Whelan, J., David, P., Javot, H., et al. (2011). Evidence for a SAL1-PAP Chloroplast Retrograde Pathway That Functions in Drought and High Light Signaling in Arabidopsis. Plant Cell *23*, 3992–4012.

Etard, C., Gradl, D., Kunz, M., Eilers, M., and Wedlich, D. (2005). Pontin and Reptin regulate cell proliferation in early Xenopus embryos in collaboration with c-Myc and Miz-1. Mech. Dev. *122*, 545–556.

Faulkner, C., Petutschnig, E., Benitez-Alfonso, Y., Beck, M., Robatzek, S., Lipka, V., and Maule, A.J. (2013). LYM2-dependent chitin perception limits molecular flux via plasmodesmata. Proc. Natl. Acad. Sci. U. S. A. *110*, 9166–9170.

Fernandez-Calvino, L., Faulkner, C., Walshaw, J., Saalbach, G., Bayer, E., Benitez-Alfonso, Y., and Maule, A. (2011). Arabidopsis plasmodesmal proteome. PLoS One *6*, e18880.

Fichtenbauer, D., Xu, X.M., Jackson, D., and Kragler, F. (2012). The chaperonin CCT8 facilitates spread of tobamovirus infection. Plant Signal. Behav. *7*, 318–321.

Fitzgibbon, J., Bell, K., King, E., and Oparka, K. (2010). Super-resolution imaging of plasmodesmata using three-dimensional structured illumination microscopy. Plant Physiol. *153*, 1453–1463.

Fitzgibbon, J., Beck, M., Zhou, J., Faulkner, C., Robatzek, S., and Oparka, K. (2013). A developmental framework for complex plasmodesmata formation revealed by large-scale imaging of the Arabidopsis leaf epidermis. Plant Cell *25*, 57–70.

Furuta, K., Lichtenberger, R., and Helariutta, Y. (2012). The role of mobile small RNA species during root growth and development. Curr. Opin. Cell Biol. *24*, 211–216.

Gallagher, K.L., Sozzani, R., and Lee, C.-M. (2014). Intercellular Protein Movement: Deciphering the Language of Development.

Gisel, a, Barella, S., Hempel, F.D., and Zambryski, P.C. (1999). Temporal and spatial regulation of symplastic trafficking during development in Arabidopsis thaliana apices. Development *126*, 1879–1889.

Gisel, A., Hempel, F.D., Barella, S., and Zambryski, P. (2002). Leaf-to-shoot apex movement of symplastic tracer is restricted coincident with flowering in Arabidopsis. Proc. Natl. Acad. Sci. U. S. A. *99*, 1713–1717.

Gisk, B., Yasui, Y., Kohchi, T., and Frankenberg-Dinkel, N. (2010). Characterization of the haem oxygenase protein family in Arabidopsis thaliana reveals a diversity of functions. Biochem. J. *425*, 425–434.

Gray, J.C., Hansen, M.R., Shaw, D.J., Graham, K., Dale, R., Smallman, P., Natesan, S.K. a, and Newell, C. a. (2012). Plastid stromules are induced by stress treatments acting through abscisic acid. Plant J. *69*, 387–398.

Guseman, J.M., Lee, J.S., Bogenschutz, N.L., Peterson, K.M., Virata, R.E., Xie, B., Kanaoka, M.M., Hong, Z., and Torii, K.U. (2010). Dysregulation of cell-to-cell connectivity and stomatal patterning by loss-of-function mutation in Arabidopsis chorus (glucan synthase-like 8). Development *137*, 1731–1741.

Ham, B.-K., Li, G., Kang, B.-H., Zeng, F., and Lucas, W.J. (2012). Overexpression of Arabidopsis Plasmodesmata Germin-Like Proteins Disrupts Root Growth and Development. Plant Cell *24*, 3630–3648.

Han, X., Hyun, T., Zhang, M., Kumar, R., Koh, E.J., Kang, B.H., Lucas, W., and Kim, J.Y. (2014). Auxin-Callose-Mediated Plasmodesmal Gating Is Essential for Tropic Auxin Gradient Formation and Signaling. Dev. Cell *28*, 132–146.

Hanson, M.R., and Sattarzadeh, A. (2011). Stromules: recent insights into a long neglected feature of plastid morphology and function. Plant Physiol. *155*, 1486–1492.

Harries, P., and Ding, B. (2011). Cellular factors in plant virus movement: At the leading edge of macromolecular trafficking in plants. Virology *411*, 237–243.

Heinlein, M. (2015). Plasmodesmata: channels for viruses on the move. In Plasmodesmata: Methods and Protocols2, M. Heinlein, ed. (New York: Springer), pp. 25–54.

Holt, B.F., Boyes, D.C., Ellerström, M., Siefers, N., Wiig, A., Kauffman, S., Grant, M.R., and Dangl, J.L. (2002). An evolutionarily conserved mediator of plant disease resistance gene function is required for normal Arabidopsis development. Dev. Cell *2*, 807–817.

Holzinger, a., Buchner, O., Lütz, C., and Hanson, M.R. (2007). Temperature-sensitive formation of chloroplast protrusions and stromules in mesophyll cells of Arabidopsis thaliana. Protoplasma *230*, 23–30.

Holzinger, A., Kwok, E.Y., and Hanson, M.R. (2008). Effects of arc3, arc5 and arc6 mutations on plastid morphology and stromule formation in green and nongreen tissues of arabidopsis Thaliana. Photochem. Photobiol. *84*, 1324–1335.

Huang, a H.C. (1992). Oil Bodies and Oleosins in Seeds. Annu. Rev. Plant Physiol. Plant Mol. Biol. *43*, 177–200.

Hughes, J. (2013). Hughes cytoplasmic signaling. Annu Rev Plant Biol *64 SRC -*, 377–402.

Izumi, N., Yamashita, A., Iwamatsu, A., Kurata, R., Nakamura, H., Saari, B., Hirano, H., Anderson, P., and Ohno, S. (2010). AAA+ proteins RUVBL1 and RUVBL2 coordinate PIKK activity and function in nonsense-mediated mRNA decay. Sci. Signal. *3*, ra27.

Jewell, J.L., and Guan, K.L. (2013). Nutrient signaling to mTOR and cell growth. Trends Biochem. Sci. *38*, 233–242.

Joly, D., and Carpentier, R. (2011). Rapid isolation of intact chloroplasts from spinach leaves.

Jónsson, Z.O., Jha, S., Wohlschlegel, J. a., and Dutta, A. (2004). Rvb1p/Rvb2p recruit Arp5p and assemble a functional Ino80 chromatin remodeling complex. Mol. Cell *16*, 465–477.

Kakihara, Y., and Houry, W. a. (2012). The R2TP complex: Discovery and functions. Biochim. Biophys. Acta - Mol. Cell Res. *1823*, 101–107.

Kakihara, Y., Makhnevych, T., Zhao, L., Tang, W., and Houry, W. a (2014). Nutritional status modulates box C/D snoRNP biogenesis by regulated subcellular relocalization of the R2TP complex. Genome Biol. *15*, 404.

Kapahi, P., Chen, D., Rogers, A.N., Katewa, S.D., Li, P.W.L., Thomas, E.L., and Kockel, L. (2010). With TOR, less is more: A key role for the conserved nutrient-sensing TOR pathway in aging. Cell Metab. *11*, 453–465.

Kim, I., and Zambryski, P. (2005). Cell-To-Cell communication via plasmodesmata during embryogenesis. Curr. Opin. Plant Biol. *8*, 593–599.

Kim, I., Hempel, F.D., Sha, K., Pfluger, J., and Zambryski, P.C. (2002). Identification of a developmental transition in plasmodesmatal function during embryogenesis in Arabidopsis thaliana. Development *129*, 1261–1272.

Kim, I., Cho, E., Crawford, K., Hempel, F.D., and Zambryski, P.C. (2005a). Cell-to-cell movement of GFP during embryogenesis and early seedling development in Arabidopsis. Proc. Natl. Acad. Sci. U. S. A. *102*, 2227–2231.

Kim, I., Kobayashi, K., Cho, E., and Zambryski, P.C. (2005b). Subdomains for transport via plasmodesmata corresponding to the apical-basal axis are established during Arabidopsis embryogenesis. Proc. Natl. Acad. Sci. U. S. A. *102*, 11945–11950.

King, T.H., Decatur, W. a, Bertrand, E., Maxwell, E.S., and Fournier, M.J. (2001). A well-connected and conserved nucleoplasmic helicase is required for production of box C/D and H/ACA snoRNAs and localization of snoRNP proteins. Mol. Cell. Biol. *21*, 7731–7746.

Kobayashi, K., Otegui, M.S., Krishnakumar, S., Mindrinos, M., and Zambryski, P. (2007). INCREASED SIZE EXCLUSION LIMIT 2 encodes a putative DEVH box RNA helicase involved in plasmodesmata function during Arabidopsis embryogenesis. Plant Cell *19*, 1885–1897.

Köhler, R.H., Cao, J., Zipfel, W.R., Webb, W.W., and Hanson, M.R. (1997). Exchange of protein molecules through connections between higher plant plastids. Science *276*, 2039–2042.

Kong, D., Karve, R., Willet, a., Chen, M.-K., Oden, J., and Shpak, E.D. (2012). Regulation of Plasmodesmatal Permeability and Stomatal Patterning by the Glycosyltransferase-Like Protein KOBITO1. Plant Physiol. *159*, 156–168.

Koussevitzky, S., Nott, A., Mockler, T.C., Hong, F., Sachetto-Martins, G., Surpin, M., Lim, J., Mittler, R., and Chory, J. (2007). Signals from chloroplasts converge to regulate nuclear gene expression. Science *316*, 715–719.

Kragler, F., Monzer, J., Shash, K., Xoconostle-Cázares, B., and Lucas, W.J. (1998). Cell-to-cell transport of proteins: Requirement for unfolding and characterization of binding to a putative plasmodesmal receptor. Plant J. *15*, 367–381.

Lai, a. G., Doherty, C.J., Mueller-Roeber, B., Kay, S. a., Schippers, J.H.M., and Dijkwel, P.P. (2012). CIRCADIAN CLOCK-ASSOCIATED 1 regulates ROS homeostasis and oxidative stress responses. Proc. Natl. Acad. Sci. *109*, 17129–17134.

Latrasse, D., Benhamed, M., Henry, Y., Domenichini, S., Kim, W., Zhou, D.-X., and Delarue, M. (2008). The MYST histone acetyltransferases are essential for gametophyte development in Arabidopsis. BMC Plant Biol. *8*, 121.

Lee, J.Y., Yoo, B.C., and Lucas, W.J. (2000). Parallels between nuclear-pore and plasmodesmal trafficking of information molecules. Planta *210*, 177–187.

Lee, J.-Y., Colinas, J., Wang, J.Y., Mace, D., Ohler, U., and Benfey, P.N. (2006). Transcriptional and posttranscriptional regulation of transcription factor expression in Arabidopsis roots. Proc. Natl. Acad. Sci. U. S. A. *103*, 6055–6060.

Lee, J.-Y., Wang, X., Cui, W., Sager, R., Modla, S., Czymmek, K., Zybaliov, B., van Wijk, K., Zhang, C., Lu, H., et al. (2011). A plasmodesmata-localized protein mediates crosstalk between cell-to-cell communication and innate immunity in Arabidopsis. Plant Cell *23*, 3353–3373.

Lefebvre, V., North, H., Frey, A., Sotta, B., Seo, M., Okamoto, M., Nambara, E., and Marion-Poll, A. (2006). Functional analysis of Arabidopsis NCED6 and NCED9 genes indicates that ABA synthesized in the endosperm is involved in the induction of seed dormancy. Plant J. *45*, 309–319.

Levy, A., Erlanger, M., Rosenthal, M., and Epel, B.L. (2007). A plasmodesmata-associated beta-1,3-glucanase in Arabidopsis. Plant J. *49*, 669–682.

Liarzi, O., and Epel, B.L. (2005). Development of a quantitative tool for measuring changes in the coefficient of conductivity of plasmodesmata induced by developmental, biotic, and abiotic signals.

March-Díaz, R., García-Domínguez, M., Lozano-Juste, J., León, J., Florencio, F.J., and Reyes, J.C. (2008). Histone H2A.Z and homologues of components of the SWR1 complex are required to control immunity in Arabidopsis. Plant J. *53*, 475–487.

Masclaux, C., Valadier, M.H., Brugière, N., Morot-Gaudry, J.F., and Hirel, B. (2000). Characterization of the sink/source transition in tobacco (Nicotiana tabacum L.) shoots in relation to nitrogen management and leaf senescence. Planta *211*, 510–518.

Mason, M.G., Ross, J.J., Babst, B. a., Wienclaw, B.N., and Beveridge, C. a. (2014). Sugar demand, not auxin, is the initial regulator of apical dominance. Proc. Natl. Acad. Sci. 201322045.

Maule, A.J., Gaudioso-Pedraza, R., and Benitez-Alfonso, Y. (2013). Callose deposition and symplastic connectivity are regulated prior to lateral root emergence. Commun. Integr. Biol. *6*.

Menand, B., Desnos, T., Nussaume, L., Berger, F., Bouchez, D., Meyer, C., and Robaglia, C. (2002). Expression and disruption of the Arabidopsis TOR (target of rapamycin) gene. Proc. Natl. Acad. Sci. U. S. A. *99*, 6422–6427.

Michalska, J., Zauber, H., Buchanan, B.B., Cejudo, F.J., and Geigenberger, P. (2009). NTRC links built-in thioredoxin to light and sucrose in regulating starch synthesis in chloroplasts and amyloplasts. Proc. Natl. Acad. Sci. U. S. A. *106*, 9908–9913.

Mönke, G., Seifert, M., Keilwagen, J., Mohr, M., Grosse, I., Hähnel, U., Junker, A., Weisshaar, B., Conrad, U., Bäumlein, H., et al. (2012). Toward the identification and regulation of the Arabidopsis thaliana ABI3 regulon. Nucleic Acids Res. *40*, 8240–8254.

Montané, M.H., and Menand, B. (2013). ATP-competitive mTOR kinase inhibitors delay plant growth by triggering early differentiation of meristematic cells but no developmental patterning change. J. Exp. Bot. *64*, 4361–4374.

Mushegian, A.R., and Elena, S.F. (2015). Evolution of plant virus movement proteins from the 30K superfamily and of their homologs integrated in plant genomes. Virology *476*, 304–315.

Nambara, E., and Marion-Poll, A. (2005). Abscisic acid biosynthesis and catabolism. Annu. Rev. Plant Biol. *56*, 165–185.

Nambara, E., Keith, K., McCourt, P., and Naito, S. (1994). Isolation of an internal deletion mutant of the Arabidopsis thaliana ABI3 gene. Plant Cell Physiol. *35*, 509–513.

Nano, N., and Houry, W. a (2013). Chaperone-like activity of the AAA+ proteins Rvb1 and Rvb2 in the assembly of various complexes. Philos. Trans. R. Soc. Lond. B. Biol. Sci. *368*, 20110399.

Natesan, S.K. a, Sullivan, J. a., and Gray, J.C. (2005). Stromules: A characteristic cell-specific feature of plastid morphology. J. Exp. Bot. *56*, 787–797.

Natesan, S.K. a, Sullivan, J. a., and Gray, J.C. (2009). Myosin XI is required for actin-associated movement of plastid stromules. Mol. Plant *2*, 1262–1272.

Niehl, A., and Heinlein, M. (2011). Cellular pathways for viral transport through plasmodesmata. Protoplasma *248*, 75–99.

Niklas, K.J. (2014). The evolutionary-developmental origins of multicellularity. Am. J. Bot. *101*, 6–25.

Niklas, K.J., and Newman, S. a. (2013). The origins of multicellular organisms. Evol. Dev. *15*, 41–52.

Nomura, H., Komori, T., Uemura, S., Kanda, Y., Shimotani, K., Nakai, K., Furuichi, T., Takebayashi, K., Sugimoto, T., Sano, S., et al. (2012). Chloroplast-mediated activation of plant immune signalling in Arabidopsis. Nat. Commun. *3*, 926.

Oparka, K.J., Roberts, a. G., Boevink, P., Cruz, S.S., Roberts, I., Pradel, K.S., Imlau, a., Kotlizky, G., Sauer, N., and Epel, B. (1999a). Simple, but not branched, plasmodesmata allow the nonspecific trafficking of proteins in developing tobacco leaves. Cell *97*, 743–754.

Oparka, K.J., Roberts, a. G., Boevink, P., Cruz, S.S., Roberts, I., Pradel, K.S., Imlau, a., Kotlizky, G., Sauer, N., and Epel, B. (1999b). Simple, but not branched, plasmodesmata allow the nonspecific trafficking of proteins in developing tobacco leaves. Cell *97*, 743–754.

Pagant, S., Bichet, A., Sugimoto, K., Lerouxel, O., Desprez, T., McCann, M., Lerouge, P., Vernhettes, S., and Höfte, H. (2002). KOBITO1 encodes a novel plasma membrane protein necessary for normal synthesis of cellulose during cell expansion in Arabidopsis. Plant Cell *14*, 2001–2013.

Palevitz, B. a., and Hepler, P.K. (1985). Changes in dye coupling of stomatal cells of Allium and Commelina demonstrated by microinjection of Lucifer yellow. Planta *164*, 473–479.

Petrillo, E., Herz, M. a G., Fuchs, A., Reifer, D., Fuller, J., Yanovsky, M.J., Simpson, C., Brown, J.W.S., Barta, A., Kalyna, M., et al. (2014). A chloroplast retrograde signal regulates nuclear alternative splicing. Science *344*, 427–430.

Pickard, W.F. (2003). The role of cytoplasmic streaming in symplastic transport. Plant, Cell Environ. *26*, 1–15.

Priest, D.M., Ambrose, S.J., Vaistij, F.E., Elias, L., Higgins, G.S., Ross, a. R.S., Abrams, S.R., and Bowles, D.J. (2006). Use of the glucosyltransferase UGT71B6 to disturb abscisic acid homeostasis in Arabidopsis thaliana. Plant J. *46*, 492–502.

Provencher, L.M., Miao, L., Sinha, N., and Lucas, W.J. (2001). Sucrose export defective1 encodes a novel protein implicated in chloroplast-to-nucleus signaling. Plant Cell *13*, 1127–1141.

Reichheld, J.-P., Khafif, M., Riondet, C., Droux, M., Bonnard, G., and Meyer, Y. (2007). Inactivation of thioredoxin reductases reveals a complex interplay between thioredoxin and glutathione pathways in Arabidopsis development. Plant Cell *19*, 1851–1865.

Rim, Y., Huang, L., Chu, H., Han, X., Cho, W.K., Jeon, C.O., Kim, H.J., Hong, J.C., Lucas, W.J., and Kim, J.Y. (2011). Analysis of Arabidopsis transcription factor families revealed extensive capacity for cell-to-cell movement as well as discrete trafficking patterns. Mol. Cells *32*, 519–526.

Rinne, P.L., and van der Schoot, C. (1998). Symplasmic fields in the tunica of the shoot apical meristem coordinate morphogenetic events. Development *125*, 1477–1485.

Roberts, A., Cruz, S., Roberts, I., Prior, D., Turgeon, R., and Oparka, K. (1997a). Phloem Unloading in Sink Leaves of Nicotiana benthamiana: Comparison of a Fluorescent Solute with a Fluorescent Virus. Plant Cell *9*, 1381–1396.

Roberts, A., Cruz, S., Roberts, I., Prior, D., Turgeon, R., and Oparka, K. (1997b). Phloem Unloading in Sink Leaves of Nicotiana benthamiana: Comparison of a Fluorescent Solute with a Fluorescent Virus. Plant Cell *9*, 1381–1396.

Roberts, I.M., Boevink, P., Roberts, a. G., Sauer, N., Reichel, C., and Oparka, K.J. (2001). Dynamic changes in the frequency and architecture of plasmodesmata during the sink-source transition in tobacco leaves. Protoplasma *218*, 31–44.

Rosenbaum, J., Baek, S.H., Dutta, A., Houry, W. a, Huber, O., Hupp, T.R., and Matias, P.M. (2013). The emergence of the conserved AAA+ ATPases Pontin and Reptin on the signaling landscape. Sci. Signal. *6*, mr1.

Roy, S., Huang, H., Liu, S., and Kornberg, T.B. (2014). Cytoneme-mediated contact-dependent transport of the Drosophila decapentaplegic signaling protein. Science *343*, 1244624.

Rutschow, H.L., Baskin, T.I., and Kramer, E.M. (2011). Regulation of solute flux through plasmodesmata in the root meristem. Plant Physiol. *155*, 1817–1826.

Sager, R., and Lee, J.-Y. (2014). Plasmodesmata in integrated cell signalling: insights from development and environmental signals and stresses. J. Exp. Bot. *65*, 6337–6358.

Schattat, M.H., and Klösgen, R.B. (2011). Induction of stromule formation by extracellular sucrose and glucose in epidermal leaf tissue of Arabidopsis thaliana. BMC Plant Biol. *11*, 115.

Schattat, M., Barton, K., Baudisch, B., Klösgen, R.B., and Mathur, J. (2011). Plastid stromule branching coincides with contiguous endoplasmic reticulum dynamics. Plant Physiol. *155*, 1667–1677.

Schattat, M.H., Griffiths, S., Mathur, N., Barton, K., Wozny, M.R., Dunn, N., Greenwood, J.S., and Mathur, J. (2012a). Differential Coloring Reveals That Plastids Do Not Form Networks for Exchanging Macromolecules. Plant Cell *24*, 1465–1477.

Schattat, M.H., Klösgen, R.B., and Mathur, J. (2012b). New insights on stromules: Stroma filled tubules extended by independent plastids. Plant Signal. Behav. *7*, 1132–1137.

Schiefelbein, J., Huang, L., and Zheng, X. (2014). Regulation of epidermal cell fate in Arabidopsis roots: the importance of multiple feedback loops.

Schmid, M., Davison, T.S., Henz, S.R., Pape, U.J., Demar, M., Vingron, M., Schölkopf, B., Weigel, D., and Lohmann, J.U. (2005). A gene expression map of Arabidopsis thaliana development. Nat. Genet. *37*, 501–506.

Schulz, A., Knoetzel, J., Scheller, H. V, and Mant, A. (2004). Uptake of a fluorescent dye as a swift and simple indicator of organelle intactness: import-competent chloroplasts from soil-grown Arabidopsis. J. Histochem. Cytochem. *52*, 701–704.

Sevilem, I., Yadav, S., and Helariutta, Y. (2015). Plasmodesmata: channels for intercellular signaling during plant growth and development. In Plasmodesmata: Methods and Protocols, M. Heinlein, ed. (New York: Springer), pp. 3–24.

Simpson, C., Thomas, C., Findlay, K., Bayer, E., and Maule, A.J. (2009). An Arabidopsis GPI-anchor plasmodesmal neck protein with callose binding activity and potential to regulate cell-to-cell trafficking. Plant Cell *21*, 581–594.

Sowiński, P., Bilska, A., Barańska, K., Fronk, J., and Kobus, P. (2007). Plasmodesmata density in vascular bundles in leaves of C4 grasses grown at different light conditions in respect to photosynthesis and photosynthate export efficiency. Environ. Exp. Bot. *61*, 74–84.

Stadler, R., Wright, K.M., Lauterbach, C., Amon, G., Gahrtz, M., Feuerstein, A., Oparka, K.J., and Sauer, N. (2005). Expression of GFP-fusions in Arabidopsis companion cells reveals non-specific protein trafficking into sieve elements and identifies a novel post-phloem domain in roots. Plant J. *41*, 319–331.

Stahl, Y., Grabowski, S., Bleckmann, A., Kühnemuth, R., Weidtkamp-Peters, S., Pinto, K.G., Kirschner, G.K., Schmid, J.B., Wink, R.H., Hülsewede, A., et al. (2013). Moderation of arabidopsis root stemness by CLAVATA1 and ARABIDOPSIS CRINKLY4 receptor kinase complexes. Curr. Biol. *23*, 362–371.

Stonebloom, S., Burch-Smith, T., Kim, I., Meinke, D., Mindrinos, M., and Zambryski, P. (2009). Loss of the plant DEAD-box protein ISE1 leads to defective mitochondria and increased cell-to-cell transport via plasmodesmata. Proc. Natl. Acad. Sci. U. S. A. *106*, 17229–17234.

Stonebloom, S., Brunkard, J.O., Cheung, a. C., Jiang, K., Feldman, L., and Zambryski, P. (2012). Redox States of Plastids and Mitochondria Differentially Regulate Intercellular Transport via Plasmodesmata. Plant Physiol. *158*, 190–199.

Storms, M.M.H., Van der Schoot, C., Prins, M., Kormelink, R., Van Lent, J.W.M., and Goldbach, R.W. (1998). A comparison of two methods of microinjection for assessing altered plasmodesmal gating in tissues expressing viral movement proteins. Plant J. *13*, 131–140.

Takai, H., Xie, Y., De Lange, T., and Pavletich, N.P. (2010). Tel2 structure and function in the Hsp90-dependent maturation of mTOR and ATR complexes. Genes Dev. *24*, 2019–2030.

Templeton, G.W., and Moorhead, G.B.G. (2005). The phosphoinositide-3-OH-kinase-related kinases of Arabidopsis thaliana. EMBO Rep. *6*, 723–728.

Terry, M.J., and Smith, A.G. (2013). A model for tetrapyrrole synthesis as the primary mechanism for plastid-to-nucleus signaling during chloroplast biogenesis. Front. Plant Sci. *4*, 14.

Thimm, O., Bläsing, O., Gibon, Y., Nagel, A., Meyer, S., Krüger, P., Selbig, J., Müller, L. a., Rhee, S.Y., and Stitt, M. (2004). MAPMAN: A user-driven tool to display genomics data sets onto diagrams of metabolic pathways and other biological processes. Plant J. *37*, 914–939.

Thomas, C.L., Bayer, E.M., Ritzenthaler, C., Fernandez-Calvino, L., and Maule, A.J. (2008). Specific targeting of a plasmodesmal protein affecting cell-to-cell communication. PLoS Biol. *6*, 0180–0190.

Tilsner, J., Amari, K., and Torrance, L. (2011). Plasmodesmata viewed as specialised membrane adhesion sites. Protoplasma *248*, 39–60.

Turgeon, R. (1989). The Sink-Source Transition in Leaves. Annu. Rev. Plant Physiol. Plant Mol. Biol. *40*, 119–138.

Vatén, A., and Bergmann, D.C. (2012). Mechanisms of stomatal development: an evolutionary view. Evodevo *3*, 11.

Veley, K.M., Marshburn, S., Clure, C.E., and Haswell, E.S. (2012). Mechanosensitive channels protect plastids from hypoosmotic stress during normal plant growth. Curr. Biol. *22*, 408–413.

Venteicher, A.S., Meng, Z., Mason, P.J., Veenstra, T.D., and Artandi, S.E. (2008). Identification of ATPases Pontin and Reptin as Telomerase Components Essential for Holoenzyme Assembly. Cell *132*, 945–957.

Wang, X., Sager, R., Cui, W., Zhang, C., Lu, H., and Lee, J.-Y. (2013). Salicylic acid regulates Plasmodesmata closure during innate immune responses in Arabidopsis. Plant Cell *25*, 2315–2329.

White, R.G., and Barton, D. a. (2011). The cytoskeleton in plasmodesmata: A role in intercellular transport? J. Exp. Bot. *62*, 5249–5266.

Wildman, S.G., Hongladarom, T., and Honda, S.I. (1962). Chloroplasts and Mitochondria in Living Plant Cells: Cinephotomicrographic Studies. Science *138*, 434–436.

Willmer, C.M., and Sexton, R. (1979). Stomata and plasmodesmata. Protoplasma *100*, 113–124.

Woodson, J.D., and Chory, J. (2008). Coordination of gene expression between organellar and nuclear genomes. Nat. Rev. Genet. *9*, 383–395.

Wu, X., Dinneny, J.R., Crawford, K.M., Rhee, Y., Citovsky, V., Zambryski, P.C., and Weigel, D. (2003). Modes of intercellular transcription factor movement in the Arabidopsis apex. Development *130*, 3735–3745.

Wullschleger, S., Loewith, R., and Hall, M.N. (2006). TOR signaling in growth and metabolism. Cell *124*, 471–484.

Xiao, Y., Savchenko, T., Baidoo, E.E.K., Chehab, W.E., Hayden, D.M., Tolstikov, V., Corwin, J. a., Kliebenstein, D.J., Keasling, J.D., and Dehesh, K. (2012). Retrograde signaling by the plastidial metabolite MEcPP regulates expression of nuclear stress-response genes. Cell *149*, 1525–1535.

Xiong, Y., and Sheen, J. (2012). Rapamycin and glucose-target of rapamycin (TOR) protein signaling in plants. J. Biol. Chem. *287*, 2836–2842.

Xiong, Y., McCormack, M., Li, L., Hall, Q., Xiang, C., and Sheen, J. (2013). Glucose-TOR signalling reprograms the transcriptome and activates meristems. Nature *496*, 181–186.

Xu, M., Cho, E., Burch-Smith, T.M., and Zambryski, P.C. (2012a). Plasmodesmata formation and cell-to-cell transport are reduced in decreased size exclusion limit 1 during embryogenesis in Arabidopsis. Proc. Natl. Acad. Sci. *109*, 5098–5103.

Xu, M., Cho, E., Burch-Smith, T.M., and Zambryski, P.C. (2012b). Plasmodesmata formation and cell-to-cell transport are reduced in decreased size exclusion limit 1 during embryogenesis in Arabidopsis. Proc. Natl. Acad. Sci. *109*, 5098–5103.

Xu, X.M., Wang, J., Xuan, Z., Goldshmidt, A., Borrill, P.G.M., Hariharan, N., Kim, J.Y., and Jackson, D. (2011). Chaperonins facilitate KNOTTED1 cell-to-cell trafficking and stem cell function. Science *333*, 1141–1144.

Yadav, R.K., Perales, M., and Gruel, J. (2011). WUSCHEL protein movement mediates stem cell homeostasis in the Arabidopsis shoot apex WUSCHEL protein movement mediates stem cell homeostasis in the Arabidopsis shoot apex. Genes Dev. *25*, 2025–2030.

Yamamoto, a., Yoshii, M., Murase, S., Fujita, M., Kurata, N., Hobo, T., Kagaya, Y., Takeda, S., and Hattori, T. (2014). Cell-by-Cell Developmental Transition from Embryo to Post-Germination Phase Revealed by Heterochronic Gene Expression and ER-Body Formation in Arabidopsis leafy cotyledon Mutants. Plant Cell Physiol. *55*, 2112–2125.

Zambryski, P., and Crawford, K. (2000). Plasmodesmata: gatekeepers for cell-to-cell transport of developmental signals in plants. Annu. Rev. Cell Dev. Biol. *16*, 393–421.

Zavaliev, R., Ueki, S., Epel, B., and Citovsky, V. (2011). Biology of callose (β-1, 3-glucan) turnover at plasmodesmata. Protoplasma *248*, 1–36.

Zhang, C., Cao, L., Rong, L., An, Z., Zhou, W., Ma, J., Shen, W., Zhu, Y., and Dong, A. (2015). The chromatin-remodeling factor AtINO80 plays crucial roles in genome stability maintenance and in plant development. Plant J. *82*, 655–668.